BOSTON UNIVERSITY

GRADUATE SCHOOL OF ARTS AND SCIENCES

Dissertation

ANOMALIES OF WATER AND SIMPLE LIQUIDS

by

ZHENYU YAN

B.S., Tongji University, 2000
M.S., Clark Atlanta University, 2002

Submitted in partial fulfillment of the

requirements for the degree of

Doctor of Philosophy

2009

Approved by

First Reader
_____

H. Eugene Stanley, Ph.D.
University Professor and Professor of Physics

Second Reader
_____

William Skocpol Ph.D.
Professor of Physics

ACKNOWLEDGMENTS

ANOMALIES OF WATER AND SIMPLE LIQUIDS

(Order No.   )

ZHENYU YAN

Boston University Graduate School of Arts and Sciences, 2009

Major Professor: H. Eugene Stanley, University Professor and Professor of Physics

ABSTRACT

This thesis applies statistical physics approaches and computer simulations to investigate quantitatively the relationship between the structure and the dynamic and thermodynamic anomalies observed in water and some other simple liquids.

In Chapter 1, we give a general introduction to the properties of water. In Chapter 2 we address the question of whether spherically-symmetric potentials are also able to reproduce the structural anomalies found in systems with local tetrahedral order. We find that water-like structural order anomalies exist for the two-scale "ramp potential". Our findings suggest that the water-like relationship between structural order and anomalies is related to the presence of two different length scales in the potential.

In Chapter 3, we use the ratio of characteristic length scales of the two-scale ramp potential as a control parameter to investigate the evolution of dynamic, thermodynamic and structural anomalies. In this manner we show that the family of tunable spherically-symmetric potentials so generated evolves continuously between water-like and hard sphere behavior. These findings suggest that strong orientational interactions in the first shell of water are not necessary for a liquid to show thermodynamic, dynamic and structural anomalies, and highlight the importance of the second shell of water.

In Chapter 4, we investigate how much orientation-dependent first-shell interaction and the second-shell environment each contribute to water's anomalies. We show that the changes in the second shell of water are the structural bases for the anomalies. In Chapter 5, we study the quantitative connection between our ideal-

ized ramp potential and water's pair potential, as well as the relation between the regions of anomalies in their respective phase diagrams. Finally in Chapter 6 we show that the "two-body excess entropy" is a useful quantity for predicting the regions of thermodynamic, dynamic and structural anomalies of water.

Contents

List of Figures

LIST OF ABBREVIATIONS

SPC/E	Simple Point Charge/Extended
PCF	Pair Correlation Function
RDF	Radial Distribution Function
TIP5P	Five Point Transferable Intermolecular Potential
MD	Molecular Dynamics
1SRP	One-scale Ramp Potential
2SRP	Two-scale Ramp Potential
ED	Errington and Debenedetti
TMD	Temperature of Maximum Density
DM	Diffusivity Minima and Maxima
O-O	Oxygen-Oxygen
LDL/HDL	Low Density Liquid/High Density Liquid
LLCP	Liquid-Liquid Critical Point
N	Number of Particles
V	Volume
T	Temperature
T_M	Melting Temperature
T_g	Glass Transition Temperature
T_X	Crystallization Temperature
k_T	Isothermal Compressibility
C_P	Isobaric Heat Capacity

α_P	Thermal Expansion Coefficient
S	Entropy
S_{ex}	Excess Entropy
$S^{(2)}$	Two-body Contribution to Excess Entropy

Chapter 1

General Introduction

1.1 Phase Diagram of Water: Low Density and High Density Water

Water is the most important substance on earth and is essential for human life. Water can exist in different solid, liquid and gas states and has many peculiar properties that are important to the normal functions of biological bodies. Effort in this thesis will concentrate on one topic, understanding the anomalies of water. First we begin with a general introduction to water's properties.

Fig. 1.1 shows the phase diagram of water in a vast range of natural conditions: the temperature 0 K$< T <$ 1000 K, and pressure 0.1 Pa$< P <$ 1 TPa. The typical conditions exist on Earth, Mars and Venus are marked on the figure. Water at atmosphere pressure $P = 1$ atm is a stable liquid in the range between the melting point $T_M = 273$ K and boiling point $T_B = 373$ K. Below the melting point, water has hexagonal ice structure at atmosphere pressure [1]. For $T > T_B$ or $T < T_M$, liquid water can also exist in a metastable state as superheated or supercooled water with respect to gas or ice phase. In nature the impurities in the water provide nucleation
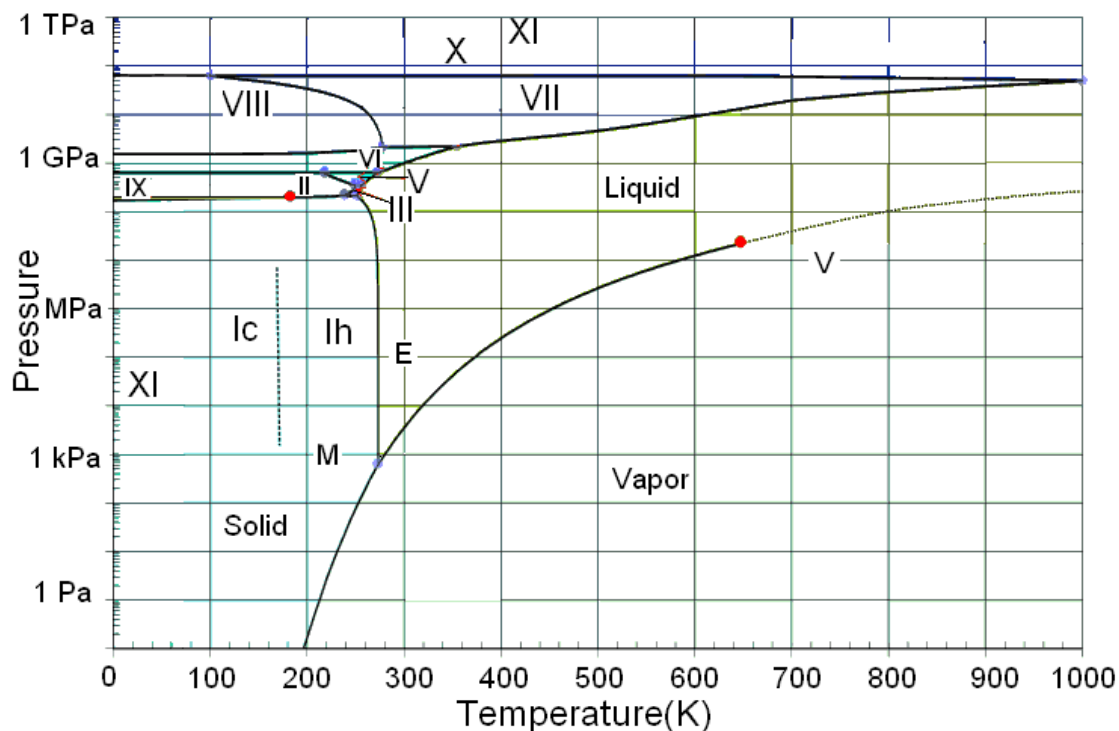
Figure 1.1: The phase diagram of water in a large range of temperature and pressure. The letters 'E', 'M' and 'V' indicate typical surface conditions on Earth, Mars and Venus. It shows water can be in gas state at low pressure and high temperature, in liquid state at medium pressure and temperature, and in solid state at low temperature and high pressure. Water can have many different solid ice structures. Under the normal condition of our living earth (marked by 'E'), water is in liquid state, which will change into solid state if temperature is lowered, or change into gas state if temperature is increased. In the figure, the lines are the coexistence lines of different gas, liquid and solid phases. (Figure from Prof. M. Chaplin http://www.lsbu.ac.uk/)

centers, and water easily freezes below T_M and boils above T_B [2].

In Fig. 1.1 there is also a triple point where solid, liquid and gas phase water coexist stably. There is a liquid-gas critical point (circle) at high temperature $T = 647$ K (pressure 22 MPa, density 322 kg/m^3), because at this point liquid water is hot enough and gaseous water is under enough pressure so that their densities become identical, and the two phases become indistinguishable from each other. Many of the solid forms of water at low temperature are metastable at low pressure, which means water can be supercooled to very low temperature without crystallization. There is also a possible second liquid-liquid critical point (circle) at low temperature $T = 217$ K, (pressure 340 MPa, density 1130 kg/cm^3), where metastable high density liquid and low density liquid coexist and become indistinguishable.

The phase diagram in Fig. 1.1 shows that water can be in at least twelve forms of ice at low temperature and high pressure. Impurities in water will help the formation of ice crystals in water, a process called "heterogeneous nucleation". If experiments can avoid such impurities and irregularities in the wall of container, water can be supercooled to the "homogeneous nucleation" temperature T_H (see Fig. 1.2), although it is not clear yet if T_H in the figure is the absolute limit of metastability or whether a lower T_H value can be achieved. Under usual situations when water is cooled slowly, for example, with a cooling rate ($q_c \approx 1$ K/s) below T_H one obtains ice I_h. However if it is cooled rapidly ($q_c \approx 10^5$ K/s) to very low $T < T_g$, the glass transition temperature, water can bypass crystallization and become an amorphous solid, or glassy water as shown in the photos of Fig. 1.3. Glassy water lacks long-range structural order compared with crystalline phase, and possesses a similar structure to the liquid. Glassy water is rigid and hard to diffuse like a solid.

Heated from very low temperature, water crystallizes at crystallization temperature T_X. Therefore in the temperature range $T_X < T < T_H$, water will crystallize. It is hard to get metastable liquid water in this range, which is called "no man's land". The glassy water at atmosphere pressure is low-density amorphous (LDA)

ice. Increasing pressure will increase the density of LDA and high-density amorphous (HDA) ice can be obtained as shown in the photos of Fig. 1.3 [3]). The two types of glassy water LDA and HDA have been extensively studied and are found to be different in structure. The transition from one form to another is abrupt with about a 25% change in density and can be reversed. Such change suggests a thermodynamic phase transition.

A coherent picture of supercooled and glassy water has been pursued. Based on the HDA-LDA phase transition of glassy water, the liquid-liquid phase transition theory hypothesizes that there is a first order phase transition between low density liquid (LDL) and high density liquid (HDL) in the region of "no man's land", and the transition between HDA and LDA is the low temperature observation of this liquid-liquid phase transition [4] (see Fig. 1.2). Computer simulations show the LDL and HDL can coexist and separate in liquid water and LDL water has smaller local density than average, while HDL has larger local density [3] (see Fig. 1.3). HDL and LDL phases are indistinguishable at higher $T > T_{C'}$, the temperature of the liquid-liquid critical point (LLCP). Above T'_C the critical fluctuation associated with the critical point can explain well the dramatic change in thermodynamic response functions such as isothermal compressibility K_T, specific heat C_P and thermal expansion coefficient α_P.

1.2   Anomalies of Water

Most liquids become denser upon cooling and more viscous upon compression. However, water and many other liquids with local tetrahedral order [5] (e.g., silica, silicon, and carbon) show a decrease in density upon cooling (density anomaly) and a decrease of viscosity upon pressurizing (diffusion anomaly). These liquids share many other thermodynamically anomalous properties than those mentioned above. For instance, experiments in phosphorus indicate the presence of a liquid-liquid phase
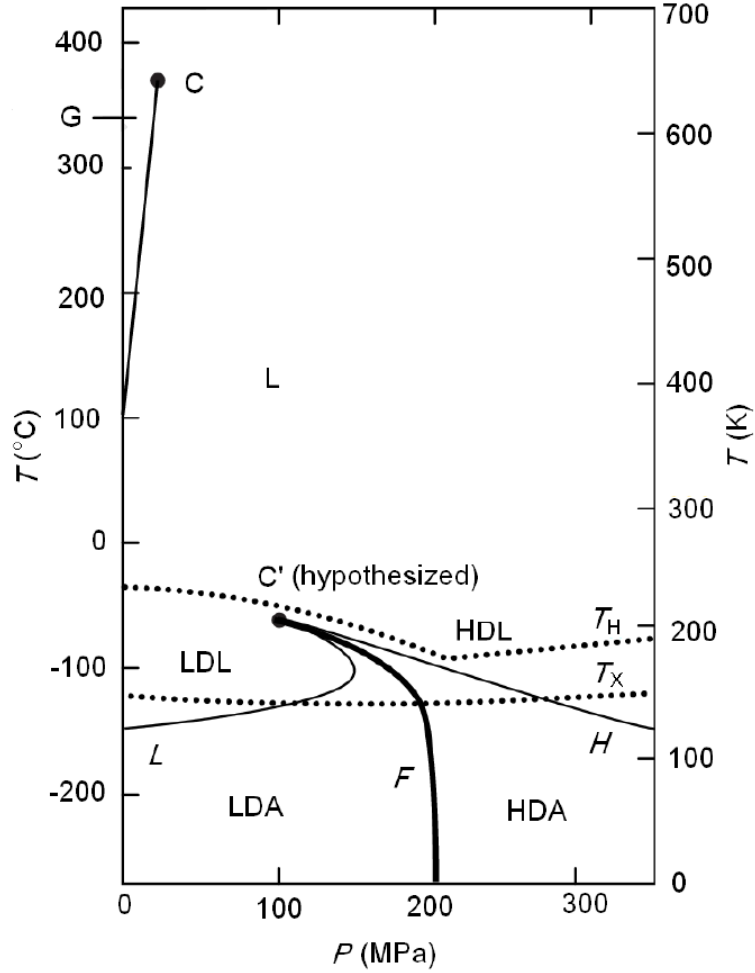
Figure 1.2: Phase diagram of water reproduced from Ref. [3], showing the phase relations between liquid water, LDL, HDL, LDA and HDA: C denotes the known liquid-gas critical point and C' the hypothesized 'second' (liquid-liquid) critical point, F denotes the line of first-order phase transitions that emanates from C' and separates the high-density and low-density phases HDL and LDL that occur for temperatures below $T_{c'}$. The curves denoted L and H are the limits of metastability of the HDA and LDA phases, respectively. Cooling supercooled water with a cooling rate (≈ 1 K/s) below T_H produces ice I_h crystal. But water can be hyperquenched from $T > T_H$ and transforms into glassy water at $T < T_g$, and then crystallize at T_X if heated again. So there is a "no man's land" between T_H and T_g. T_g is the glass transition temperature below T_X, which is the crystallization temperature.
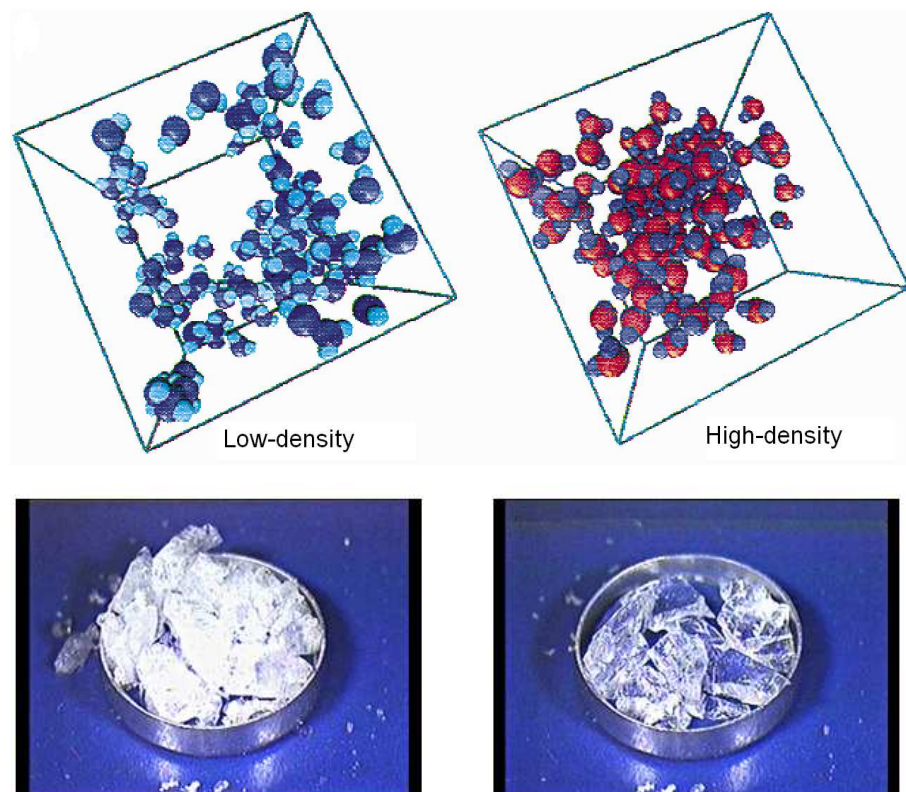
Figure 1.3: Low density and high density water. Upper two panels reproduced from Ref. [3] show configurations of LDL and HDL from molecular dynamics trajectories, coexisting and separating in liquid water. Lower two panels are photo shots of low density and high density amorphous ice. Photos from Prof. Osamu Mishima http://www.nims.go.jp/water/top.html.

transition [6] and similar results are obtained from computer simulations in silica [7], silicon [8], and water [4].

Among the different thermodynamic, dynamic and structural properties of water, lots of anomalies have been found compared to typical liquids. The most well known is that water's density reaches maximum at $4°C$ degree (Fig 1.4). Experiments also show that water has a diffusion anomaly because it can diffuse faster upon compression in some range of temperature and pressure [9] (Fig 1.5). The response functions of water in Fig. 1.6 increase sharply upon cooling below melting temperature T_M compared to the slow change of typical liquids [10]. The response functions are associated with the microscopic fluctuations of entropy and volume: $kTVK_T =< (\delta V)^2 >$, $kC_P =< (\delta S)^2 >$, and $kTV\alpha_P =< \delta V \delta S >$. Therefore below T_M, the thermodynamic fluctuations increase sharply. Recently the fluctuations have been connected with the so called Widom line of water, which basically is the extension of the liquid-liquid coexistence line into the one-phase region at temperature $T > T_{C'}$ above the liquid-liquid critical point, and there are maximum fluctuations of volume and entropy in the Widom line region due to the competition between the LDL and HDL liquids [11]. It is also shown that response functions actually reach a maximum at the Widom line instead of increasing to infinity [11].

One interesting question is to identify the regions of anomalies in the phase diagram. For example from experiment [9](Fig. 1.5), one can identify the range of density where diffusion increases with pressure for different T, and find this region in the $P - T$ phase diagram. Fig. 1.7 shows anomalous region of density and diffusion [12] using experimental data [9]. Fig. 1.7 also shows the similar anomalous regions obtained from molecular dynamic simulation of SPC/E water. The simulation can generate data for negative pressure, therefore it includes a complete region compared to the only positive pressure region of experiment.
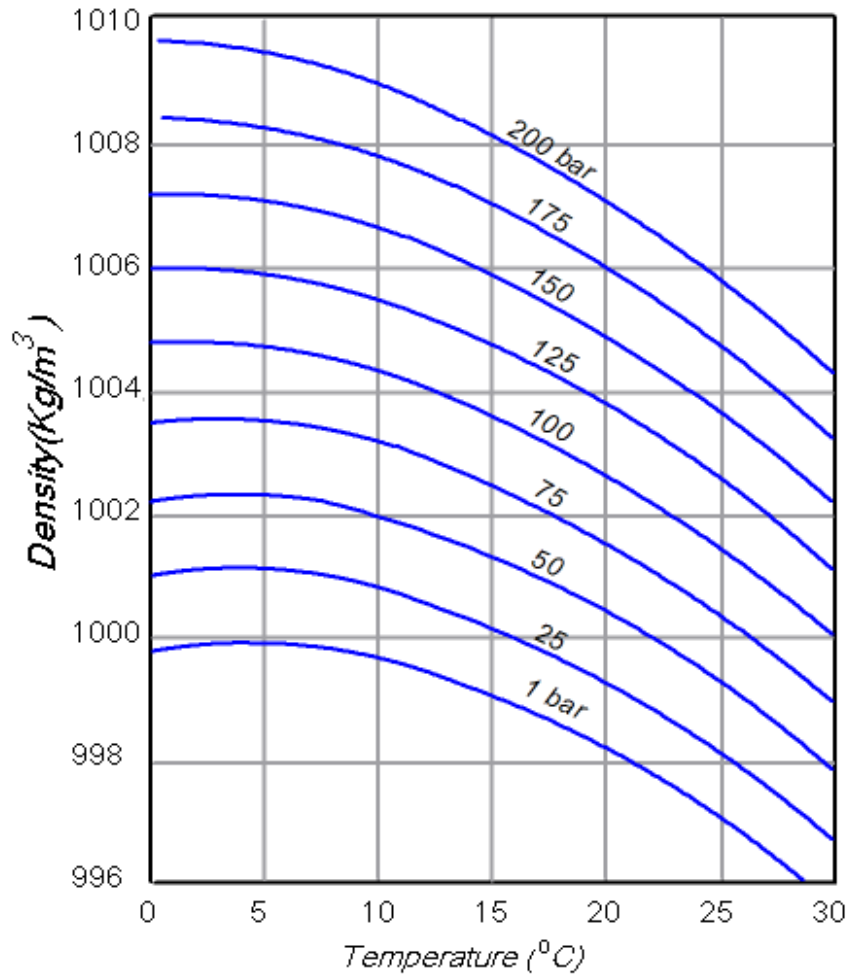
Figure 1.4: Density anomaly of water. Density of water as a function of temperature at different pressures shows that water at atmospheric pressure has maximum density at $T = 277$ K, which is the temperature of maximum density (TMD). Below this temperature, water expands upon cooling and this is called the density anomaly of water. There is a region of density anomaly in the phase diagram of liquid water spanning a range of temperature and pressure (see Fig. 1.7). (Figure from http://www.engineeringtoolbox.com/)
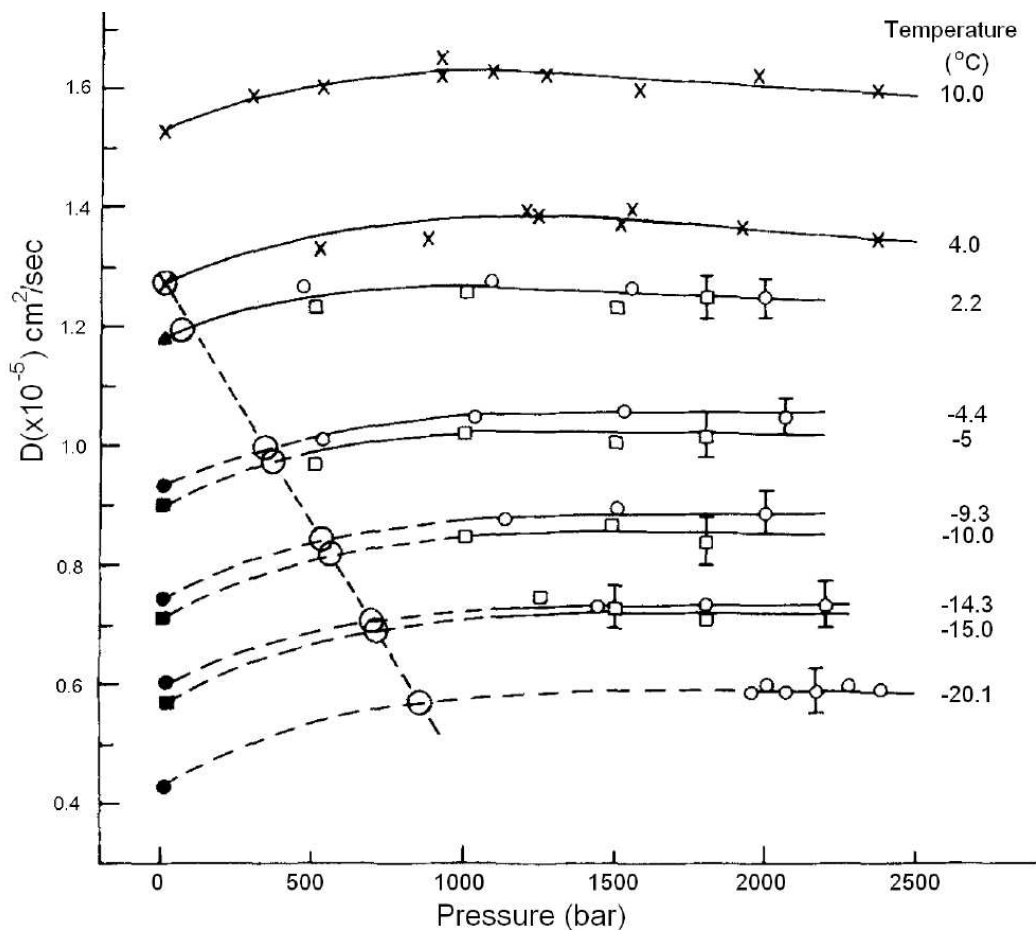
Figure 1.5: Diffusion anomaly of water. Temperature and pressure dependence of self diffusion coefficient of water. The data from different experiments are plotted with different symbols. The data consistently show that water's diffusivity increases with pressure in a range of temperature and pressure, and this is called diffusion anomaly. There is also a region of diffusion anomaly in the phase diagram of water (see Fig. 1.7). The dashed line corresponds to the temperature and pressure of the TMD line. (For details, see original figure in Ref [9]).
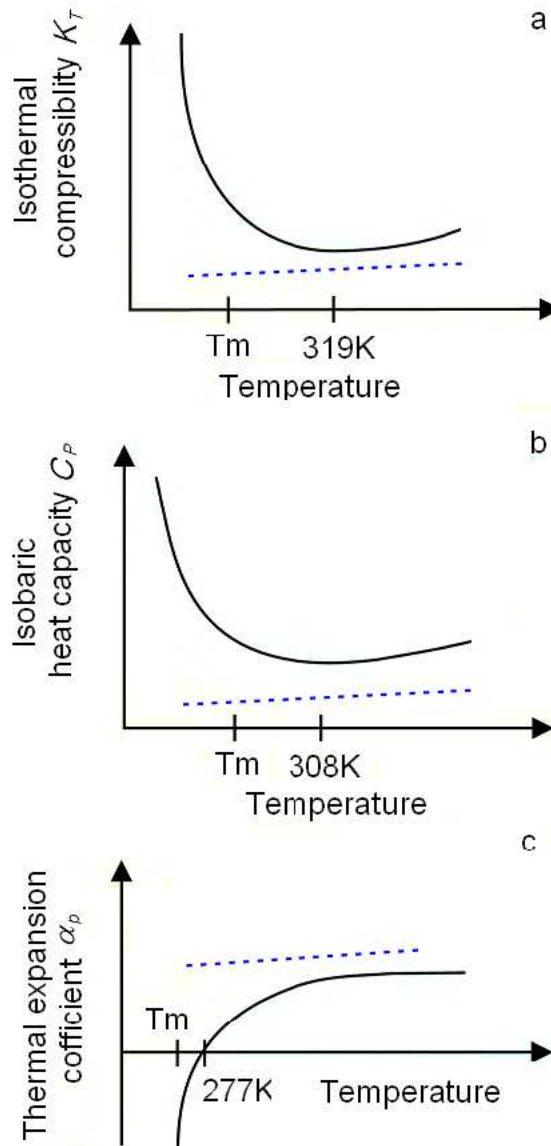
Figure 1.6: Schematic figures of thermodynamic response functions of water. (a) the isothermal compressibility $K_T \equiv (\partial \ln \rho / \partial P)_T$, (b) the constant pressure specific heat $C_P \equiv T(\partial S/\partial T)_P$, and (c) the thermal expansion coefficient $\alpha_P \equiv -(\partial \ln \rho / \partial T)_P$. The dashed lines are for the typical liquid. The thermodynamic fluctuations of supercooled water become much larger below the melting temperature T_M and the functions have sharp change. (Figures from Stanley *et al.* [13])
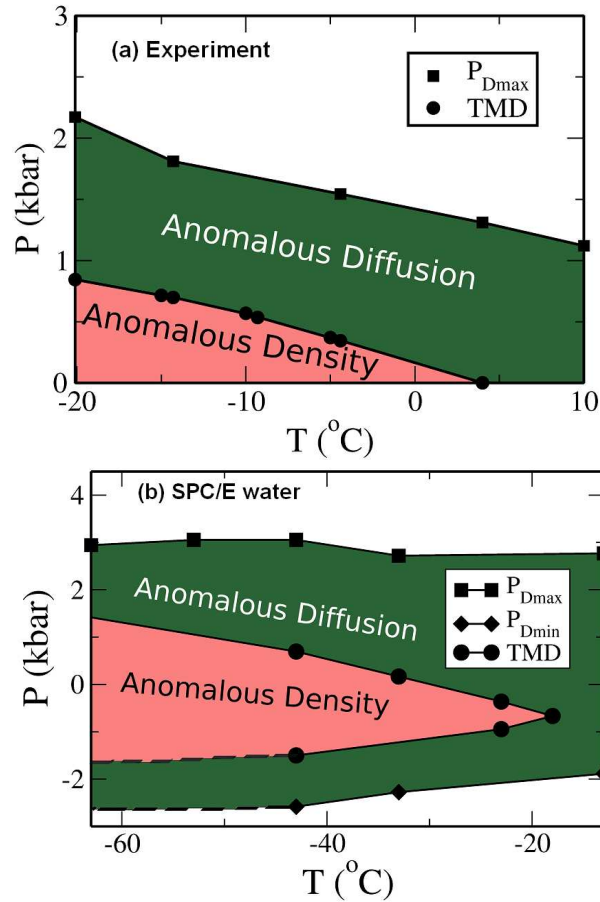
Figure 1.7: Anomalous regions of water. Upper panel: Regions of density and diffusion anomalies in the $P - T$ phase diagram of water obtained from experimental data [9, 12]. The diffusion anomaly region is wider than the density anomaly region. Lower panel: Regions of density and diffusion anomalies in the $P - T$ phase diagram of water obtained from SPC/E MD simulation [12, 14]. The experimental data can only show the region in the positive pressure range, while simulations can also show region in negative pressure. (Figures are reproduced from Ref. [12].)

1.3 Relation Between Structure and Anomalies of Water

Much effort has been expended to understand the relationship between the structure and the dynamic and thermodynamic anomalies observed in water. These anomalies are not unique to water. Other liquids with local tetrahedral order (e.g., silica and silicon) also exhibit thermodynamic and dynamic anomalies [5]. A possible explanation of these anomalies is the tendency of these substances to form local open structures not present in simple liquids. For water, the hydrogen bonding between each molecule and its four nearest neighbors form the open tetrahedral structure as shown in Fig. 1.8.

It has been proposed that these anomalies may arise from a liquid-liquid critical point (LLCP) in the deeply supercooled state of water [4]. The change of water structure between LDL (with low density, low entropy, low energy) and HDL (with high density, high entropy, and high energy) is related to water's thermodynamic and dynamic anomalies. For example, the structure change from HDL to LDL upon cooling (see Fig. 1.2) is related to the negative correlation between the total entropy and volume fluctuations, and the negative thermal expansion coefficient (density anomaly) is due to the relation $kTV\alpha_P =< \delta V \delta S >$. The structural anomaly is also related to the anomalous diffusion increase with density due to Adam-Gibbs equation $D \propto \exp[-B/(TS_c)]$, where S_c is the configurational entropy [23], proportional to the logarithm of the number of configurations of the system.

However, establishing a precise and quantitative link between the microscopic structure and the dynamic and thermodynamic anomalies of tetrahedral liquids has proved elusive until recently. Errington and Debenedetti [19] (ED) have studied the microscopic structural order in liquid water (SPC/E model) by using simple geometrical metrics or order parameters. They used two different metrics: a translational order parameter t [20], quantifying the tendency of particle pairs to adopt preferential
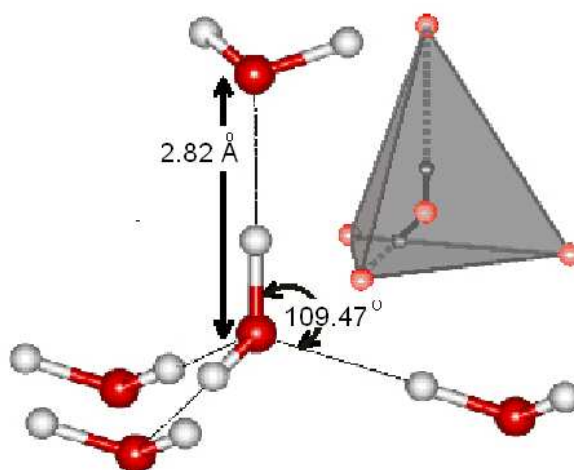
Figure 1.8: Tetrahedral structure of water molecules. The typical tetrahedral structure formed by a water molecule and its four nearest neighbors through the hydrogen bonding interaction. Two hydrogen atoms (donor) of a water molecule bond to two oxygen atoms (acceptor) of two nearby water molecules, at the same time its oxygen atom bonds to two hydrogen atoms of two other water molecules. Hydrogen bond lifetimes are 1 - 20 ps [15] whereas broken bond lifetimes are about 0.1 ps, and the fraction of breaking hydrogen bonding persisting for longer than a picosecond is insignificant [16–18], meaning that the tetrahedral network is essentially complete at ambient temperatures. At high temperature and pressure, the tetrahedral structure becomes disordered and one can use the local tetrahedral order parameter to quantify the change of local structural order of water [19]. (Figure from Prof. M. Chaplin http://www.lsbu.ac.uk/)
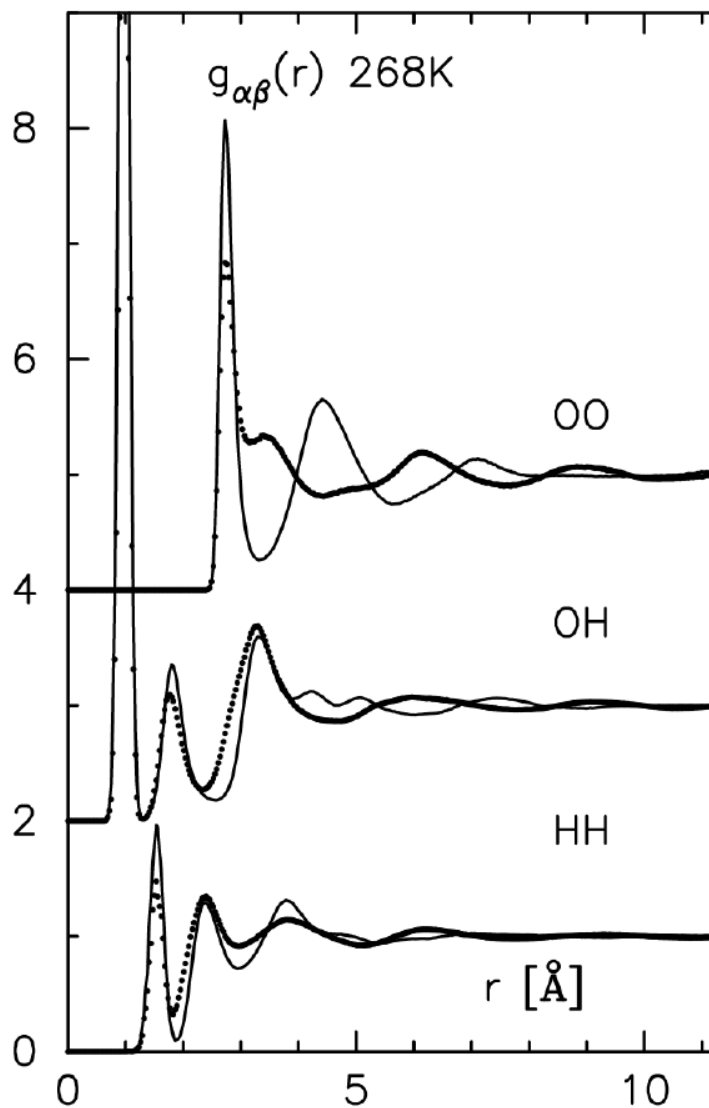
Figure 1.9: The radial distribution function $g(r)$ between oxygen-oxygen, oxygen-hydrogen and hydrogen-hydrogen atoms of water molecules under low (solid line) or high (dashed line) pressures. Results were obtained from neutron diffraction [22]. $g(r)$ defines the probability to find a molecule at distance r from a center molecule located at origin. $g(r)$ changes with temperature and pressure accompanied by the change in local structural order. One can also quantify the translational order of system by integrating over $g(r)$ [20, 21]. (Figure from A. K. Soper *et al.* [22])

separations as shown in Fig. 1.9, and a bond-orientational order parameter q [19, 24] quantifying the extent to which a molecule and its four nearest neighbors arrange in a tetrahedral local structure, as is the case in hexagonal ice (Fig. 1.8).

Ref. [19] found that the structural order of water changes abnormally with density. The *decrease* in order upon compression constitutes a structural anomaly (see Fig. 1.10): simple hard spheres or Lennard Jones liquids, in contrast, always become more ordered upon compression. They also found a dome-shaped region in the (T, ρ) plane within which isothermal compression leads to a decrease in t and q. ED further found that dynamic and thermodynamic anomalies define nested domes in the (T, ρ) plane: the structural anomalies dome contains the dynamic anomalies dome, which in turn contains the thermodynamic anomalies dome (Fig. 1.10(b)). This means that whenever the thermal expansion coefficient is negative, the diffusivity must necessarily increase and structural order must decrease upon isothermal compression,

A useful way of investigating structural order in liquids is to map state points into the $t - q$ plane (Fig. 1.11). Such a representation was introduced by Torquato and coworkers [26], who first applied it to sphere packing and referred to it as an order map. ED used the order map to investigate structural order in SPC/E water [19]. Because of the distinctive features discovered in the ED study, in what follows we refer to water-like order maps as the ED order map. Using molecular dynamics simulation of the SPC/E [27] model, ED found that the state points accessible to liquid water define a two-dimensional region in the $t - q$ plane (Fig. 1.11 right panel inset), meaning that in general t and q are independently variable in liquid water (i.e., equilibrium state paths exist along which one order metric varies while the other does not). ED showed that all state points exhibiting structural, dynamic or thermodynamic anomalies define a line on the (t, q) plane (Fig. 1.11 right panel), meaning that when SPC/E water exhibits anomalous behavior, its translational and orientational order metrics become strictly coupled. This is clear evidence of the relationship between structure and water anomalies. Simulations of Shell *et al.* subsequently found
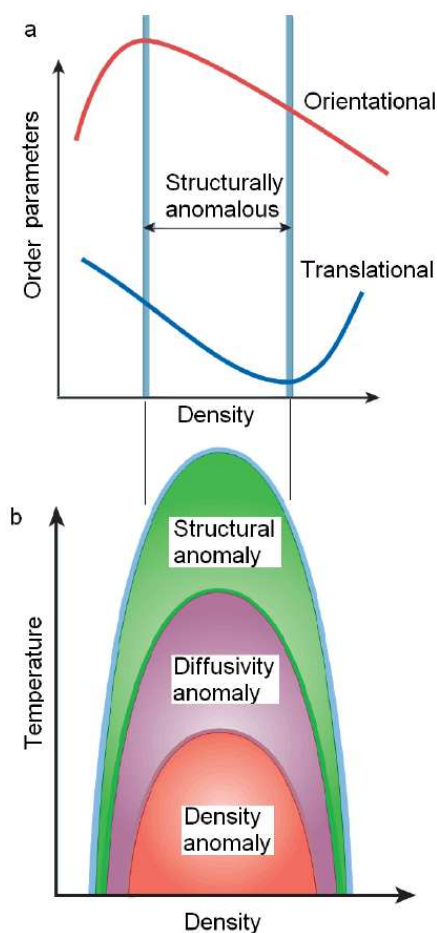
Figure 1.10: Relation between structure and anomalies of SPC/E water. (a) The orientational and translational order parameters of water can be computed for different temperatures and densities. The sketch shows both structural orders of water as a function of density at constant temperature. There is a maximum in orientational order at a low density and a minimum in translational order at a high density. Between the low and high densities, both structural orders decrease with density, and this is defined as structural anomaly. (b) Errington *et al.* [19] find that SPC/E water has a structural anomaly and there is a region of structural anomaly in the phase diagram of liquid water spanning over a range of temperature and pressure, which encloses the density and diffusion anomaly regions. (From S. Sastry [25]).
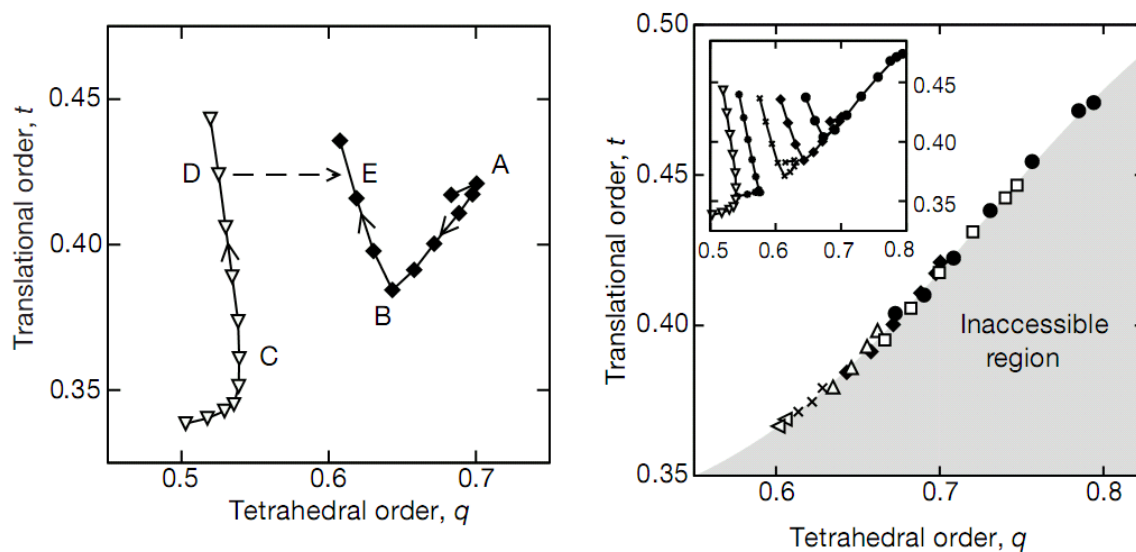
Figure 1.11: Order map of simulated SPC/E water. To further investigate relationship between the orientational structural order and translational order of water, Errington *et al.* [19] plot the translational and orientational orders against each other on the order map. They find that the two order parameters inside the structural anomalous region are correlated because they fall on a narrow strip region just above the inaccessible region in the order map. (Figure from Errington *et al.* [19])

qualitatively similar behavior in molten silica's order map [28]. However, in the case of silica, it was found that state points corresponding to anomalous behavior define a narrow stripe in the (t, q) plane instead of a strict line. Furthermore, unlike in water, the region of dynamic anomalies was found to contain that of structural anomalies.

1.4   Simple Liquids with Water-like Anomalies

Compared to water, typical simple liquids such as hard sphere and Lennard Jones liquids have no anomalous behavior in their thermodynamic, dynamic and structural properties (Fig. 1.6 dashed lines). The structures of simple liquids are more closely packed and simple atoms usually have twelve nearest neighbors in the first shell compared to the tetrahedrally coordinated four neighbors in water's first shell as shown in Fig. 1.12. For simple spherically-symmetric liquids, including hard spheres [26, 29] and Lennard-Jones [20] the order map has a positively-sloped line in the (t, q) plane, indicating that translational and orientational orders are always strictly and positively correlated. In this case the appropriate metric for orientational order does not measure tetrahedrality; rather, the bond-orientational order parameter introduced by Steinhardt *et al.* [30] measures the degree to which the nearest neighbors adopt a fcc or hcp structure. An important result from these studies is the fact that the order map for the Lennard-Jones system above its critical density is identical to that of hard spheres. Furthermore, in these simple systems that do not exhibit thermodynamic or dynamic anomalies, compression always leads to an increase in the order metrics.

But there are exceptions because some simple liquids show waterlike thermodynamic and dynamic anomalies and compression leads to an decrease in their order metrics. In 1970 Hemmer and Stell [32] showed that in fluids interacting via pairwise-additive, spherically-symmetric potentials consisting of a hard core plus an attractive tail, softening of the repulsive core can produce additional phase transitions. This pioneering study elicited a considerable body of work on core-softened potentials [32–
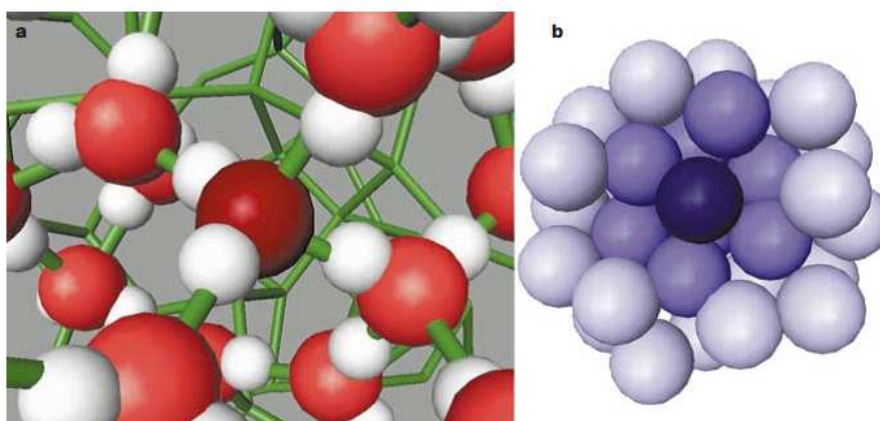
Figure 1.12: Difference between the structures of water and simple liquids. (a) Water molecules typically form hydrogen bonds with four neighbors on the corner of tetrahedral structure, and water molecules have open, loosely packed network structure. The first coordination shell of water has only four to five neighbors depending on pressure and temperature. (b) In a simple atomic liquid, the packing is much more dense, and there is no tetrahedral structure due to the lack of orientational bonds, instead there is usually a fcc, or hcp structure in its crystal phase. There are usually twelve neighbors in the first coordination shell of simple atomic liquid. (Figure from S. Sastry [25])
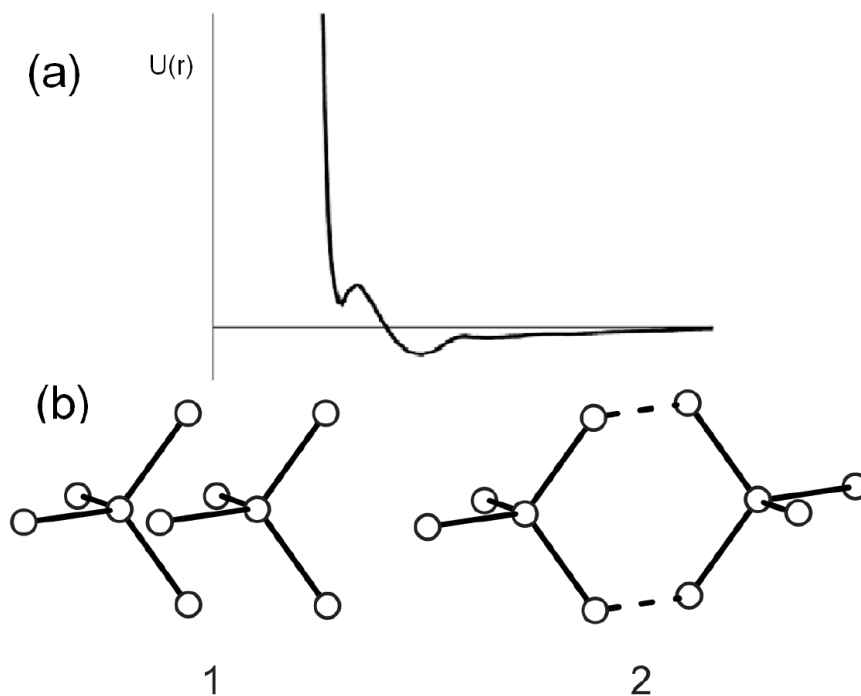
Figure 1.13: Effective potential of water. Upper panel: Effective potential of water-water interaction computed from radial distribution function of water [31]. There is a soft core ramp (energy barrier) in the effective potential, which water molecules need to overcome to move closer to each other when low density water becomes high density water under pressure. Lower panel shows the typical low density and high density configurations of water clusters. Simple potentials can be derived from the effective potential. Simple liquid system can be studied using such simple potentials to see whether water-like anomalies can be obtained from simple potentials even without orientational interactions in the potential. (Figures reproduced from [31] and [3])

40]. This generic term denotes continuous potentials with inflections in the repulsive core [33], discontinuous potentials with the core softened by shoulders or ramps (see Fig. 1.13 and Fig. 1.14) [32, 34, 36–39], or lattice models with nearest-neighbor attraction and next-nearest neighbor repulsion [40]. It is now well-established that such potentials can generate water-like density and diffusion anomalies [32–37, 39–41] and can even show a liquid-liquid transition [38] because the different length scales in the potential allow the structural change between low and high density liquids. As shown in Fig. 1.13(a) the core-softened potentials are originated from the effective potential of water, with the soft core mimicking the energy barrier in the effective potential of water.

1.5   Overview of Thesis

These important findings about simple liquids with water-like anomalies imply that strong orientational interactions, such as those that exist in water and silica, are not a necessary condition for a liquid to have thermodynamic and dynamic anomalies. But it is still not clear whether such strong orientational interactions are necessary for a liquid to have structural anomalies. Here in Chapter 2 and 3 of this thesis we investigate the question of whether spherically-symmetric potentials are also able to reproduce the structural anomalies found in systems with local tetrahedral order. We also systematically investigate the effect of tuning the parameters of simple potentials.

It is also not clear why simple liquids interacting via spherically-symmetric potentials can generate water-like structural, dynamic and thermodynamic anomalies and what are the structural bases for these anomalies? In Chapter 4, we investigate how much orientation-dependent first-shell interactions and the second-shell environment each contribute to water's anomalies. We show that the changes in the second shell of water provide the structural bases for the anomalies.

In Chapter 5, we study the quantitative connection between the two-scale ramp
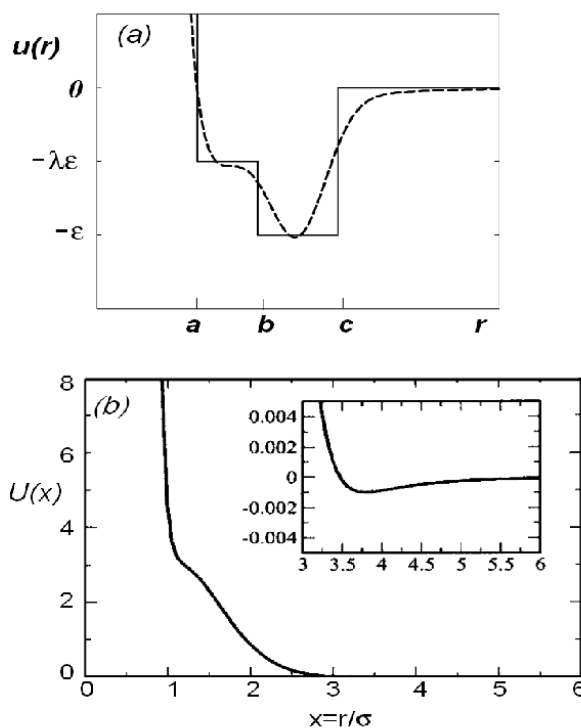
Figure 1.14: Different core-softened models. Different types of simple potentials are able to generate water-like anomalies. (a) the square well potential [36], or (b) the model potential formulated by combining the Lennard Jones potential and the Gaussian potential [42]. The simple potential can be changed in different forms by tuning parameters of potential, but in order to have water-like anomalies, they all need to have a soft core (a well, or a ramp) in the potential acting like the energy barrier in the effective potential of water. The soft core can cause water-like structural change between low density and high density simple liquids when simple particles migrate from soft core towards hard core upon compression. The other anomalies of simple liquids are related to the structural changes. (Figure from [36] and [42])

potential and water's pair potential, as well as the relation between the regions of anomalies in their respective phase diagrams.

Finally in Chapter 6 we investigate the relation of water anomalies to the excess entropy, We find that the excess entropy can not only predict the regions of structural, dynamic and thermodynamic anomalies of water, but also predict the location of the Widom line of water in the phase diagram.

Chapter 2

Structural Order for One-Scale and Two-Scale Potentials

2.1   Introduction

Most liquids become denser upon cooling and more viscous upon compression. However, water and many other liquids with local tetrahedral order [5] (e.g., silica, silicon, carbon, and phosphorus) show a decrease in density upon cooling (density anomaly) and an increase of diffusivity upon pressurizing (diffusion anomaly). These liquids share many other thermodynamic anomalous properties than those mentioned above. For instance, experiments in phosphorous indicate the presence of a liquid-liquid phase transition [6] and similar results are obtained from computer simulations in silica [7], silicon [8], and water [4]. A possible explanation of these anomalies is the tendency of these liquids to form bonds resulting in local open structures not present in simple liquids. Therefore, much effort has been expended to understand the relationship between the structure and the dynamic and thermodynamic anomalies observed in tetrahedral liquids.

Several recent studies have investigated thermodynamic and dynamic anomalies using spherically-symmetric potentials. Simple spherically-symmetric potentials with

a 'core-softened' or a repulsive interaction at short distances are able to generate water-like density and diffusion anomalies [33, 34, 36–41, 43], and can even show a liquid-liquid transition [38]. These findings in simple liquids imply that strong orientational interactions (as observed in water or silica) are not a *necessary* condition for a liquid to have thermodynamic and dynamic anomalies. It is still not clear whether such strong orientational interactions are necessary for a liquid to have structural anomalies. Here we address the question of whether spherically-symmetric potentials are also able to reproduce the structural anomalies found in systems with local tetrahedral order.

Errington and Debenedetti [19] (ED) have studied the microscopic structural order in liquid water by using simple geometrical metrics or order parameters. The structural order was characterized using two different metrics: a translational order parameter t [20], quantifying the tendency of particle pairs to adopt preferential separations, and a bond-orientational order parameter q [19, 24] quantifying the extent to which a molecule and its four nearest neighbors arrange in a tetrahedral local structure, as is the case in hexagonal ice. A useful way of investigating structural order in liquids is to map state points onto the $t-q$ plane. Such a representation was introduced by Torquato and coworkers [26], who applied it to sphere packings and referred to it as an order map. ED used the order map to investigate structural order in SPC/E water [19]. Because of the distinctive features discovered in that study, in what follows we refer to water-like order maps as the ED order map. ED found that the state points accessible to the liquid state in the order map fall into a two-dimensional area, meaning that in general t and q are independent. However, for those state points where the dynamic and thermodynamic anomalies occur, the $t-q$ parameters fall on a line in the ED order map, meaning that they are strictly correlated. This is a clear evidence of the relationship between structure and water anomalies. Shell *et al.* [28] used simulation to test the ED order map in silica, another liquid with local tetrahedral order. They studied the ED order map in silica

and found it qualitatively similar to water. However, in this case, the $t - q$ values corresponding to the state points in the ED order map for anomaly regions do not fall on a single line as in water but fall on a stripe region. Further, the state points showing diffusion anomaly are not all contained in this stripe region of ED order map.

In this chapter we perform molecular dynamics simulations to investigate the relationship between structural order and water-like dynamic and thermodynamic anomalies in spherically-symmetric potentials having either one or two characteristic length scales. The first potential has only one length scale which is the diameter of the ramp without the hard core, and the second potential has two length scales: one is the diameter of a ramp(softcore) and another one is the diameter of a hard core with a ratio of 1.76. Structural order is characterized by translational and orientational order parameters analogous to those used in previous cases for water and silica. We find that dynamic and thermodynamic anomalies exist for both one-scale and two-scale ramp potentials, and water-like structural order anomalies exist only for the two-scale ramp potential. Our findings suggest that the water-like relationship between structural order and anomalies is related to the presence of two different length scales in the potential.

2.2   Methods: Molecular Dynamic Simulation and Structural Order

It is possible to define order metrics analogous to the $t - q$ parameters used for water or silica. The ED order map was studied for different models of spherically symmetric potentials, e.g., hard spheres [26, 29] and Lennard-Jones [20] system. In these systems, where no dynamic or thermodynamic anomalies are observed, the liquid state points *always* fall on a single line on the ED order map. In other words, in contrast to the case of silica or water, the $q - t$ parameters are *always* strongly correlated. In light of these findings, it is natural to inquire about the ED order

map of systems that are spherically symmetric and, in addition, exhibit water-like anomalies in their thermodynamic and transport properties.

Here we perform discrete molecular dynamics simulations to study the ED order map of a liquid with spherically symmetric atomic interactions that shows both thermodynamic and dynamic water-like anomalies. This model was introduced by Jagla [34] (see Fig. 2.1).

The potential energy $U(r)$ of a pair of particles separated by a distance r is given by (see Fig. 2.1)

$$
U(r) = \begin{cases} \infty & r < \sigma_0 \\ U_1(\sigma_1 - r)/\sigma_1 & \sigma_0 < r < \sigma_1 \\ 0 & r > \sigma_1 \end{cases} \tag{2.1}
$$

The shorter distance σ_0 corresponds to the hard-core distance, and the longer distance σ_1 characterizes a softer repulsion range that can be overcome at high pressure. We will identify the model defined by Eq. (2.1) with $\lambda \equiv \sigma_1/\sigma_0 = 1.76$ as the two-scale ramp potential (2SRP) model, and the model with $\sigma_0 = 0$ as the one-scale ramp potential (1SRP) model. We use NVT ensemble for a system composed by $N = 1728$ (2SRP) or 850 (1SRP) particles with periodic boundary conditions and control the temperature with the Berendsen thermostat. The details of the simulation are given in Ref. [39]. However, we note that we use different units than in Ref. [39]: lengths are measured in units of σ_1 and energy is measured in units of U_1. We also check that the results do not depend on the number of particles and the value of σ_1 and U_1 after renormalization.

We use the translational order parameter [19, 20, 28], used in water [19], silica [28], and Lennard-Jones systems [20],

$$
t \equiv \int_0^{s_c} |g(s) - 1| ds. \tag{2.2}
$$

Here $s \equiv r \rho_n^{1/3}$ is the radial distance scaled by the mean interparticle distance, $g(s)$ is the pair correlation function, and s_c a numerical cutoff that can be set to a suitable value (we choose s_c so that it corresponds to one-half the simulation box size). For
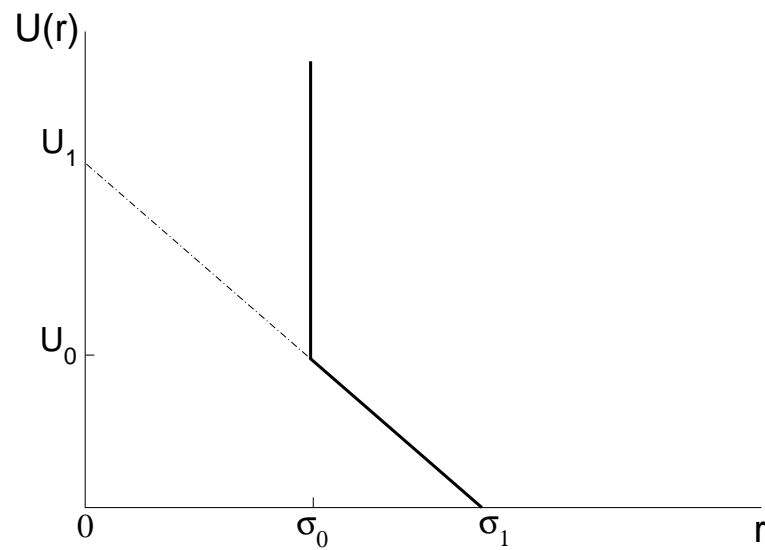
Figure 2.1: The ramp potential introduced by Jagla [34]. σ_0 corresponds to the hard-core distance, σ_1 characterizes a softer repulsion range that can be overcome at high pressure. The 1SRP has $\sigma_0 = 0$, while the 2SRP has two length scales with $\lambda \equiv \sigma_1/\sigma_0$. Typically $\lambda = 1.76$ corresponds to the ratio of distance of the first and the second shell of water.

a completely uncorrelated system, $g(s) \equiv 1$, and thus $t = 0$. For systems with long-range order, the modulations in $g(s)$ persist over large distances, causing t to grow.

An orientational order parameter introduced by Steinhardt *et al.* [30] and used in Refs. [20, 26, 29, 44] is modified to characterize the average local order of the system. For each particle, we define 12 vectors (or bonds) connecting the central particle with each of its 12 nearest neighbors. Each bond is characterized by two angles (θ, φ) and the corresponding spherical harmonic $Y_{\ell m}(\theta, \varphi)$ can be computed. The orientational order parameter associated with each particle i is

$$Q_{\ell i} \equiv \left[\frac{4\pi}{2\ell + 1} \sum_{m=-\ell}^{m=\ell} |\overline{Y}_{\ell m}|^2 \right]^{\frac{1}{2}}. \tag{2.3}$$

Here, $\overline{Y}_{\ell m}(\theta, \varphi)$ denotes the average of $Y_{\ell m}(\theta, \varphi)$ over the 12 bonds associated with particle i. For $\ell = 6$ [20], Q_ℓ has maximum value for most crystals such as fcc, hcp and bcc [30]. The values of Q_{6i} for each molecule in the system obey a Gaussian distribution, and the averaged value of Q_{6i} over all the particles [45], Q_{6s}, is used to characterize the local order of the system. In general, Q_{6s} grows in value as the crystallinity of a system increases. For example, in fcc lattice, $Q_{6s}^{\text{fcc}} = 0.574$, and for uncorrelated system, $Q_{6s} = 1/\sqrt{12} \approx 0.289$. Thus, Q_{6s} provides a measure of orientational order in the system. We note that fcc is the structure of the stable crystal at low pressure in the 1SRP and 2SRP models [39].

2.3   Results: Two-scale Ramp Potential has Waterlike Anomalies

Figs. 2.2(a) and 2.2(b) show the density dependence of t for the 1SRP and 2SRP at different temperatures T. The behavior of $t(\rho)$ is qualitatively the same in both models. At low-T, $t(\rho)$ shows a clear minimum and maximum and, hence, a range of ρ where t decreases with increasing ρ. This anomaly implies that the system becomes

less ordered upon compression. In fact, for the case of hard-spheres and LJ systems, t increases monotonically with ρ [20]. As T increases, the extrema in $t(\rho)$ disappear. At high-T, for the 2SRP, t is a monotonically increasing function of ρ, as is the case in normal liquids. However, for the 1SRP, t decreases with ρ. This behavior at high T is probably a consequence of the absence of a hard core in the 1SRP pair interaction potential. Therefore, upon compression particles can pass through each other and, as ρ increases, the structure of the liquid resembles more the structure of the gas. As expected, $t(T)$ and $Q_{6s}(T)$ in both models decrease with T at fixed ρ, meaning that the system becomes more disordered upon heating (Fig. 2.2).

Q_{6s} as a function of density for both models is shown in Figs. 2.2(c) and 2.2(d). At low T, $Q_{6s}(\rho)$ for the 1SRP is a monotonically increasing function of ρ, i.e., orientational order increases upon compression. Instead, $Q_{6s}(\rho)$ for the 2SRP at low T shows a clear maximum, indicating a range of density for which $Q_{6s}(\rho)$ decreases with ρ. We also note that at high pressure/density, the two models have different crystal structures, hcp for 1SRP and rhombohedral for 2SRP. Thus the different $Q_{6s}(\rho)$ in liquid state may be related to the difference in crystal formation. This anomalous behavior where orientational order decreases upon compression disappears at high T. At high-T, for both the 1SRP and 2SRP, Q_{6s} is weakly ρ-dependent as is the case in hard sphere and LJ systems [20] compared to low-T. At high-T, for both the 1SRP and 2SRP, the ρ-dependence of Q_{6s} is weak as is the case in hard sphere and LJ systems [20]. We also note from Fig. 2.2 that, as expected, $Q_{6s}(T)$ in both models decreases with T at fixed ρ, meaning that the system becomes more disordered upon heating.

Fig. 2.3 shows the isotherms from Fig. 2.2 in the ED order map representation. For both the 1SRP and 2SRP, the state points fall on a two-dimensional region, i.e., t and Q_{6s} can be changed independently. As is the case of silica and water [19, 28], we also find an inaccessible region in the ED order map where no liquid state points can be found. The structural anomalies correspond to the section of the isotherms
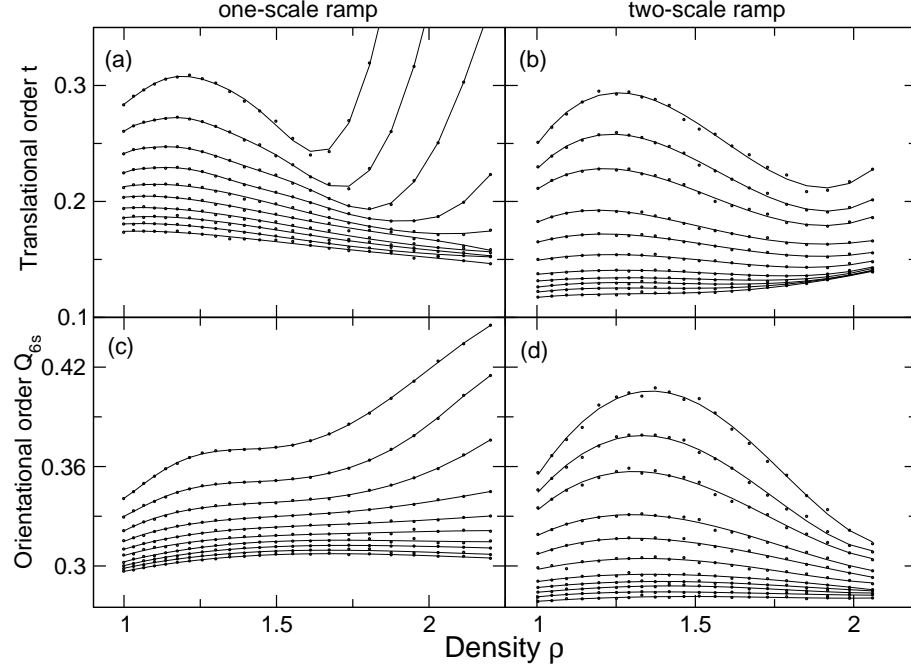
Figure 2.2: Density-dependence of the structural order parameters. The upper panels show the density-dependence of the translational order parameter t. The solid lines are polynomial fits to the data, introduced as a guide to the eye. (a) One-scale ramp potential ($\sigma_0 = 0$). From top to bottom isotherms correspond to $T =$ 0.04, 0.05, 0.06, 0.07, 0.08, 0.09, 0.10, 0.11, 0.12, and 0.13. At low temperature $T < 0.08$, there is a range of ρ where t decreases with density, and there is translational order anomaly for 1SRP. (b) Two-scale ramp potential with $\sigma_1/\sigma_0 = 1.76$. From top to bottom isotherms correspond to $T =$ 0.027, 0.036, 0.045, 0.063, 0.082, 0.109, 0.145, 0.172, 0.2, 0.236, and 0.290. At low temperature $T < 0.2$, there is also a range of ρ where t decreases with density, and there is translational order anomaly for 2SRP. The lower panels (c)–(d) show the density-dependence of the orientational order parameter Q_{6s} for same sets of isotherms. 1SRP has no anomaly in Q_{6s}, while 2SRP has anomaly in Q_{6s}.
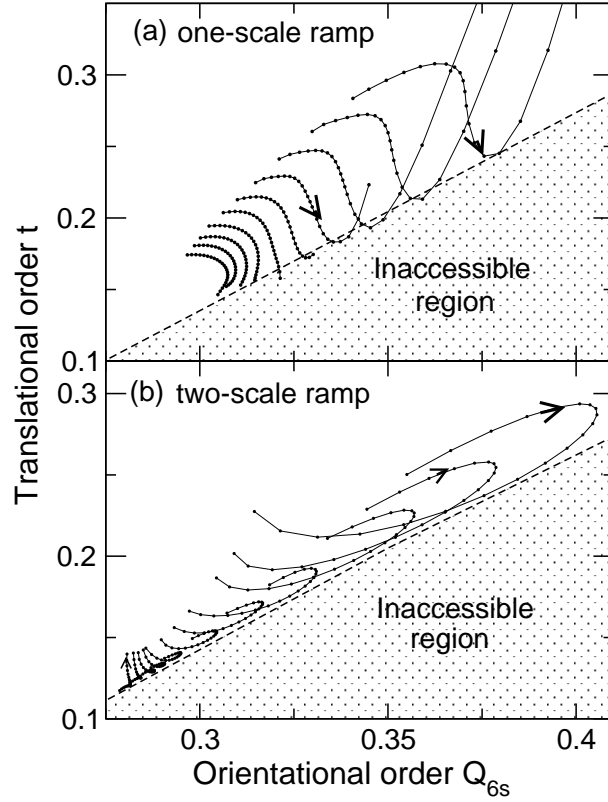
Figure 2.3: Order map of one-scale and two-scale potentials. (a) The ED order map for the one-scale ramp liquid. Isotherms correspond to $T =$0.04, 0.05, 0.06, 0.07, 0.08, 0.09, 0.10, 0.11, 0.12, and 0.13 (from top to bottom), and arrow indicates the direction of increasing density. For $T \leq 0.08$, t has a maximum at a low density and a minimum at a high density but Q_{6s} shows no maximum. (b) The ED order map for the two-scale ramp liquid. Isotherms correspond to $T =$0.027, 0.036, 0.045, 0.063, 0.082, 0.109, 0.145, 0.172, 0.2, 0.236, and 0.290 (from top to bottom). Q_{6s} and t have maxima at low densities, and t has minima at high densities. We can identify a structurally anomalous region bounded by loci of maximum orientational order (at low densities) and minimum translational order (at high densities) in which both t and Q_{6s} decrease upon compression. All state points within the structurally anomalous region fall in a narrow stripe region adjacent to the inaccessible region where no liquid state point can be found.

in Fig. 2.2 where both Q_{6s} and t decrease upon compression. Only for the 2SRP we find such anomalies, as have been observed in both silica and water. The state points corresponding to the structural anomalies do not fall, strictly speaking, on a single line delimiting the inaccessible region in the ED order map (Fig. 2.3(b)). Instead, these state points form a narrow stripe region, resembling the water ED order map much more closely than the ED order map found for silica [28].

Next, we discuss the regions in the phase diagram where the structural, dynamic, and thermodynamic anomalies occur. In water, the region in the T-ρ or P-T plane corresponding to both structural anomalies contains the region corresponding to the diffusion anomaly which in its turn contains the region corresponding to the density anomaly. In silica, the diffusion anomaly region contains the structural anomaly region, which also contains the density anomaly region. Fig. 2.4 shows the temperature of maximum density (TMD) line and the diffusivity maxima/minima (DM) line for our 1SRP and 2SRP models. The TMD defines the boundary where the density anomaly occurs while the DM defines the boundary where the diffusion anomaly occurs. The ED order map in Fig. 2.3(b) shows that the points along isotherms where both t and Q_{6s} decrease with density fall between the Q_{6s} maximum and the t minimum along the isotherms. By definition, the structural anomaly region in the $T - \rho$ plane is delimited by the location in the $T - \rho$ plane of the Q_{6s} maximum and the t minimum. Fig. 2.5(b) shows the different anomaly regions on the $T - \rho$ plane for 2SRP. Fig. 2.5(b) shows that the relation among the regions of various anomalies for the 2SRP is the same as in the case of water [19], i.e., the structural anomaly region contains the diffusion anomaly region which also contains the density anomaly region.

For the 1SRP, there is no clear Q_{6s} maximum (i.e., Q_{6s} shows no anomaly), so we are not able to identify a structural anomaly region. However, in this case the structural anomaly can be identified by those state points along an isotherm where t decreases upon compression. Therefore, the maximum and minimum values of t in Fig. 2.3(a) define the structural anomaly region. Fig. 2.5(a) shows that with this
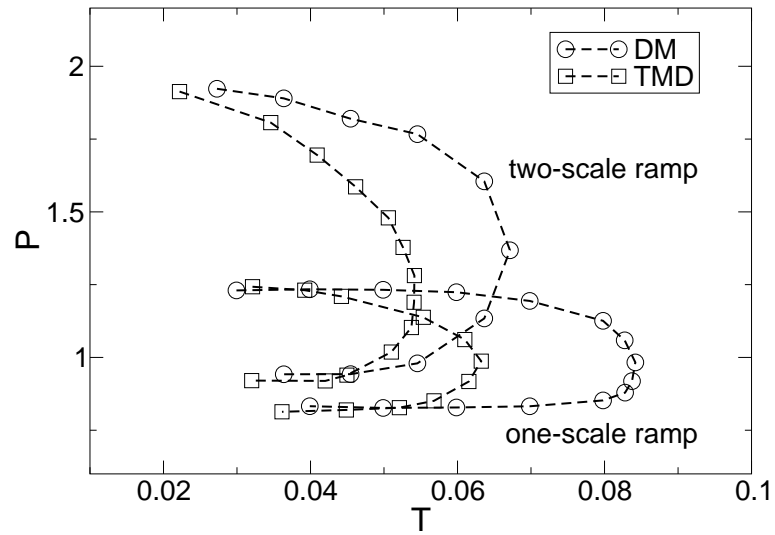
Figure 2.4: Density and diffusion anomalies in the P-T plane. Temperature of maximum density (TMD) and diffusivity minima and maxima (DM) lines for the two potentials in the P-T plane. The region of diffusion anomaly is defined by the loci of DM inside which the diffusivity increases with density. The thermodynamically anomalous region is defined by TMD line, inside which the density increases when the system is heated at constant pressure.

definition the structural anomaly region contains the diffusion anomaly region which also contains the density anomaly region. We show in Fig. 2.5(b) that for the 2SRP, defining the structural anomaly boundaries using the extrema of t does not alter the relationship between the regions of various anomalies. Furthermore, comparing Figs. 2.5(a) and 2.5(b), we observe that the effect of reducing the hard core distance σ_0 is to open the structural anomaly region (curves C and A).

In summary, we find that the 2SRP shows not only density and diffusion anomalies but also the same structural anomalies found in tetrahedral liquids such as silica and water. Furthermore, the 2SRP also shows the same relation among structural, dynamic and density anomalies. Our finding suggests that the water-like relationship between structural order and anomalies may be due to the presence of two different length scales. When eliminating the hard core interaction with $\sigma_0 \to 0$, we find no water-like relation between structure and dynamics. This suggests that the ratio between the two length scales in the 2SRP, σ_1/σ_0 is the relevant variable in the interaction potential.
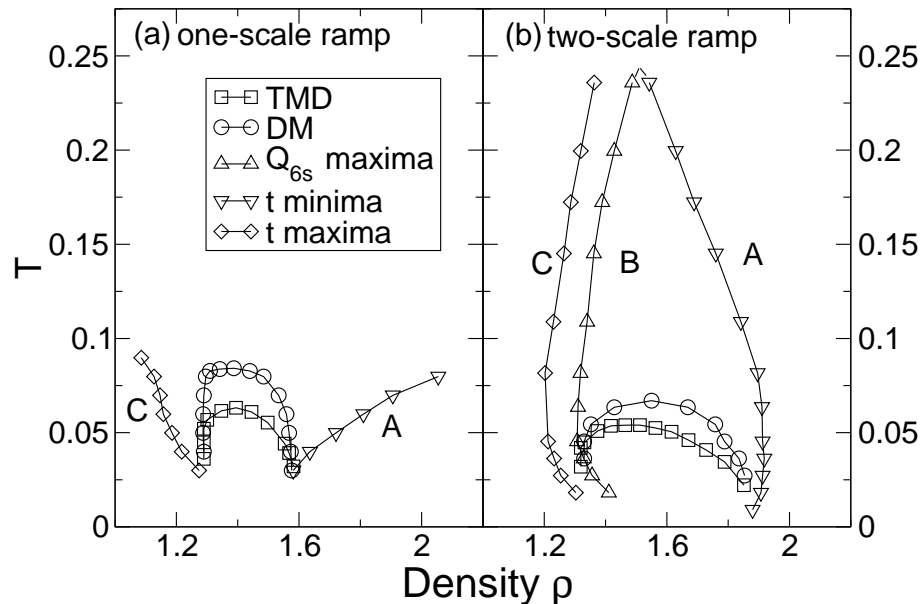
Figure 2.5: Relationship between the structural order and the density and diffusion anomalies. (a) For the one-scale ramp liquid, the open region bounded by the loci of t minima (curve A) and t maxima (curve C) [see Fig. 2.3(a)] defines the structurally anomalous region. This region contains the diffusion anomaly (delimited by the DM) and the density anomaly (delimited by the TMD). (b) For the two-scale ramp liquid, the structurally anomalous region can be defined by the region between the loci of t minima (curve A) and by the loci of either t maxima (curve C) or Q_{6s} maxima (curve B) [see Fig. 2.3(b)]. The structurally anomalous region contains the diffusion anomaly region which also contains the density anomaly region. Only the two-scale ramp potential shows the same relation between the structural, diffusion, and density anomaly regions as observed in water.

Chapter 3

A Family of Tunable Spherically-Symmetric Potentials

3.1 Introduction

Water's density and diffusion anomalies, which disappear at high enough temperature and pressure, are not unique to water. Other liquids with local tetrahedral order (e.g., silica and silicon) also exhibit thermodynamic and dynamic anomalies [5]. A possible explanation of these anomalies is the tendency of these substances to form local open structures not present in simple liquids. However, establishing a precise and quantitative link between the microscopic structure and the dynamic and thermodynamic anomalies of tetrahedral liquids has proved elusive until recently.

Ref. [19] studied the relation between microscopic structure and the anomalies of liquid water by introducing two simple metrics: a translational order parameter t [20], and an orientational order parameter q [19, 24]. Using molecular dynamics simulation of the SPC/E [27] model, ED found a dome-shaped region in the (T, ρ) plane within which isothermal compression leads to a decrease in t and q. This *decrease* in order upon compression constitutes a structural anomaly: simple liquids, in contrast, always become more ordered upon compression. ED further found that dynamic and

thermodynamic anomalies define nested domes in the (T, ρ) plane: the structural anomalies dome contains the dynamic anomalies dome, which in turn contains the thermodynamic anomalies dome. This means that whenever the thermal expansion coefficient is negative, the diffusivity will increase upon isothermal compression. ED showed that all state points exhibiting structural, dynamic or thermodynamic anomalies define a line on the (t, q) plane, meaning that when water exhibits anomalous behavior, its translational and orientational order metrics become strictly coupled. This is clear evidence of the relationship between structure and water anomalies. Shell *et al.* subsequently found qualitatively similar behavior in molten silica's order map [28]. However, in the case of silica, it was found that state points corresponding to anomalous behavior define a narrow stripe in the (t, q) plane instead of a strict line. Furthermore, unlike in water, the region of dynamic anomalies was found to contain that of structural anomalies.

For simple spherically-symmetric liquids, including hard spheres [26, 29] and Lennard-Jones [20] the order map was found to be a positively-sloped line in the (t, q) plane, indicating that translational and orientational order are always strictly and positively correlated. In this case, of course, the appropriate metric for orientational order does not measure tetrahedrality; rather, the bond-orientational order parameter introduced by Steinhardt *et al.* [30] was used. An important result from these studies is the fact that the order map for the Lennard-Jones system above its critical density is identical to that of hard spheres. Furthermore, in these simple systems that do not exhibit thermodynamic or dynamic anomalies, compression always leads to an increase in the order metrics.

In 1970 Hemmer and Stell [32] showed that in fluids interacting via pairwise-additive, and spherically-symmetric potentials consisting of a hard core plus an attractive tail, softening of the repulsive core can produce additional phase transitions. This pioneering study elicited a considerable body of work on so-called core-softened potentials [32–40]. This generic term denotes continuous potentials with inflections

in the repulsive core [33], discontinuous potentials with the core softened by shoulders or ramps [32, 34, 36–39], or lattice models with nearest-neighbor attraction and next-nearest neighbor repulsion [40]. It is now well-established that such potentials can generate water-like density and diffusion anomalies [32–41, 46–48]. This important finding implies that strong orientational interactions, such as those that exist in water and silica, are not a necessary condition for a liquid to have thermodynamic and dynamic anomalies.

The above discussion implies the existence of two well-defined classes of liquids: simple and water-like. The former which interact via spherically-symmetric non-softened potentials, do not exhibit thermodynamic nor dynamic anomalies, and their order map is a line. In water-like liquids, interactions are orientation-dependent; these liquids exhibit dynamic and thermodynamic anomalies, and their order map is in general two-dimensional but becomes linear (or quasi-linear) when the liquid exhibits structural, dynamic or thermodynamic anomalies. Intermediate between these well-defined extremes is the class of core-softened liquids, which interact via spherically-symmetric potentials but can also exhibit water-like thermodynamic and dynamic anomalies.

Two questions arise naturally from this emerging taxonomy of liquid behavior. First, is structural order in core-softened fluids hard-sphere or water-like ? Second, is it possible to seamlessly connect the range of liquid behavior from hard spheres to water-like by a simple and common potential, simply by changing a physical parameter ?

In Chapter 2 [21] we addressed the first question. We showed that a core-softened potential with two characteristic length scales can not only give rise to water-like diffusive and density anomalies, but also to an ED water-like order map. This implies that orientational interactions are not necessary in order for a liquid to have structural anomalies. In this work we address the second question. Specifically, we use the ratio of characteristic length scales as a control parameter to investigate the

evolution of dynamic, thermodynamic and structural anomalies. In this manner we show that the family of tunable spherically-symmetric potentials so generated evolves continuously between water-like and hard sphere behavior. To our knowledge this is the first time that essential aspects of the wide range of liquid behavior encompassed by hard spheres and tetrahedrally-coordinated network-formers can be systematically traversed by varying a single control parameter.

This chapter is structured as follows. Sections 3.2, 3.3, and 3.4 provide details on the interaction potential, simulation method, and order parameters, respectively. Results are presented in Section 3.5. Conclusions and some suggestions for future work are provided in Section 3.6.

3.2   Tunable Ramp potential

We perform discrete MD simulations to study the equation of state, diffusion coefficient and structural order as measured by the ED order map, for a fluid whose particles interact via a pairwise-additive, spherically-symmetric potential that gives rise to both thermodynamic and dynamic water-like anomalies. The model was introduced by Jagla [34]; the potential energy $U(r)$ between a pair of particles separated by a distance r is given by the same equation as Eq. (2.1) in Chapter 2 (see Fig. 3.1), $U(r) = U_1(\sigma_1 - r)/\sigma_1$ for $\sigma_0 < r < \sigma_1$, while $U(r) = \infty$ for $r < \sigma_0$ and $U(r) = 0$ for $r > \sigma_1$. Because of the shape of potential, it is called the ramp potential. The constant slope of the ramp potential for $\sigma_0 < r < \sigma_1$ keeps the force between particles f constant, so the product of separation and force rf will decrease when the separation r decreases. This satisfies the mathematical meaning of core-softening [40] and under these conditions the thermodynamic (density) anomaly can be qualitatively explained by invoking the virial theorem [40].

Of interest is the ratio between the two characteristic length scales, σ_0 and σ_1,

$$\lambda \equiv \sigma_0/\sigma_1, \tag{3.1}$$
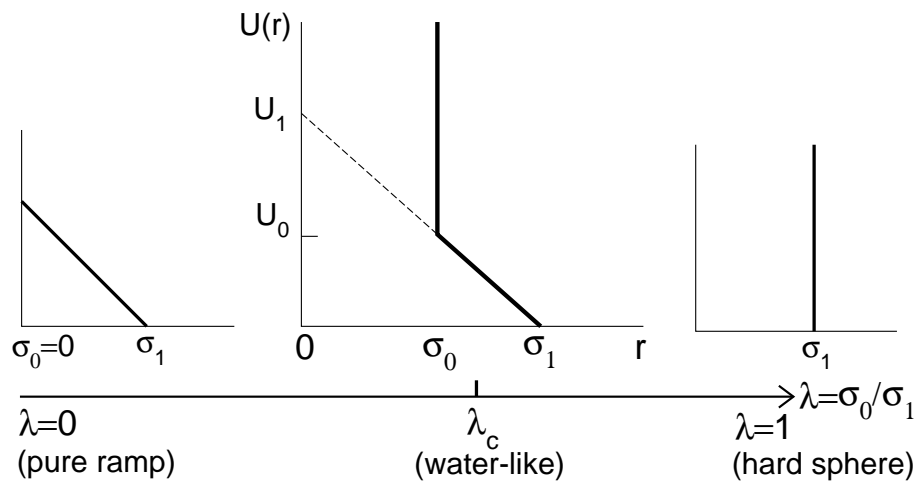
Figure 3.1: Ramp potential with two tunable length scales. The middle figure shows the ramp potential with two characteristic length scales. σ_0 corresponds to the hard core, σ_1 characterizes the onset of soft repulsion. When $\lambda = 0$ (left figure) we have a pure ramp potential (no hard core). When $\lambda = 1$ (right figure) we have a hard sphere potential. $\lambda_c \sim 0.6$ is the ratio near which the system exhibits water-like structural, dynamic and thermodynamic behavior.

which can vary between 0 and 1. Ref. [21] investigated the one-scale ($\lambda = 0$) and two-scale ($\lambda = 4/7$) ramp potentials. Here we investigate the full range $0 \leq \lambda < 1$, with

$$\lambda = 0, 2/7, 4/7, 5/7, 6/7. \tag{3.2}$$

3.3 MD simulation

We use discrete MD simulation; details are given in Ref. [39]. We use the NVT ensemble for a system composed of 850 particles with periodic boundary conditions, and we control the temperature with the Berendsen thermostat [49]. However, we note that we use different units than in Ref. [39]: the distance r, number density ρ, pressure P and temperature T are all normalized with respect to the soft core distance σ_1 and the potential U_1 at $r = 0$ (i.e., densities are reported as $\rho\sigma_1^3$, and temperature as kT/U_1). We also investigate systems with different number of particles ($N = 1728$) and different σ_1, U_1 values, and confirm that the results do not depend on the number of particles, the value of σ_1 and U_1 after normalization. The ratio λ is the only determinating factor of properties here, so the results from different ratios can be put in the same normalized frame to be analyzed. The simulation ranges of temperature and density fully cover the region where density, diffusion and structural anomalies occur.

The location of freezing lines for soft potentials requires special attention [50]. We verify that the systems we have studied are in the liquid phase by applying the technique described in Ref. ([39]), in which the ramp potential's phase diagram is investigated for $\lambda = 4/7$, including both the melting and homogeneous nucleation lines. In the supercooled state, the system can be equilibrated for a sufficiently long time, and quantities such as the pressure and the potential energy fluctuate without drift about average values that can be computed with high accuracy. As soon as nucleation occurs, the potential energy decreases sharply, and the pressure experi-

ences periodic jumps because of finite system size and the use of periodic boundary conditions. When such an event occurs we disregard the data obtained after nucleation. Moreover, it has been shown for the hard-sphere [26, 29] and Lennard-Jones systems [20], that the structural order parameters jump discontinuously when the system crystallizes. In our system we observe only continuous changes in the order parameters, which clearly indicates that the system is in the liquid state.

3.4 Translational and orientational order parameters

3.4.1 Translational order parameter

The translational order parameter [19, 20, 28] is defined same as Eq. (2.2), $t \equiv \int_0^{s_c} |g(s) - 1| ds$. We choose s_c so that it corresponds to one-half the simulation box size, and we verify that our system size is always large enough so that $g(s) = 1$ at half the box size. For a completely uncorrelated system, $g(s) \equiv 1$, and thus $t = 0$. For systems with long-range order, the modulations in $g(s)$ persist over large distances, causing t to grow. Between these limits, t will change as a consequence of the dependence of $g(r)$ upon T and ρ.

3.4.2 Orientational order parameter

An orientational order parameter based on spherical harmonic function was introduced by Steinhardt *et al.* [30] and used in Refs. [20, 26, 29, 44]. In this definition, all vectors connecting nearest neighbors (i.e., particle pairs whose separation is less than the first minimum of the radial distribution function) are considered. Each of these vectors, also called 'bond', defines an azimuthal and polar angle, and the corresponding spherical harmonic function is evaluated. The orientational order parameter used in Refs. [20, 26, 29, 44] involves the average of each spherical harmonic function over

all bonds.

The orientational order parameter used for water and silica in Refs. [19, 28] involves, first, the evaluation of the local tetrahedral order for each particle with respect to its four nearest neighbors, and then, the average of this quantity over all the molecules of the system. In the definition of the orientational order parameter used in Refs. [20, 26, 29, 44] there is no such concept of 'local order' for an individual particle. Moreover, the number of bonds associated to each particle is not fixed, but instead it changes with temperature and pressure. These two differences led, in Ref. [21], to the introduction of a slightly modified version of the original orientational order parameter introduced by Steinhardt et al. in ref. [9]. The resulting order metric is based on the idea of a 'local order' for each particle, analogous to Refs. [19, 28]. The ED maps obtained with the original (global) and modified (local) definitions of orientational order are qualitatively similar.

In this work we use the same order parameter introduced in Ref. [21]. We define twelve bonds connecting each particle with its twelve nearest neighbors. Each bond is characterized by its azimuthal and polar angles (θ, φ) and the corresponding spherical harmonic $Y_{\ell m}(\theta, \varphi)$ is computed. The orientational order parameter associated with each particle i is same as Eq. (2.3), $Q_{\ell i} \equiv \left[\frac{4\pi}{2\ell+1} \sum_{m=-\ell}^{m=\ell} |\overline{Y}_{\ell m}|^2 \right]^{\frac{1}{2}}$. This definition of order parameter is analogous to that used in water. For water, the solid at low pressure is hexagonal ice where each molecule has four neighbors. The orientational order parameter is maximum in the ice configuration and decreases as the system becomes less ice-like. For the ramp potential, the solid phase at low pressure has a fcc structure where each particle has twelve nearest neighbors. Q_6 has a maximum value in the fcc lattice ($Q_6^{\text{fcc}} = 0.574$) and decreases as the system becomes less correlated (for uncorrelated systems, $Q_6 = 1/\sqrt{12} = 0.289$).

3.5 Results and Discussion

3.5.1 Structural anomalies and order map

Since the pair correlation function $g(r)$ is used to compute the translational order parameter t (Eq. (2.2)), we first discuss the effect of density on $g(r)$. Fig. 3.2 shows the effects of compression on $g(r)$ at low temperature, $T = 0.04$, for the various values of λ considered in this study. In all cases, there is no inner peak at $r = \sigma_0$ for $\rho = 1$ and 1.21, and only the outer peak at $r = \sigma_1$ is present at these densities. The inner peak at $r = \sigma_0$, which is broad and of modest height at $\rho = 1.66$, becomes sharper and more pronounced upon further compression. Interestingly, structural changes brought about by compression become progressively longer-ranged as λ increases. Thus, for $\lambda = 0$ and 2/7, the major changes in $g(r)$ involve the development of structure at length scales $\leq \sigma_1$ associated with the growth of the inner peak at $r = \sigma_0$. However, for $\lambda = 4/7, 5/7$ and 6/7, structural changes upon compression occur at distances larger than σ_1. In particular, for $\lambda = 6/7$, the effects of compression are clearly discernible at $r = 3\sigma_1$.

These effects of density on the pair correlation function underlie the evolution of t upon compression, shown in Figs. 3.3(a1)-(e1). Consider for example the $T = 0.04$ isotherm when $\lambda = 2/7$. It can be seen that t displays a non-monotonic dependence on density: it increases upon compression at low densities, $1.0 < \rho < 1.22$, decreases over the intermediate density range $1.22 < \rho < 1.76$, and increases again at high densities, $\rho > 1.76$. The initial increase at low densities is associated with the growth of $g(\sigma_1)$. The emergence of structure associated with the inner (hard) core causes t to decrease at intermediate densities because the initial, modest growth of g at $r \sim \sigma_0$ causes $|g-1|$ to decrease with respect to its low-density value of 1 (see Eq. (2.2)). Upon further compression, the growth of $g(\sigma_0)$ above 1 eventually contributes additional area to the integral of $|g - 1|$, causing t to increase. This qualitative behavior of t is similar for $\lambda = 0, 2/7$ and 4/7, and is more pronounced at low T. For $\lambda = 6/7$, close to the
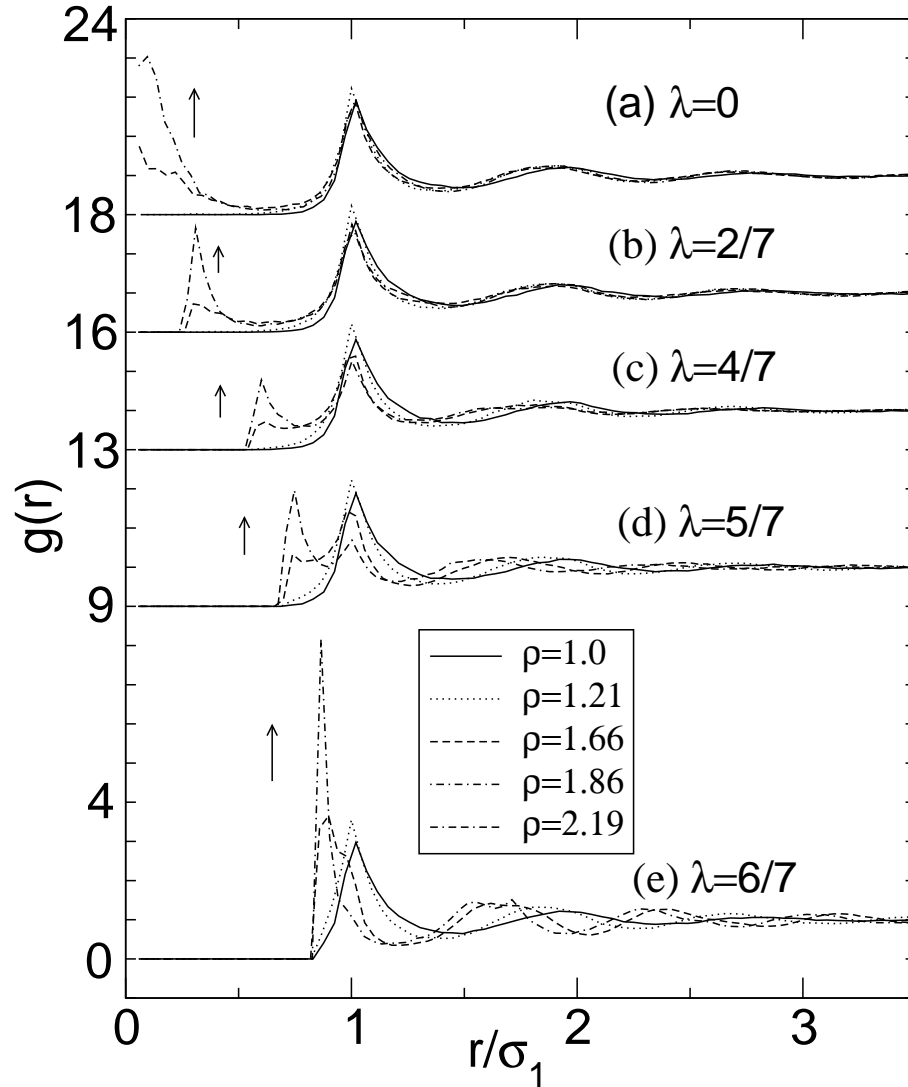
Figure 3.2: Radial distribution function $g(r)$ at $T = 0.04$ for different $\lambda \equiv \sigma_0/\sigma_1$ values. The arrows indicate the direction of increasing density. The density values are 1.0, 1.21, 1.66, 2.19 for $\lambda = 2/7, 4/7, 5/7$ and 1.0, 1.21, 1.66, 1.86 for $\lambda = 0, 6/7$. The distance r is normalized by σ_1, the soft core length. The curves for different λ are shifted vertically by integer numbers for clarity.
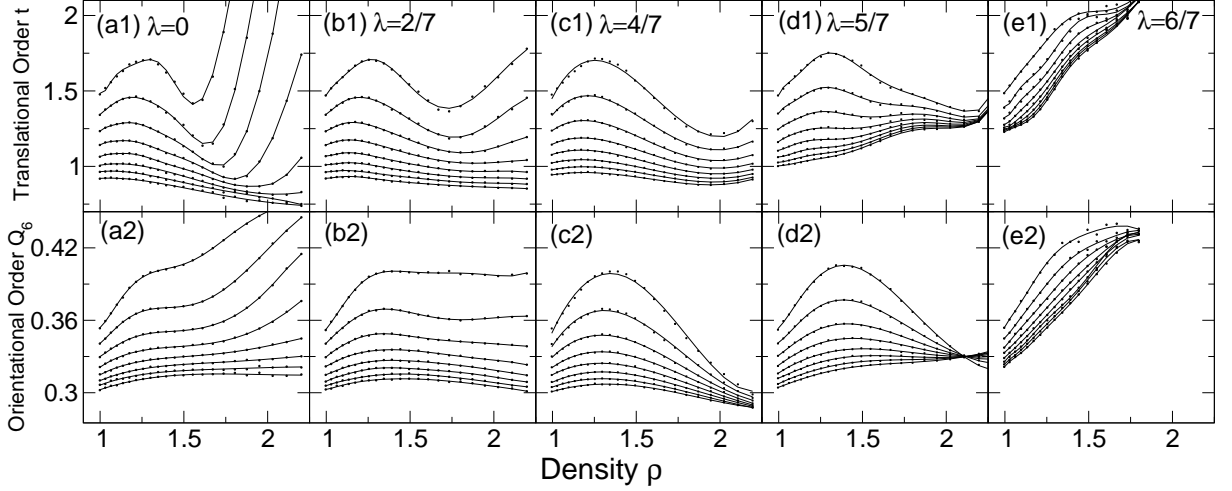
Figure 3.3: Density-dependence of structural orders for different λ. The upper and lower panels (a1)–(e1) and (a2)–(e2) show the density-dependence of the translational order parameter t and orientational order parameter Q_6 for $\lambda = 0$ (a1, a2), 2/7 (b1, b2), 4/7 (c1, c2), 5/7 (d1, d2), and 6/7 (e1, e2). The solid lines are polynomial fits to the data. In each panel, the different curves correspond to isotherms (top to bottom) $T = 0.03, 0.04, 0.05, 0.06, 0.07, 0.08, 0.09, 0.10$.

hard sphere limit, the pronounced growth of the inner peak upon compression gives rise to a monotonic density dependence of t, and structural changes upon compression occurring at distances larger than σ_1 have less effect since g converges to 1 by $r/\sigma_1 \sim$ 3. The case $\lambda = 5/7$ is clearly transitional, with non-monotonic behavior at low temperature changing to hard-sphere-like monotonic growth of t upon compression at high temperature.

Orientational order, as measured by Q_6, shows a pronounced dependence on λ, illustrated in Figs. 3.3(a2)–(e2). When $\lambda = 0$ (no hard core), Q_6 increases monotonically with density for all T. When $\lambda = 2/7$, Q_6 begins to exhibit non-monotonic behavior upon compression. For this particular value of λ the trend is very mild, and is best described as a virtual insensitivity of Q_6 to compression, except for an initial increase at low enough densities. For $\lambda = 4/7$ and 5/7, orientational order exhibits a

marked non-monotonic dependence on density, especially at low temperatures. When coupled with the corresponding behavior of t, this corresponds to a water-like structural anomaly, whereby both order metrics decrease upon isothermal compression. When $\lambda = 6/7$, which is close to the hard sphere value ($\lambda = 1$), orientational order increases monotonically upon compression. Thus, there exists a narrow interval of λ within which the ramp fluid shows water-like structural order, whereas in the pure ramp ($\lambda = 0$) and quasi-hard-sphere limits ($\lambda \sim 1$) Q_6 behaves conventionally upon compression. The fact that t displays strongly non-monotonic behavior for $\lambda = 0$ and $2/7$, while Q_6 only shows very mild non-monotonic behavior at $\lambda = 2/7$ illustrates the much weaker coupling of the two order metrics compared to the water-like case ($\lambda = 4/7$).

Cross-plotting the order metrics against each other generates the order map, whose evolution as a function of λ is depicted in Fig. 3.4. For all values of λ except $6/7$, state points fall on a two-dimensional region, signifying that t and Q_6 can be varied independently. As is the case for silica and water [19, 28], we find, for all values of λ, an inaccessible region where no liquid state points can be found. In the pure ramp ($\lambda = 0$) case, the pronounced non-monotonic dependence of t on density gives rise to isotherms with well-characterized t-minima, the locus of which defines the boundary between the accessible and inaccessible regions of the order map. For $\lambda = 2/7$, the barely discernible non-monotonic dependence of Q_6 on density gives rise to loops along isotherms. The non-monotonic behavior of Q_6 is fully developed for $\lambda = 4/7$. This gives rise to an order map with states corresponding to structural anomalies lying on a narrow stripe of the order map adjacent to the boundary between the accessible and inaccessible regions. This behavior is strikingly analogous to that of water. The insensitivity of structural order to temperature, a distinguishing feature of hard spheres, can be clearly seen in Fig. 3.4(e) by the virtual collapse of all isotherms in the $\lambda = 6/7$ case. The transition from water-like to hard sphere order map occurs in the narrow interval $4/7 < \lambda < 6/7$. In particular, for $\lambda = 5/7$, there is a clear evolution
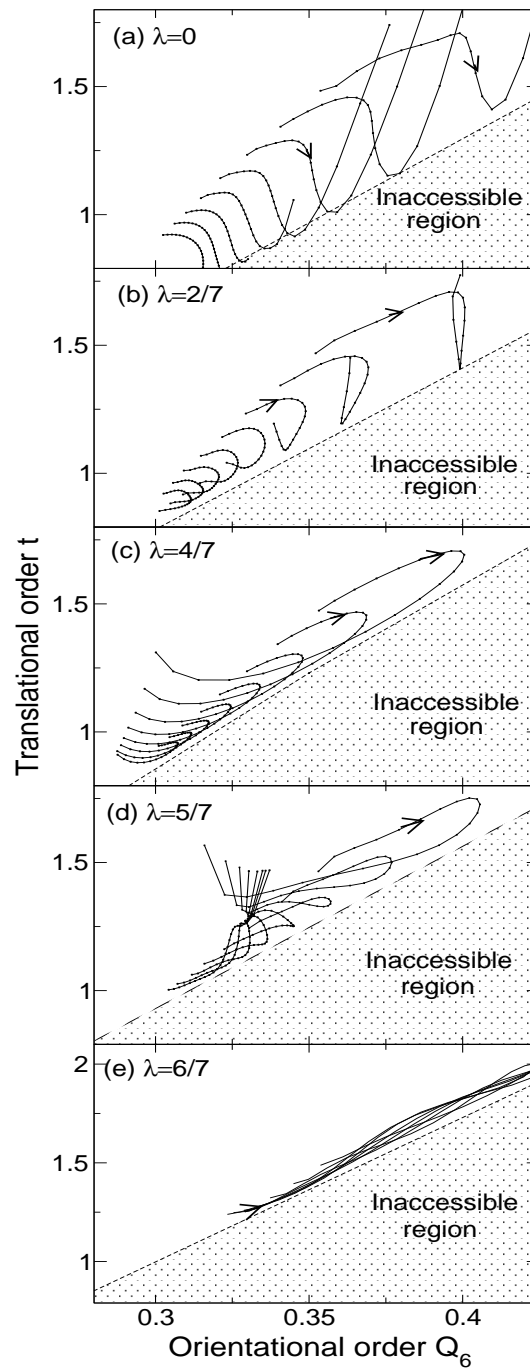
Figure 3.4: Order map of the ramp fluid for different λ. For each λ, the eight isotherms (right to left) correspond to $T = 0.03, 0.04, 0.05, 0.06, 0.07, 0.08, 0.09, 0.10$, and the arrow indicates the direction of increasing density.

from water-like low-T behavior ($T < 0.07$) to hard-sphere-like high-T behavior ($T > 0.07$).

3.5.2   Thermodynamic, dynamic, and structural anomalies

We now discuss the regions of the phase diagram where structural, dynamic and thermodynamic anomalies occur. In water [19], structural, dynamic, and thermodynamic anomalies occur as nested domes in the (T, ρ) or (T, P) planes. Structural anomalies define the outer dome, within which isothermal compression results in a decrease of both translational and orientational order. Dynamic anomalies define an intermediate dome, lying entirely within the structural anomalies dome, and within which isothermal compression leads to an increase in the diffusion coefficient. Thermodynamic anomalies define the innermost dome, within which water expands when cooled isobarically. In silica [28], dynamic anomalies define the outer dome, structural anomalies the intermediate dome, and thermodynamic anomalies define the inner dome. Thus, in both cases negative thermal expansion implies also diffusive and structural anomalies, but in silica diffusive anomalies occur over a broader range of densities and temperatures than structural anomalies, the opposite being true in water.

Fig. 3.5 shows the loci of dynamic and thermodynamic anomalies for three values of λ. The latter line was traced by locating extrema of isochores in the (P, T) plane. Similar to water and silica, in ramp fluids thermodynamic anomalies occur over a narrower temperature and density range than dynamic anomalies. In other words, if a ramp fluid is at a state point where it expands when cooled isobarically, its diffusion coefficient necessarily increases upon isothermal compression. It can be seen that upon increasing λ, the range of temperatures where anomalies occurs shrinks, and there are no anomalies for $\lambda = 6/7$, whereas the upper limit of density (or pressure) where anomalies can occur increases. The shrinking of the temperature range where anomalies occur follows from the fact that increasing λ makes the fluid progressively
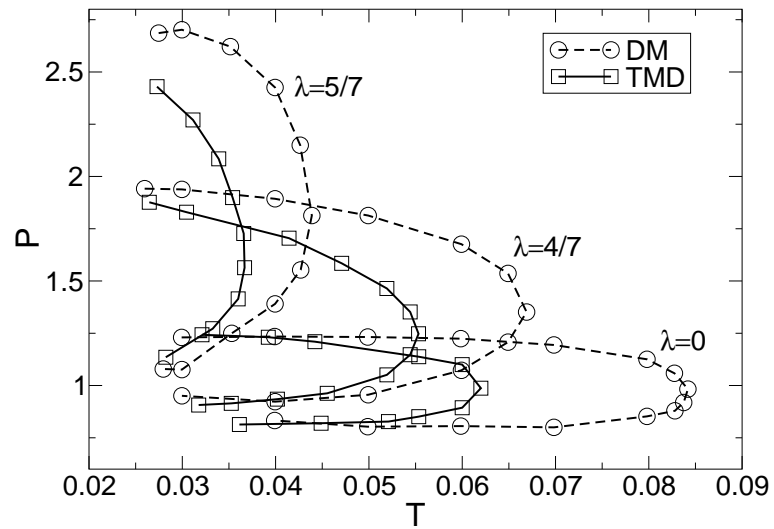
Figure 3.5: Loci of thermodynamic and dynamic anomalies for ramp fluids with different λ values. The region of diffusion anomalies is defined by the loci of diffusion minima and maxima (DM) inside which the diffusivity increases upon isothermal compression. The thermodynamically anomalous region is defined by locus of temperatures of maximum density (TMD), inside of which the density increases when the system is heated at constant pressure.
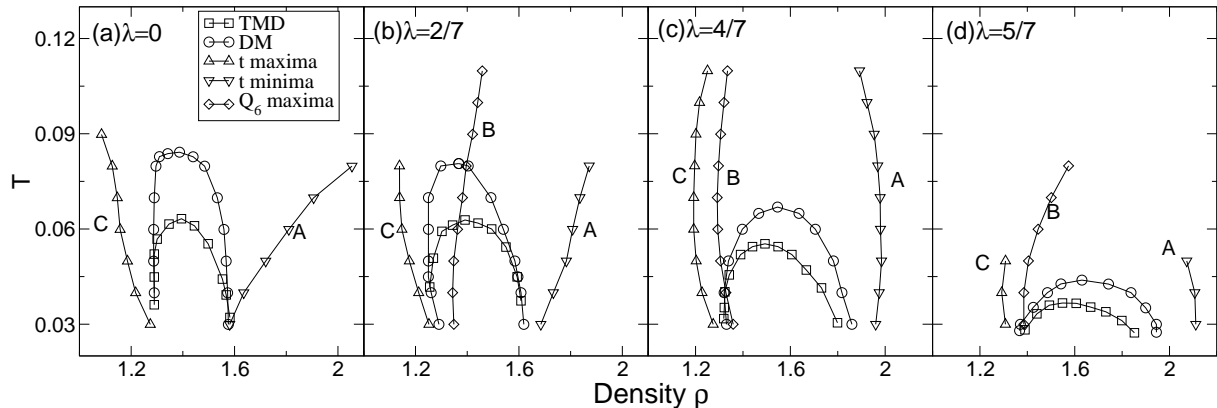
Figure 3.6: Relationship between structural order and the density and diffusion anomalies in the T-ρ plane. For $\lambda = 0$ and 2/7, the domes of dynamic and thermodynamic anomalies are bounded by loci of t maxima (C) and minima (A), between which isothermal compression cause a *decrease* in translational order. For $\lambda = 4/7$ and 5/7, the domes of dynamic and thermodynamic anomalies are bounded by loci of Q_6 maxima (B) and t minima (A), between which isothermal compression cause a *decrease* in both translational and orientational order (structural anomaly). This cascade of anomalies is characteristic of water.

hard-sphere-like, and there are no anomalies in a hard sphere fluid.

Fig. 3.6 shows the relationship between the loci of dynamic, thermodynamic and structural anomalies. In water, the low-density and high-density branches of the dome of structural anomalies correspond to tetrahedrality maxima and translational order minima, respectively. For the pure ramp case ($\lambda = 0$), the orientational order increases monotonically with density over the range of temperatures explored here. Accordingly, as seen in Fig. 3.6(a), the dynamic and thermodynamic anomalies domes are bounded by loci of translational order extrema (maxima: line C; minima: line A). Between lines C and A, compression leads to a decrease in translational order. For $\lambda = 4/7$ and 5/7, the locus of orientational order maxima (B) provides a low-density bound to the existence of thermodynamic and dynamic anomalies. Thus, for these two values of λ, ramp fluids exhibit a water-like cascade of anomalies (structural,

dynamic, thermodynamic). For $\lambda = 2/7$, Q_6 maxima are barely discernible and the two order metrics are only weakly coupled to each other. Accordingly, the locus of weak orientational order maxima (B) is not a relevant indicator of dynamic or thermodynamic anomalies.

3.6   Conclusion

In this work we have investigated thermodynamic, dynamic and structural anomalies in ramp potential fluids, as a function of the ratio λ of length scales corresponding to the inner hard core, and to the outer edge of the ramp. We find that thermodynamic and dynamic anomalies exist for $\lambda = 0$, $2/7$, $4/7$ and $5/7$, but not for $= 6/7$. As in water and silica, the loci of anomalies form nested domes in the (T, ρ) plane, inside which the thermal expansion coefficient is negative (inner dome) and the diffusivity increases upon compression (outer dome). The limit $\lambda = 1$ corresponds to hard spheres, and the absence of anomalies for $\lambda = 6/7$ indicates approach to hard sphere behavior. The order map of this family of ramp fluids is water-like at $\lambda = 4/7$ and hard-sphere-like at $\lambda = 6/7$. Thus, by varying the ratio of characteristic length scales, the family of ramp potentials spans the range of liquid behavior from hard spheres to water-like.

These findings show that orientational interactions are not necessary for the existence of thermodynamic, dynamic, or structural anomalies. Instead, water-like behavior apparently emerges in this spherically-symmetric family of fluids through the existence of two competing length scales, with their ratio λ being the single control parameter. Although thermodynamic and dynamic anomalies exist almost over the entire range of the control parameter, the combination of thermodynamic and dynamic anomalies plus a water-like order map occurs over a narrow range of λ. It is interesting to note that a distinguishing feature of water is the fact that the ratio of radial distances to the first and second peaks of the oxygen-oxygen pair correlation

function is not $\sim 1/2$, as in simple liquids, but ~ 0.6. This is close to 0.571 ($\lambda = 4/7$, the ratio of σ_0 to σ_1 that gives rise to water-like structural, dynamic and thermodynamic anomalies). In water, isothermal compression pushes molecules from the second shell towards the first shell, gradually filling the interstitial space [51]. Likewise, in the ramp potential, isothermal compression pushes molecules from the soft core (σ_1) to the hard core (σ_0). Further work is needed to establish whether a ratio of competing length scales close to 0.6 is generally associated with water-like anomalies in other core-softened potentials, for example linear combinations of Gaussian [52] potentials. In this work we used the terminology water-like to denote structural, diffusion, and density anomalies. The increase in water's isothermal compressibility upon isobaric cooling, another of this liquid's canonical anomalies, is also trivially captured by the ramp potential, because thermodynamic consistency arguments [53] mandate that the compressibility increase upon cooling whenever there exists a negatively-sloped locus of density maxima in the (P, T) plane.

The ramp potential, when supplemented by explicit [11, 35] or mean-field attractions [34], gives rise to liquid-liquid immiscibility and a critical point distinct from the one associated with the vapor-liquid transition. A liquid-liquid transition has been observed experimentally in phosphorus [6, 54], n-butanol [55] and triphenyl phosphite [56], and strong experimental evidence consistent with liquid-liquid immiscibility also exists for water [3, 57, 58]. Computer simulations of silicon [8], silica [7, 59], carbon [60] and water [4, 61–66] also indicate the presence of a liquid-liquid transition. A systematic study of the effects of λ and the ratio of characteristic energies (U_1 and the attractive well depth) on the existence of a liquid-liquid transition, the positive or negative slope of the line of first-order liquid-liquid transitions in the (P, T) plane, and the relationship, if any [38], between the liquid-liquid transition and density anomalies, would shed important new light on the phenomenon of liquid polyamorphism [5, 67, 68].

In summary we investigate the equation of state, diffusion coefficient, and struc-

tural order of a family of spherically-symmetric potentials consisting of a hard core and a linear repulsive ramp. This generic potential has two characteristic length scales: the hard and soft core diameters. The family of potentials is generated by varying their ratio, λ. We find negative thermal expansion (thermodynamic anomaly) and an increase of the diffusion coefficient upon isothermal compression (dynamic anomaly) for $0 \leq \lambda < 6/7$. As in water, the regions where these anomalies occur are nested domes in the (T, ρ) or (T, P) planes, with the thermodynamic anomaly dome contained entirely within the dynamic anomaly dome. We calculate translational and orientational order parameters (t and Q_6), and project equilibrium state points onto the (t, Q_6) plane, or order map. The order map evolves from water-like behavior to hard-sphere-like behavior upon varying λ between $4/7$ and $6/7$. Thus, we traverse the range of liquid behavior encompassed by hard spheres ($\lambda = 1$) and water-like ($\lambda \sim 4/7$) with a family of tunable spherically-symmetric potentials by simply varying the ratio of hard to soft-core diameters. Although dynamic and thermodynamic anomalies occur almost across the entire range $0 \leq \lambda \leq 1$, water-like structural anomalies (i.e., decrease in both t and Q_6 upon compression and strictly correlated t and Q_6 in the anomalous region) occur only around $\lambda = 4/7$. Water-like anomalies in structure, dynamics and thermodynamics arise solely due to the existence of two length scales, with their ratio λ being the single control parameter, orientation-dependent interactions being absent by design.

It is generally accepted that strong orientation-dependent interactions underlie many of the distinctive properties of associating, network-forming liquids such as water. Atomic liquids, on the other hand, exhibit simpler behavior, and in particular do not show structural, thermodynamic, or dynamic anomalies of the type discussed here. In this work we have shown that key properties of these apparently distinct categories of liquids can be bridged systematically by varying the ratio of two length scales in a family of spherically-symmetric potentials in which orientation-dependent interactions are absent by design. What other spherically-symmetric potentials, in

addition to those possessing competing length scales, may give rise to water-like anomalies, is among the interesting questions arising from this study that we will pursue in future work.

Chapter 4

Structure of the First and Second Neighbor Shells of Water

4.1 Introduction

It is known both from experiments [22, 69–72] and simulations [73–76] that the first shell of a central water molecule, usually defined by the first minimum of the oxygen-oxygen pair correlation function $g(r)$, can accomodate between four and five water molecules, depending on pressure [77]. The signature of this first shell, defined by the first maximum of $g(r)$, barely changes with pressure. In contrast, the properties of the second shell, which extends between the first and second minima of $g(r)$, are highly dependent on pressure, indicating that large structural changes occur in this shell upon compression [22, 70].

The structural order of water has been quantified by two measures [19]: a local *orientational* order parameter q, which quantifies the extent to which a molecule and its four nearest neighbors adopt a tetrahedral local structure in the first shell, and a *translational* order parameter t, which quantifies the tendency of molecular pairs to adopt preferential separations. While q depends only on the four nearest neighbors of a central molecule in its first shell, t depends on all the neighbors of the central

molecule.

Water in the *liquid* phase displays: (i) a thermodynamic anomaly (density decrease upon cooling or, equivalently, entropy increase with pressure); (ii) a dynamic anomaly (increase of diffusivity upon compression); (iii) a structural anomaly (decrease of both q and t upon compression) [19]. Several other liquids with local tetrahedral order [5] such as silica, silicon, carbon and phosphorous also show waterlike anomalies. In the case of water [19] and silica [28], computer simulation studies show that the anomalies (i)-(iii) in the liquid phase are closely related. For example, in the case of water, the region of thermodynamic anomaly in the temperature-density (T-ρ) plane is enclosed by the region of dynamic anomaly, which in turn is enclosed by the region of structural anomaly [19].

Recent studies show that simple liquids interacting via spherically-symmetric potentials can exhibit waterlike anomalies [21, 34, 35, 39, 78], suggesting that strong orientational interactions in the first shell are not *necessary* for a liquid to show thermodynamic, dynamic and structural anomalies and pointing out the importance of the second shell of water [78]. In light of these findings, it remains unclear how much the strongly orientation-dependent first-shell interactions and the second-shell environment each contribute to water's anomalies. To address these questions, we first modify the definition of first and second shells for the purpose of quantitative study. Then we define the orientational and translational order parameters within each shell and study their changes with T and ρ.

4.2   Definition of the First and Second Shells of Water

We perform constant volume isothermal (NVT) molecular dynamics simulation of 512 TIP5P (five-site transferable interaction potential) water molecules. Our simulations are performed using a cubic box with periodic boundary conditions. We
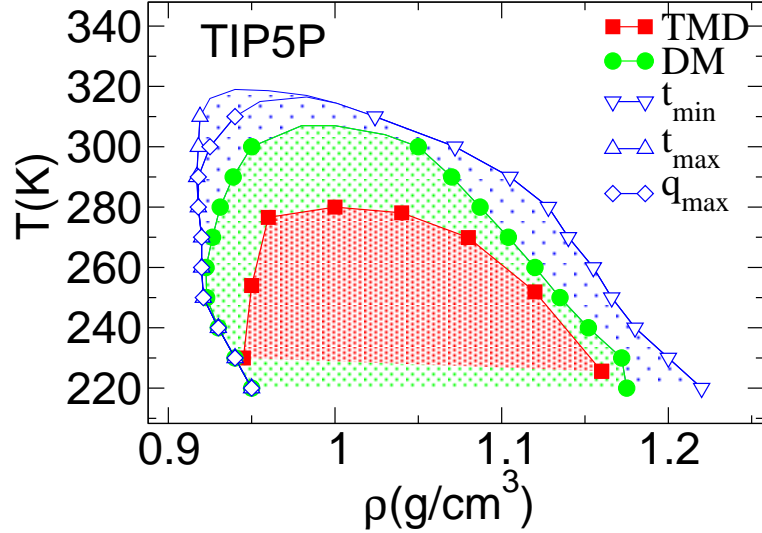
Figure 4.1: Anomalous regions in the T-ρ plane of TIP5P water. (i) The density anomaly region is defined by the locus of density maxima (TMD), inside of which the density increases when the system is heated at constant pressure. (ii) The diffusion anomaly region is defined by the loci of diffusion maxima or minima (DM), inside which the diffusivity increases with density. (iii) The structural anomaly region is defined by the loci of translational order minima (t_{min}) and maxima (t_{max}), or orientational order maxima (q_{max}), inside which both translational and orientational orders decrease with density (see Fig. 4.3).

control the temperature using a Berendsen thermostat. The TIP5P model reproduces the thermodynamic properties of liquid water over a broad region of the phase diagram [79] although it does not reproduce well the phase diagram of solid water [80]. However our study concentrates on the liquid or supercooled phase of water at low T without crystallization. In particular, we find that the TIP5P model reveals similar relations between the thermodynamic, dynamic and structural anomalies (see Fig. 4.1) as observed in ref. [19] using the SPC/E model.

The first and second shells of water can be defined according to the first and second minima of $g(r)$. For this definition, the number of molecules in each shell will

change with pressure and temperature $[51, 74, 77, 81]$. But the orientational measures that most concern us are the tetrahedral arrangement of nearest neighbors, and bond orientational order in next-nearest neighbors of a central molecule. To see how these orders evolve across a broad range of state points, we must base our comparison on a fixed number of nearest and next-nearest neighbors. Moreover, the minima in $g(r)$ become not obvious at high ρ, and $g(r)$ becomes almost featureless beyond the first peak at high ρ (see Fig. 4.2(b)). Hence we choose a less ambiguous shell definition by denoting the nearest four and next-nearest twelve neighbors of a central water molecule as the first and second shells respectively.

We first study the average effect of density on different shells by dividing $g(r)$ into three regions. We compute the average number of neighbors of a central molecule at a distance r as

$$N(r) \equiv 4\pi n \int_0^r r'^2 g(r') dr', \tag{4.1}$$

where n is the number density. We define r_1 and r_2 such that $N(r_1) = 4$ and $N(r_2) = 16$. Therefore, we can define three regions: $0 < r \leq r_1$ (first shell), $r_1 < r \leq r_2$ (second shell), and $r > r_2$, where r_1 and r_2 depend on T and ρ. We find that in general r_1 and r_2 decrease with increasing ρ for different T due to the compression effect. Fig. 4.2(a) shows $N(r)$ at $T = 280$ K and $\rho = 1.00$ g/cm^3 ($n = 33.4/\text{nm}^3$), where $r_1 = 0.32$ nm and $r_2 = 0.48$ nm.

4.3 Structural Order of Different Shells of Water: Importance of the Second Shell

Fig. 4.2(b) shows $g(r)$ of TIP5P water at $T = 280$ K and a range of density covering the anomalous regions of water of Fig. 4.1. Fig. 4.2(c) shows the change upon compression,

$$\Delta g(r) \equiv g(r)|_\rho - g(r)|_{\rho_0}, \tag{4.2}$$
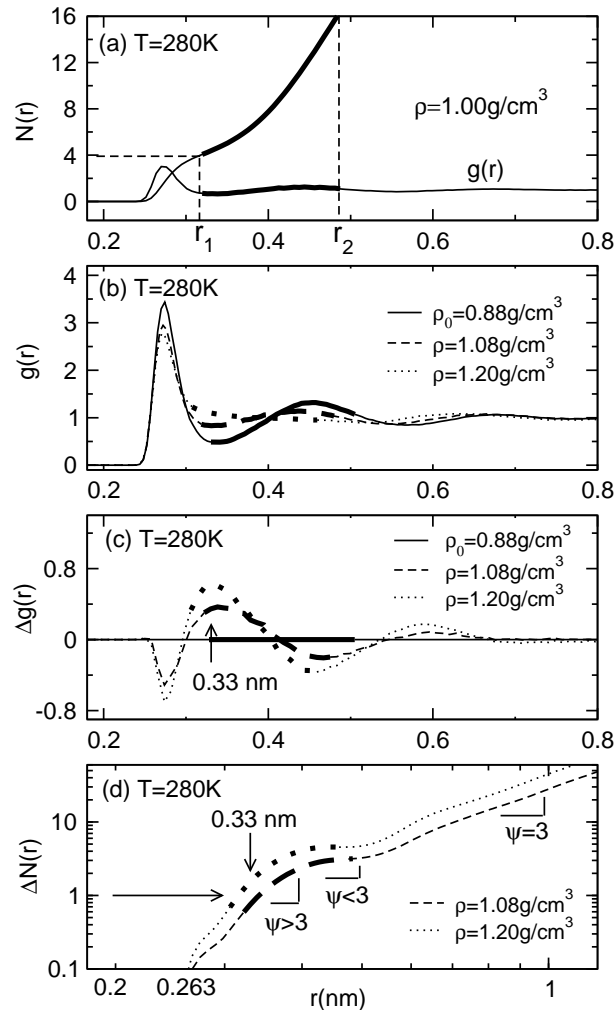
Figure 4.2: The number of neighbors $N(r)$ and Oxygen-oxygen pair correlation $g(r)$ of TIP5P water. (a) The number of neighbors $N(r)$ around a central water molecule. r_1 and r_2 correspond to the first and the second shell distances, defined such that $N(r_1) = 4$ and $N(r_2) = 16$. (b) Oxygen-oxygen pair correlation function $g(r)$. (c) Difference $\Delta g(r)$ between $g(r)$ at a given density and $g(r)$ at ρ_0, and (d) Difference $\Delta N(r)$ between $N(r)$ at a given density and $N(r)$ at ρ_0 for TIP5P water. ψ characterizes the local slope. The bold portions of the curves correspond to water's second shell, $r_1 < r \leq r_2$, showing that the largest changes upon compression occur in the second shell.

where $\rho_0 = 0.88$ g/cm^3. Fig. 4.2(d) shows the corresponding change,

$$\Delta N(r) \equiv N(r)|_\rho - N(r)|_{\rho_0}. \tag{4.3}$$

Fig. 4.2(b) shows that as ρ increases, the first peak of $g(r)$ decreases, so $\Delta g(r) < 0$ at $r = 0.28$ nm in Fig. 4.2(c). This effect of ρ on $g(r)$ is a result of having a fixed number of neighbors at $r \approx 0.28$ nm, normalized by n in the definition of $g(r)$. The change of the number of neighbors corresponding to the first peak of $g(r)$ is barely distinguishable (see Fig. 4.2(d)), i.e. $\Delta N(r) \approx 0 - 0.2$ for $r \approx 0.28$ nm. This implies that the distance defined by the first peak of $g(r)$ is practically impenetrable and thus, it roughly resembles a hard core. The main changes in $g(r)$ (Fig. 4.2(b)) and $\Delta g(r)$ (Fig. 4.2(c)) occur in the second shell. As the density increases, hydrogen bond bending allows water molecules in the second shell to shift toward the first shell, filling the interstitial space [22, 70]. The changes of $g(r)$ with pressure for $r > r_2$ are minimal.

Fig. 4.2(d) shows in double logarithmic scale the relationship between $\Delta N(r)$ and r. The slope of the curve, ψ, characterizes the power law dependence

$$\Delta N(r) \propto r^\psi. \tag{4.4}$$

There are three main regimes in the behavior of $\Delta N(r)$ as shown by the different slopes $\psi > 3$, $\psi < 3$ and $\psi = 3$. The $\psi = 3$ regime at $r > r_2$ is mainly due to the density change, since $g(r) \approx 1$ ($\Delta g(r) \approx 0$) for $r > r_2$, so $\Delta N(r)$ behaves approximately as

$$\Delta N(r) \propto \Delta \rho \, r^3, \ \Delta \rho \equiv \rho - \rho_0. \tag{4.5}$$

Both the $\psi > 3$ and $\psi < 3$ regimes are located within the second shell. The increase of $\Delta N(r)$ for $r < r_2$ is not only due to density increase, but also due to the shift of water molecules from the second shell around 0.45 nm toward the first shell around 0.28 nm. Thus, the regime where $\psi > 3$, for roughly $r < 0.4$ nm, is due to an increase of $g(r)$ ($\Delta g(r) > 0$), and $\psi < 3$ for roughly 0.4 nm $< r < r_2$ is due to the

decrease of $g(r)$ ($\Delta g(r) < 0$). Note that $\Delta N(r) = 1$ for $r \sim 0.33$ nm, corresponding to the fifth neighbor [77, 81], which is very close to the border of the first shell, where $\Delta g(r)$ has its maximum value. This fifth neighbor in the vicinity of the first shell of water can produce a defect in the tetrahedral network of water at high density. This defect leads to hydrogen bond bifurcation and offers paths with low energy barriers between different network configurations of water. The defect is also related to diffusion anomaly by lowering energy barriers for translational and rotational motions of water molecules [77, 81].

The translational order parameter t in Eq. (2.2) is introduced by Truskett *et al.* [29] and defined in refs. [19, 21, 28, 29, 82]

$$t \equiv \int_0^{s_c} |g(s) - 1| ds, \tag{4.6}$$

where the dimensionless variable $s \equiv rn^{1/3}$ is the radial distance r scaled by the mean intermolecular distance $n^{-1/3}$, and s_c usually corresponds to half of the simulation box size, which is large enough to have $g(s_c) \approx 1$. It equals to the area bounded by the PCF $g(s)$ and the line $g(s) = 1$. We can decompose the translational order parameter t into t_1, t_2, and t_3 for each shell of water by integrating

$$|g(s) - 1| \tag{4.7}$$

over the three different regions

$$0 < s \leq s_1, \ s_1 < s \leq s_2, \ s > s_2, \tag{4.8}$$

where

$$s_1 = r_1 n^{1/3}, \ s_2 = r_2 n^{1/3}. \tag{4.9}$$

We note that

$$t = t_1 + t_2 + t_3. \tag{4.10}$$

The orientational order q_i is used to quantify the tetrahedrality of the first shell, defined as [19]

$$q_i \equiv 1 - \frac{3}{8} \sum_{j=1}^{3} \sum_{k=j+1}^{4} \left[\cos \theta_{jik} + \frac{1}{3} \right]^2, \tag{4.11}$$

where θ_{jik} is the angle formed between neighbors j and k and the central molecule i. The average value

$$q \equiv \frac{1}{N} \sum_{i=1}^{N} q_i \qquad (4.12)$$

quantifies the orientational order of the system based on the molecules in the first shell. For perfect tetrahedral order, $q = 1$; for an uncorrelated system, $q = 0$.

Because the second shell of the hexagonal ice crystal forms an hcp lattice, the orientational order parameter for the second shell of water can be characterized by Q_{6i}, which quantifies the extent to which a molecule i and *twelve* of its neighbors adopt the local fcc, bcc, or hcp structures. This orientational order parameter [30] is often used for simple liquids [21, 26, 29, 82] because they have fcc or bcc crystal structures. In order to compute Q_{6i}, we first define twelve bonds connecting each water molecule i with its twelve next-nearest neighbors in the second shell, and compute for each bond its azimuthal and polar angles (θ, φ). Next we compute $\overline{Y}_{\ell m}(\theta, \varphi)$, the average of the spherical harmonic function over the 12 bonds of the molecule i. Finally we compute

$$Q_{\ell i} \equiv \left[\frac{4\pi}{2\ell + 1} \sum_{m=-\ell}^{m=\ell} |\overline{Y}_{\ell m}|^2 \right]^{\frac{1}{2}}. \qquad (4.13)$$

For $\ell = 6$, the average value $Q_6 \equiv \frac{1}{N} \sum_{i=1}^{N} Q_{6i}$ quantifies the orientational order of the system based on the molecules in the second shell. Q_6 is large [30] for most crystals such as fcc (0.574), bcc (0.511), hcp (0.485). For uncorrelated systems,

$$Q_6 = 1/\sqrt{12} = 0.289. \qquad (4.14)$$

Fig. 4.3 shows the density dependence of all six order parameters at three temperatures covering the anomalous region of TIP5P water (see Fig. 4.1). Although t_1 is much larger than t_2 and t_3, it is apparent that t_2 makes the most important contribution to the anomaly of t (decrease of t with increasing density), compared to t_1 and t_3. t_1 also makes a small contribution to the t anomaly at low $T = 240$ K due to a small decrease in the first peak of $g(r)$ upon compression. The anomalous behavior
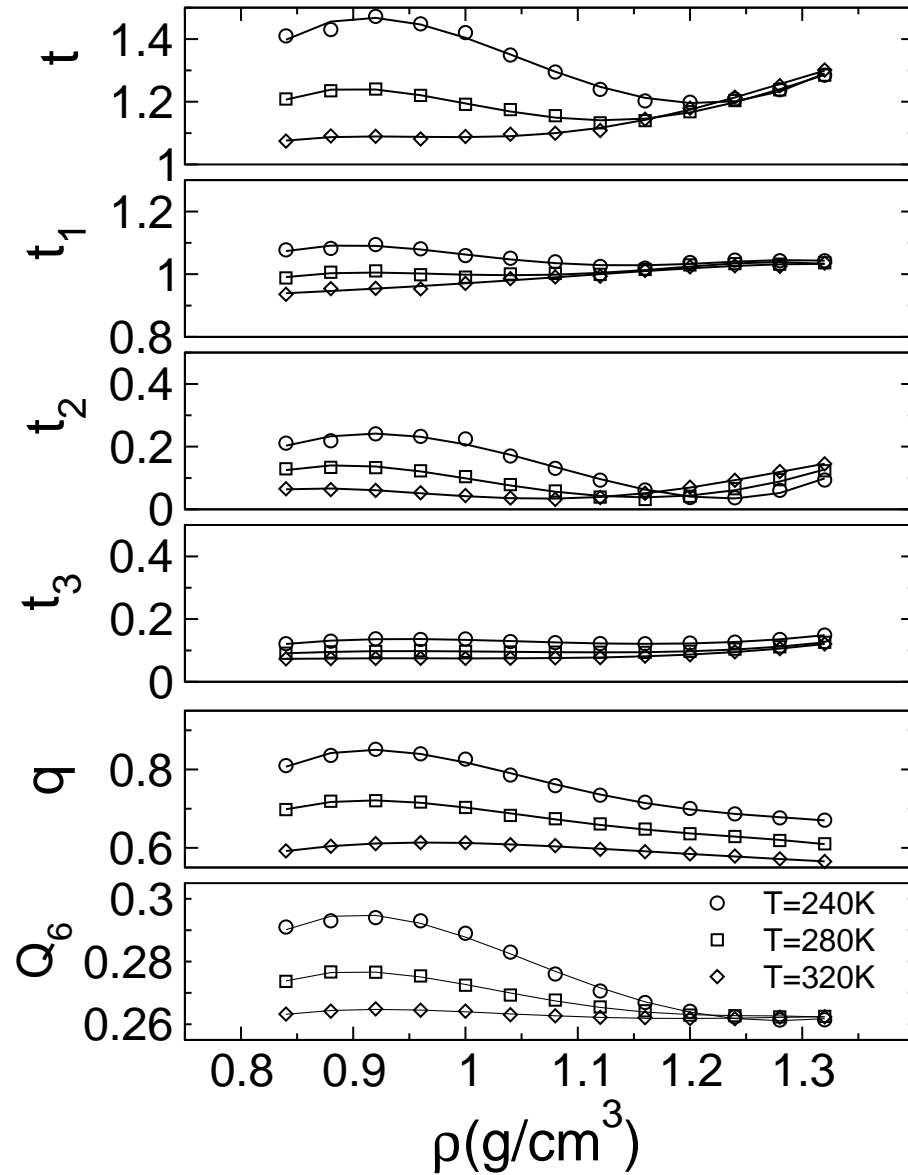
Figure 4.3: Structural order parameters for different shells of water. Translational order parameters t (total), t_1 (first shell), t_2 (second shell), t_3 and orientational order parameters q (first shell), Q_6 (second shell) of TIP5P water as function of density at different T. The anomalous decrease of orientational order upon compression occurs in both shells (q, Q_6), but the anomalous decrease of translational order upon compression mainly occurs in the second shell (t_2).

of t becomes weak at $T = 280$ K and disappears at $T = 320$ K. The orientational order parameters q and Q_6 both show similar anomalous behavior. The distribution of individual q_i shifts from high q (ice-like) at low ρ and T to low q (less tetrahedral) at high ρ and T as shown in Fig. 4.4(a) and (d), due to increased hydrogen bond bifurcation [77] as interstitial molecules move closely to the first shell (Fig. 4.4(c) and (f)). Q_{6i} always has approximately normal distribution as shown in Fig. 4.4(b) and (e) because there is no direct bonding between a central water molecule and its second shell neighbors.

4.4   Order maps of Different Shells of Water: Importance of the Second Shell

A useful way of investigating structural order in fluids is to map state points onto the t-q plane, a representation called the order map [19, 21, 26]. The order map for TIP5P water (i.e., using t and q) is shown in Fig. 4.5(a). This order map is similar to the one found in ref. [19] using the SPC/E model. Its main characteristic is the correlation of the two order parameters in the anomalous regions where both q and t decrease with density, as shown by the isotherms collapsing onto a line. Recently an entropy-based measure of structural order in water [83] has revealed that the correlated order map is invariant to the choice of different measures, suggesting that such correlation is a general feature of waterlike liquids. Fig. 4.5(b)-(h) shows the different order maps obtained by considering the order parameters in different shells. The only one that shows the states in the thermodynamically, dynamically and structurally anomalous regions collapsing onto a line, is the panel (f) (i.e. the t_2-Q_6 order map of the second shell), indicating that the changes in the second shell are related to anomalies of water.

The first shell order map t_1-q in (c) is not correlated because t_1 has only small changes with increasing density due to the impenetrable hard core at 0.28 nm, while
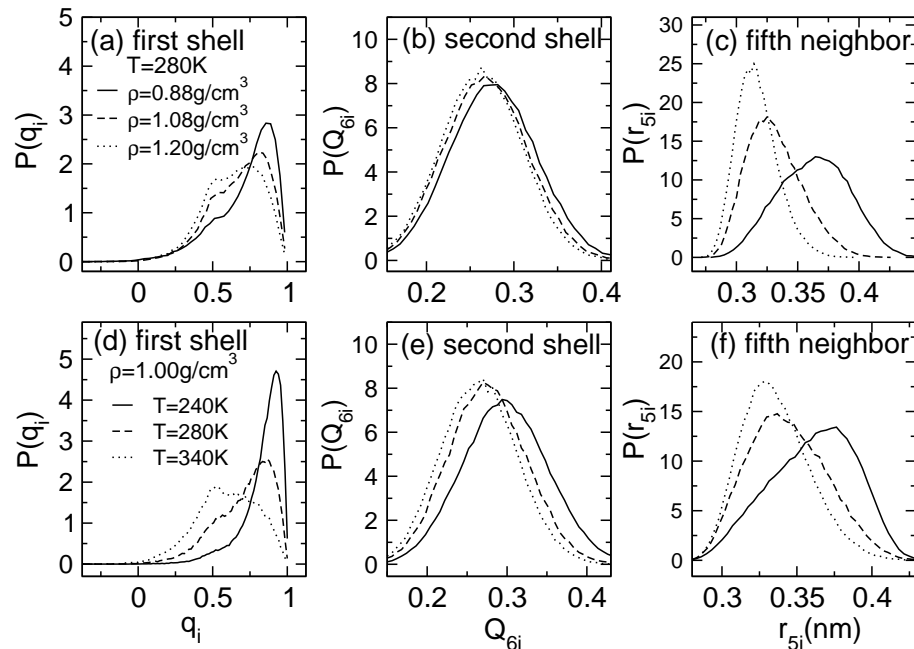
Figure 4.4: Histograms of local orientational order and the fifth neighbor distance for water. Histograms of (a) the local orientational order q_i in the first shell, (b) Q_{6i} in the second shell, and (c) distance r_{5i} between a central water molecule i and its fifth neighbor of TIP5P water. (a), (b), and (c) show the changes for three different ρ at fixed $T = 280K$. (d), (e), and (f) show the changes for three different T at fixed $\rho = 1.00$ g/cm^3. Upon compression or heating over the anomalous regions of the phase diagram, the fifth neighbor (and other interstitial water molecules in the second neighbor shell) shift towards first shell (see also Fig. 4.2 and ref. [76]), corresponding to anomalous changes of structural order in the first and second shells, as quantified by Fig. 4.3 and Fig. 4.5.
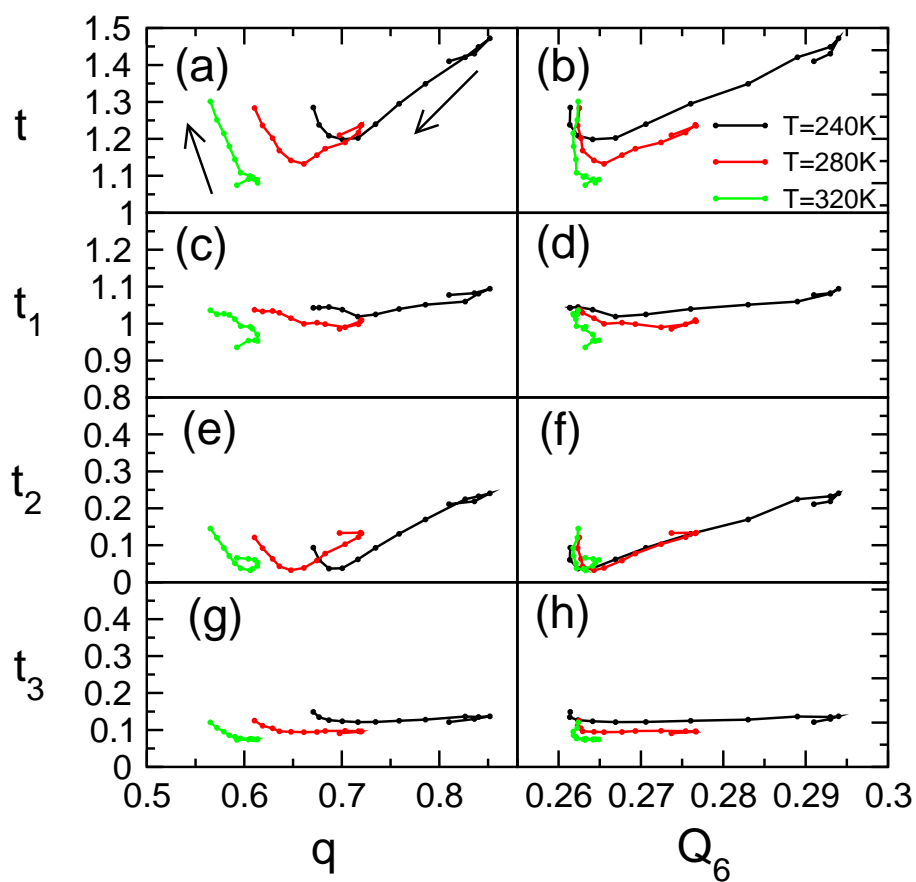
Figure 4.5: Order maps for TIP5P water. The arrows indicate the direction of increasing density from 0.84 g/cm³ to 1.32 g/cm³. Only for the second shell order map, t_2-Q_6 in (f), the isotherms collapse on a line and the decrease of translational and orientational orders is correlated.

q changes significantly with density. In the second shell, t_2 and Q_6 both change significantly and simultaneously with density so that they are well correlated. Our work quantitatively shows that the second shell is related to anomalies of water by its gradual shift towards first shell upon compression. In addition to water, other tetrahedral liquids such as silica, silicon, carbon and phosphorous [5] may also exhibit similar behavior, and a detailed, shell-based study of their order parameters may prove useful.

In summary we perform molecular dynamics simulation of water using the TIP5P model to quantify structural order in both the first shell (defined by four nearest neighbors) and second shell (defined by twelve next-nearest neighbors) of a central water molecule. We find that the anomalous decrease of orientational order upon compression occurs in both shells, but the anomalous decrease of translational order upon compression occurs *mainly in the second shell*. The decreases of translational and orientational orders upon compression ("structural anomaly") are thus correlated only in the second shell. Our findings quantitatively confirm the qualitative idea that the thermodynamic, structural and hence dynamic anomalies of water are related to changes in the second shell upon compression.

Chapter 5

Correspondence Between Water and Ramp Potential

5.1 Introduction

Liquid water is peculiar as reflected by its thermodynamic and dynamic anomalies [2, 19], such as the density decrease upon isobaric cooling (density anomaly) and the increase of diffusivity upon isothermal compression (diffusion anomaly). It has been proposed that these anomalies may arise from a liquid-liquid critical point (LLCP) in the deeply supercooled state of water [4]. Several other liquids (e.g., silica, silicon, carbon, and phosphorous) with local tetrahedral order [5, 28, 82] also may show water-like anomalies. These anomalies of water and the LLCP can be reproduced by simple liquids interacting via core-softened spherically symmetric potentials which lack the strong orientational interaction expected in tetrahedral liquids [11, 21, 32–34, 39, 42, 78, 84–88].

Water also possesses structural anomalies which occur when metrics describing both translational and orientational order decrease upon compression, as found in both the SPC/E and TIP5P (five point transferable intermolecular potential) water models [19, 89]. Water's structural anomaly is also reproduced by a family of core-

softened spherically symmetric potentials possessing two characteristic length scales σ_0 and σ_1 (see the ramp potential in Fig. 5.1(a)) [21, 86]. In order to exhibit a water-like structural anomaly, the ratio $\lambda \equiv \sigma_0/\sigma_1$ must lie within a small interval around 0.62, the ratio of the distances to water's first and second neighbor shells, 0.28 nm/0.45 nm[21].

A quantitative connection between the ramp potential and water's pair potential has not been established, as well as the relation between the regions of anomalies in their respective phase diagrams. In this work, we show that the effective pair potential derived from the TIP5P water model [79] can be approximated by a two-scale spherically symmetric repulsive ramp potential, allowing us to assign physical units to the temperature and pressure of the ramp model. We perform molecular dynamics simulations using both the TIP5P and ramp potentials and compare the regions of anomalies in the corresponding phase diagrams. We find that the regions of anomalies in both phase diagrams are *quantitatively* similar if (i) pressure P and temperature T are measured in terms of $(T - T_C)$ and $(P - P_C)$ respectively, where (T_C, P_C) are the coordinates of the LLCP of the corresponding system; and (ii) a ramp particle corresponds to two TIP5P molecules. We present quantitative arguments supporting point (ii) and provide a simple picture to explain the similarities observed in the TIP5P and ramp potentials. A ramp liquid particle corresponds *effectively* to two water molecules, one molecule plus 1/4 of each of its four neighbors. The water-like anomalies in the ramp potential are due to the ability of the particles to reproduce, upon compression or heating, the migration of water molecules from the second shell to its first shell.

5.2   Effective Potential of Water

The TIP5P model is a well-known water model and its parameters are defined in physical units, so values of P and T from simulations can be compared directly
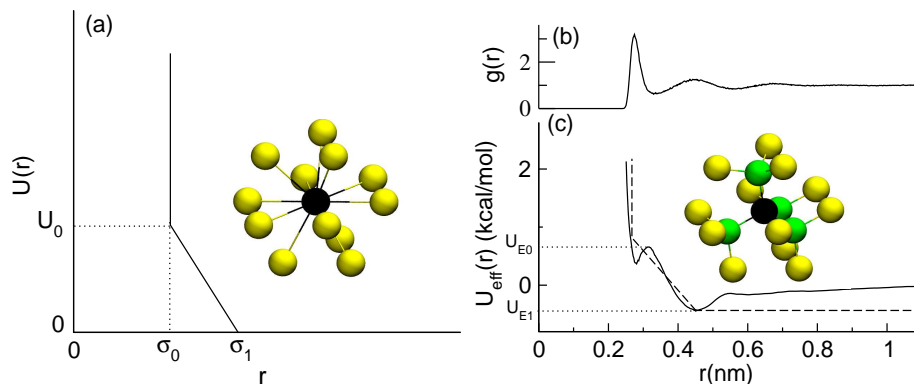
Figure 5.1: Effective potential of water approximated by a ramp potential. (a) The two-scale spherically symmetric repulsive ramp potential: σ_0 corresponds to the hard core distance, σ_1 characterizes a softer repulsion range that can be overcome at high P and T. The central ramp particle (black) and its twelve nearest neighbors form a hcp crystal structure in a range of densities corresponding to the density anomaly. (b) The pair correlation function, $g(r)$, and (c) spherically symmetric effective potential, $U_{\text{eff}}(r)$, from the simulations using the TIP5P model at $T = 280K$ and $\rho = 1.00$ g/cm^3 (solid line). For hexagonal ice, the twelve neighbors in the second shell of the center water molecule (black) also has a hcp structure while the four nearest neighbors in the first shell are located in the corner of a tetrahedron. $U_{\text{eff}}(r)$ can be approximated by a ramp potential (dashed lines). By calculating the area of $g(r)$ for $r \leq \sigma_0$ we find that the hard core of the ramp particle roughly incorporates two water molecules (see also Fig. 5.2).

with experiments [79]. Instead, thermodynamic properties in the ramp potential are given in terms of potential parameters, such as $\{\sigma_0, U_0\}$, and the particle mass, m. To compare the phase diagrams of the ramp potential to that of the TIP5P model, we will define σ_0 and U_0 in units of 'nm' and 'kcal/mol', respectively, and m in units of 'g/mol'. We do this by calculating $U_{\text{eff}}(r)$, the effective spherically symmetric pair potential between water molecules from the TIP5P model simulations.

The interaction between water molecules usually include the Van der Waals' force and Coulomb interactions. There is no direct way to get the corresponding physical parameters of water for σ_0, σ_1, U_0 and U_1 in the ramp potential. But we can compute the potential of mean force or the effective potential between the TIP5P water molecules by applying the technique in ref. [90]. To get effective potential, first we compute the oxygen-oxygen (O-O) pair correlation function (PCF), $g(r)$, from MD simulation of water. Then we get the total correlation function

$$h(r) = g(r) - 1 \tag{5.1}$$

and apply the Fourier transform of isotropic liquids to get $h(k)$. Next we solve for the direct correlation function, $c(r)$, by invoking the the Fourier transform

$$h(k) = c(k) + \mu c(k) h(k) \tag{5.2}$$

of Ornstein-Zernike (OZ) equation, which have the form

$$h(r) = c(r) + \mu \int d^3 r' c(r') h(|\vec{r} - \vec{r'}|). \tag{5.3}$$

Here μ is the number density of water molecules. Finally we use hypernetted chain (HNC) approximation [91] to get generic effective pair potential of TIP5P water

$$U_E(r) = K_b T \{g(r) - 1 - ln[g(r)] - c(r)\}. \tag{5.4}$$

$U_{\text{eff}}(r)$ is obtained from the oxygen-oxygen pair correlation function $g(r)$, by solving the Ornstein-Zernike equation and using the hypernetted chain approximation [90].

The resulting $U_{\rm eff}(r)$ depends on T and density ρ [92], but has no significant change for different state points in the anomalous region. For the TIP5P model, the range of anomalies is approximately $220\,{\rm K} < T < 320\,{\rm K}$ and $0.90\,{\rm g/cm^3} < \rho < 1.16\,{\rm g/cm^3}$ [89]. We select a state point located in the middle of the anomalous regions, at $T = 280$ K and $\rho = 1.00$ g/cm^3, and calculate $g(r)$ and $U_{\rm eff}(r)$ [see Fig. 5.1(b) and Fig. 5.1(c)]. We find that $U_{\rm eff}(r)$ is similar to the effective pair potential obtained from the experimental $g(r)$ [90], and shows a hard-core-like steep repulsion at $r \approx 0.26$ nm and an approximately linear repulsive region covering the distance spanned by the second shell of a central water molecule, approximately $0.32\,{\rm nm} < r < 0.45\,{\rm nm}$. The shallow minimum at $r = 0.28$ nm is caused by hydrogen-bonding attraction and corresponds to the first peak of $g(r)$, while the minimum at $r = 0.45$ nm with

$$U_{\rm E1} \equiv U_{\rm eff}(0.45\ nm) = -0.45\ kcal/mol \tag{5.5}$$

corresponds to the second peak of $g(r)$. $U_{\rm eff}(r)$ also shows a maximum at $r \approx 0.32$ nm with

$$U_{\rm E0} \equiv U_{\rm eff}(0.32\ nm) = 0.66\ kcal/mol \tag{5.6}$$

that corresponds to the first minimum of $g(r)$.

Fig. 5.1(c) also shows that a ramp potential is a good approximation to $U_{\rm eff}(r)$. In the figure we set $\sigma_1 = 0.45$ nm and define the ramp part of the potential such that it intersects the plot of $U_{\rm eff}(r)$ at

$$(U_{\rm E0} + U_{\rm E1})/2. \tag{5.7}$$

The intersection of the ramp part of the potential with the hard core of $U_{\rm eff}(r)$ is used to define U_0 and σ_0. This results in $\sigma_0 = 0.267$ nm, which is located between 0.28 nm, the first peak position of $g(r)$ and 0.26 nm, roughly the infinite repulsion part of $U_{\rm eff}(r)$. Therefore,

$$\lambda \equiv \sigma_0/\sigma_1 = 0.593 \tag{5.8}$$

and

$$U_0 = U_{\rm eff}(\sigma_0) - U_{\rm eff}(\sigma_1) = 1.31\ kcal/mol. \tag{5.9}$$
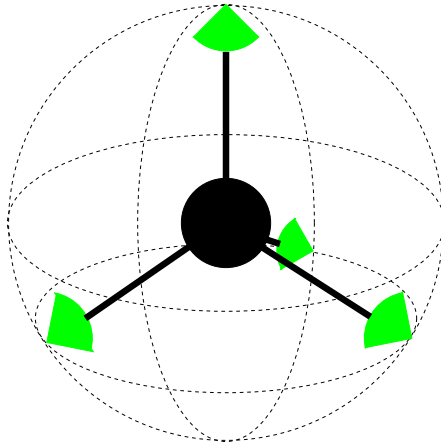
Figure 5.2: A sketch of a water molecule and 1/4 of each of its four nearest neighbors in a tetrahedral arrangement. Only oxygen atoms are shown for clarity. Mass of this unit corresponds effectively to the mass of a spherically symmetric ramp particle. The hexagonal ice (the low pressure crystal of water) can be obtained by combining these units in an hcp lattice (the low pressure crystal of the ramp potential model). We notice this figure is in the spirit of Walrafen pentamer [93] with the difference that the former consists of only two water molecules.

U_0 is approximately the energy barrier that water molecules need to overcome to migrate from the second shell to the first shell positions in terms of the effective potential. It is also roughly the energy that ramp particles need to overcome to reach the hard core distance.

5.3   Effective Physical Units of Ramp Potential

To define m in physical units, we argue that spherically symmetric ramp particle has an effective mass corresponding to the mass of two water molecules. This is based on the crystalline phases of water (hexagonal ice) and ramp potential (hcp) [see Fig. 5.1]. The hexagonal ice can be formed by combining units such as that shown in Fig. 5.2. To form the hexagonal ice, such units must form an hcp network.

Therefore, if the crystalline structure of the ramp potential model is identified with that of hexagonal ice, a ramp particle must be identified, on average, to the unit shown in Fig. 5.2. The mass of a water molecule is $m_w = 18$ g/mol, thus, the mass of a ramp particle is

$$m \approx (1 + 4 \times 1/4) \, m_w = 36 \, g/mol. \tag{5.10}$$

Alternatively, the present argument implies that the number density of the ramp potential model corresponds to twice the number density of water, and this will be relevant when comparing the pressures of the ramp and TIP5P models [94]. To test the idea that a ramp particle corresponds approximately to two water molecules, we calculate the average number of neighbors, N_0, that a water molecule has within a distance of $r < \sigma_0 = 0.267$ nm. Using the $g(r)$ from Fig. 5.1 we get

$$N_0 \equiv 4\pi n \int_0^{\sigma_0} r'^2 g(r') dr' \approx 1, \tag{5.11}$$

(here, n is the number density), in agreement with our view. The correspondence between one ramp particle and two water molecules is also supported by computer simulations of the ramp potential with $\lambda = 0.581$ and an attractive part [11, 85]. Such a ramp potential model has both liquid-gas (LG) and liquid-liquid (LL) critical points. Application of the values for σ_0, U_0, and m that we use here to the data from [11, 85] results in

$$\rho_{LG} \approx 0.314 \, g/cm^3 \tag{5.12}$$

and

$$\rho_{LL} \approx 1.188 \, g/cm^3. \tag{5.13}$$

These values approximately coincide with the experimental critical density of water [95]

$$\rho_{LG} \approx 0.322 \, g/cm^3 \tag{5.14}$$

and the LL critical density of TIP5P water [96, 97]

$$\rho_{LL} \approx 1.13 \, g/cm^3. \tag{5.15}$$

5.4 Quantitative Connection Between Water and Waterlike Simple Liquid

To compare the regions of anomalies in the phase diagrams of the TIP5P and ramp potentials, we first obtain the LLCP coordinates, (P_C, T_C, ρ_C). The LLCP in the TIP5P model is accessible in MD simulations and is located at [64, 98]

$$T_C = 217 \ K, \ P_C = 340 \ MPa, \ \rho_C = 1.13 \pm 0.04 \ g/cm^3. \tag{5.16}$$

Instead, for the ramp potential of Fig. 5.1(a), the LLCP is located at temperatures below those accessible in simulations [39]. In this case, the LLCP can be located by extrapolating the isochores in the $P - T$ phase diagram to low-T (the isochores cross each other at the LLCP). This procedure indicates that the LLCP is located at

$$T_C = 16.5 \ K, \ P_C = 967 \ MPa, \ \rho_C = 1.19 \ g/cm^3. \tag{5.17}$$

Fig. 5.3 shows the phase diagrams of the TIP5P and ramp potential models, obtained by MD simulations (for details see [21, 39, 89]). To emphasize the quantitative similarities of these diagrams we place the origins of P and T axes at the LLCP of the corresponding models. In both models, the density anomaly region is within the diffusion anomaly region, which is enclosed by the structure anomaly region. A comparison of panels (a) and (b), or (c) and (d), shows *quantitative* similarities in the regions of anomalies of both models. For example, the density anomaly region covers approximately the ranges for both models,

$$-500 < P - P_C < 0 \ MPa, \ T - T_C < 60 \ K, \ 0.9 < \rho < 1.15 \ g/cm^3. \tag{5.18}$$

Similarly, the diffusion anomaly region covers approximately the ranges for both models,

$$-500 < P - P_C < 0 \ MPa, \ T - T_C < 90 \ K, \ 0.9 < \rho < 1.2 \ g/cm^3. \tag{5.19}$$
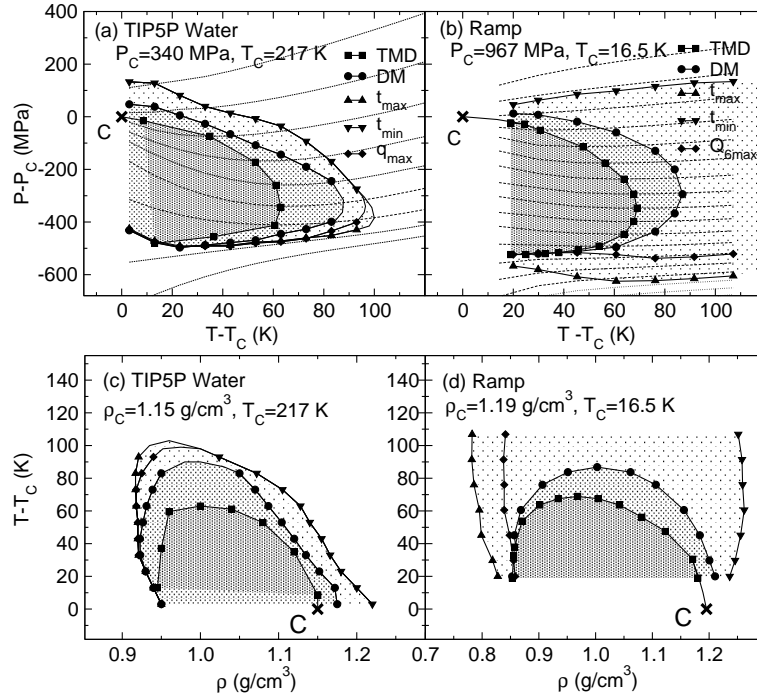
Figure 5.3: Three anomalous regions of TIP5P water. (a) Three anomalous regions of TIP5P water in modified P-T phase diagram. The dashed lines are the isochores with density ρ=1.20, 1.16, 1.12, 1.08, 1.04, 1.00, 0.96, 0.92, 0.88 g/cm^3 from top to bottom. Density anomaly region (dark shade) is defined by TMD (temperature of maxima density, filled square) lines. Diffusion anomaly region (medium shade) is defined by the loci of DM (diffusion maxima-minima, filled circle). Structural anomaly region (light shade) is defined by the loci of translational order minima (t_{min}, filled down triangle) and maxima (t_{max}, filled up triangle), or orientational order maxima q_{max} (filled diamond, $Q_{6\,max}$ for ramp liquid). Here t quantifies the tendency of molecular pairs to adopt preferential separations, and q quantify the local tetrahedrality of water (Q_6 quantify the local orientational order of twelve nearest neighbors in the first shell of a ramp particle). (b) Anomalous regions for the ramp liquid, here the values of P and ρ are doubled in order to compare with the corresponding values of water [see text]. The dashed lines are the isochores with density ρ=1.33, 1.28, 1.23, 1.18, 1.14, 1.09, 1.05, 1.02, 0.98, 0.94, 0.91, 0.88, 0.85, 0.82, 0.79, 0.77, 0.74 g/cm^3 from top to bottom. (c) and (d) are the anomalous regions in the T-ρ phase diagrams. 'C' is the location of the LLCP.
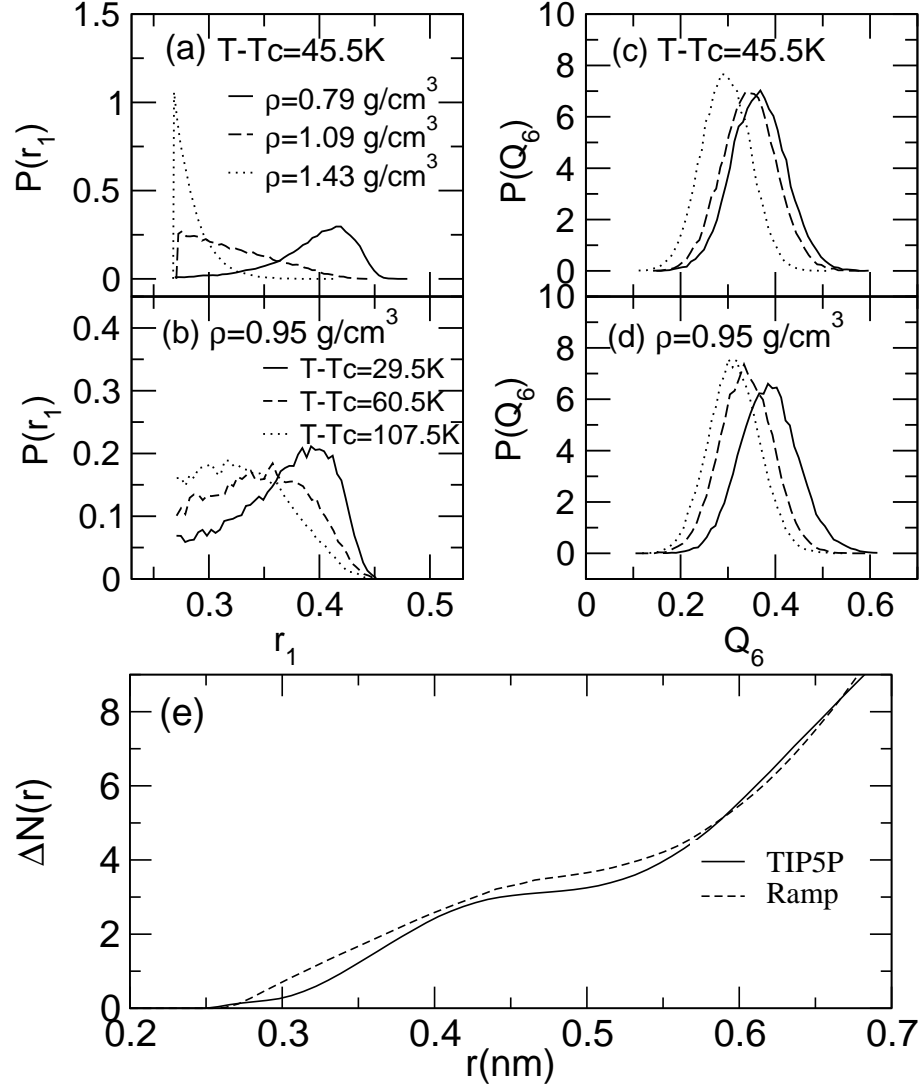
Figure 5.4: Probability distribution of the distance r_1 of a central ramp particle and its nearest neighbor at (a) constant T and (b) constant ρ. (c)-(d) Probability distribution of orientational order parameter for a ramp potential particle corresponding to panels (a) and (b), respectively. Upon heating or compression, ramp particles move from the soft-core distance toward the hard-core distance and the orientation order parameter decreases. Similar structural changes occur in water [89]. (e) Increase in the number of neighbors, $\Delta N(r) \equiv N(r)|_{\rho_1} - N(r)|_{\rho_0}$, where $\rho_1 = 0.88$ g/cm^3 and $\rho_0 = 1.08$ g/cm^3, for the TIP5P and ramp potentials. We doubled the values of $N(r)$ and $\Delta N(r)$ obtained from the simulations using the ramp potential model (see text).

The structural anomaly regions show some differences, extending to higher-T for the ramp potential model than for the TIP5P model.

Tc of water (217 K) is much higher than Tc of ramp liquid (16.5K) because of the strong attractions in the water, and it can be explained by invoking the van der Waals equation. For ramp liquid, we write the pressure, $P = P(T, \rho)$, as a function of T and ρ. The pressure exerted by the molecule on the walls of the container is related to the number and frequency of the collisions with the wall. These are both reduced by attractive forces between the molecules and included in the $-a\rho^2$ term,

$$P = P(T, \rho) - a\rho^2. \tag{5.20}$$

The molecular attractions in water decrease P and isochore with higher ρ (solid lines) will decrease much more than isochore with low ρ (dashed lines). The result is that the critical point (crossover of isochores) moves to higher T, and becomes more accessible. The anomalous regions also shift to higher T. This is also why ramp potential with long range attraction [11] show clear critical point at higher renormalized $Tc = 71$ K (using data from ref. [11]) compared to ramp without attraction [21, 39].

A possible reason for the *quantitative* similarities in the regions of anomalies of water and ramp potential model is that this model is able to reproduce *quantitatively* the observed migration of water molecules from the second shell toward the first shell upon compression or heating [76, 77, 89]. We discuss first the probability distribution, $P(r_1)$, of the distance between a ramp particle and its nearest-neighbor. Fig. 5.4(a) shows the evolution of $P(r_1)$ upon isothermal compression. As density increases, the maxima of $P(r_1)$ shifts from $r = 0.42$ nm $\approx \sigma_1$, at low density, to $r = 0.267$ nm $= \sigma_0$, at high density. Fig. 5.4(b) shows that a similar but less pronounced changes in $P(r_1)$ occur upon isobaric heating. Thus, upon compression or heating, particles move from the soft-core distance (corresponding to water's second shell) toward the hard-core distance (corresponding to water's first shell) of the ramp potential. The probability distribution, $P(Q_6)$, of the orientational order parameter, Q_6 [21], of the ramp potential particles is shown in Figs. 5.4(c) (upon isothermal compression) and 5.4(d) (upon

isobaric heating). Upon compression or heating, the maximum $P(Q_6)$ shifts to small values of Q_6, i.e. orientational order decreases. Similar structural changes occur in water [76, 77, 89]. In particular, Figs. 5.4(a), (b) and Figs. 5.4(c), (d) can be compared with the corresponding Figs. 4(c), (f) and Figs. 4(b), (e) of ref. [89] obtained for the TIP5P model. For a quantitative comparison of the structural changes in the ramp and TIP5P models, we calculate the number of neighbors, $N(r)$, as a function of the distance r from a central water molecule/ramp particle in both models. The increase of $N(r)$ with density, $\Delta N(r)$ in Fig.4(e), show similar change for both models. Thus, the ramp potential reproduces *quantitatively* the migration of water molecules from the second shell toward the first shell upon compression or heating.

In summary, our study makes a microscopic *quantitative* connection between a ramp potential and TIP5P water model and shows that orientational interactions, such as hydrogen bonding, are not necessary to reproduce water-like anomalous properties. In general, the ramp potential provides an understanding of the anomalous features of tetrahedral liquids. These features are caused by a large empty space around the tetrahedrally coordinated molecules, which is reduced as temperature and pressure increase. In the ramp liquid, this empty space is created by the repulsive soft core.

Chapter 6

Relation of Water Anomalies to the Excess Entropy

6.1 Water's Anomalies are Connected to the Structure of Water

The anomalies of water are related to its local tetrahedral structure. It is hypothesized that at very low temperatures T, water undergoes a phase transition between low density liquid (LDL) with large empty space around the tetrahedrally coordinated molecules and the high density liquid (HDL) in which additional molecules enter the first coordination shell and weaken its tetrahedrality [4, 22]. When the local structure is characterized by translational and orientational order parameters, the regions of anomalous behavior of these parameters, and also density ρ and diffusivity D are enclosed in each other on the $T - \rho$ phase diagram, thus forming a cascade of anomalies [19]. This fact indicates that various anomalies are not independent but stem from the same origin, namely the critical point which terminates the hypothesized LDL/HDL phase transition coexistence line [4]. The continuation of this coexistence line into the one-phase region forms the Widom line [11]. Response functions, such

as isothermal compressibility K_T and isobaric heat capacity C_P have maxima near the Widom line [99]. The Widom line is also related to the dynamic crossover of water [11, 100].

The models interacting with a repulsive spherically symmetric potential [21, 32, 34, 38, 84, 87, 88, 101] display waterlike anomalies despite lack of highly directional hydrogen-bonds, because the hard core of these potentials mimicks the rigid first shell of water, while the repulsive soft core mimicks the energy barrier that water molecules need to overcome to migrate from the second shell toward the first shell [21]. The repulsive soft core creates empty space in the structure which can be reduced by compression or heating, and this mimics [21] the LDL/HDL structural transition in water although there is no orientational interaction and tetrahedral structure in these models. These two-scale repulsive potentials also exhibit waterlike structural anomalies [21]. As a measure of structure, Ref.[88] used excess entropy,

$$S_{ex} \equiv S - S_{ig} \equiv S + k_B \ln \rho - c(T). \tag{6.1}$$

defined as the difference between S, the total entropy of a fluid, and $S_{ig} \equiv -k_B \ln \rho + c(T)$, the ideal gas entropy, where k_B is the Boltzmann constant. Ref.[88] successfully predicts the density and dynamic anomaly regions for a repulsive simple liquid with waterlike anomalies. The connection between two-body excess entropy $S^{(2)}$ and the "cascade of anomalies" also applies for fluids of particles with short-range attractions relative to their diameter. This, and the relationship of the colloidal system's properties to liquid water's behavior, was first discussed in the Ref. [102]. The excess entropy approach shows promise for application to molecular liquids. For example, study of SPC/E water shows that $S^{(2)}$ can capture the structural anomaly of water [19, 103]. The scaling relation between the excess entropy and transport properties of different materials has also been investigated [104].

These findings suggest that the anomalous properties of water are closely related to its LDL/HDL structural changes. We propose that the excess entropy, as a measure of structure and correlation between particles, can predict the regions of structural,

dynamic and thermodynamic anomalies of water, and it can also predict the location of the Widom line. To test this proposal, we perform constant volume isothermal (NVT) molecular dynamics (MD) simulations of 512 TIP5P (five-site transferable intermolecular potential) molecules [64]. TIP5P water model is able to reproduce the thermodynamic properties of water over a broad region of phase diagram, such as the temperature of maximum density of water around $T = 277$ K at atmosphere pressure. TIP5P model also has a second critical point in the accessible region of the phase diagram. Our simulations are performed using a cubic box with periodic boundary conditions. We control the temperature using a Berendsen thermostat.

Figure 6.1 shows the anomalous regions in the P-T phase diagram obtained from our MD simulations results. Our results are similar to results for the SPC/E water [19]. We compute D from the long-time behaviour of the mean square displacement of the water molecules $\langle r^2(t) \rangle$, using the Einstein relationship $6D = d\langle r^2(t) \rangle / dt$. We also compute the translational and orientational (tetrahedral) order parameters of water for different state points. Both order parameters have been widely used to investigate the structure of model liquids [19, 21, 28, 87].

6.2 Excess Entropy as a Measure of Structure: Relation to Translational Order

The excess entropy of water can be estimated from the two-body contribution $S^{(2)}$ arising in the expansion of the entropy in terms of partial N-body distribution functions using structural information in the form of oxygen-oxygen (O-O) pair correlation function (PCF) $g(r)$ [87, 88, 105]

$$S_{ex} \approx S^{(2)} = -2\pi \rho k_B \int \{g(r) \ln[g(r)] - [g(r) - 1]\} r^2 dr, \tag{6.2}$$

and it can estimate the excess entropy to a reasonable level of accuracy for different model liquids [106–108]. It also captures the structural anomaly of liquid silica [87]
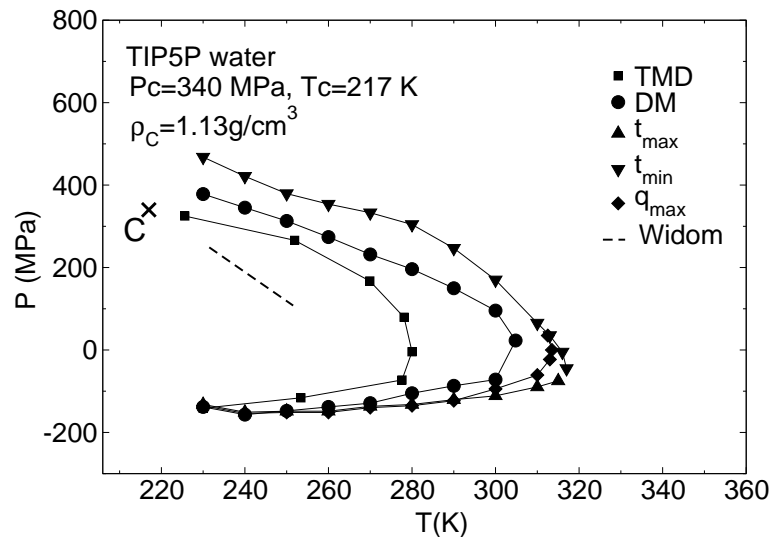
Figure 6.1: Three regions of the TIP5P phase diagram obtained from our MD simulations. Figures regenerated from Refs. [21]. Density anomaly region is defined by TMD (temperature of maxima density, ■) lines, inside which the density increases when the system is heated at constant pressure. Diffusion anomaly region is defined by the loci of DM (diffusivity maxima-minima, ●), inside which the diffusivity increases with density at constant T. The structural anomaly region is defined by the loci of translational order minima (t_{min}, ▼) and maxima (t_{max}, ▲), or orientational order maxima q_{max} (♦), inside which both translational and orientational orders decrease with density at constant T (see refs. [19, 21] for details). The dashed line (Widom line) is the loci of the response function maximum (specific heat C_P). C is the hypothesized liquid-liquid critical point according to simulations of Ref. [64].

and SPC/E water [103].

The main change of $g(r)$ of water upon compression occurs in the range of the second coordination shell [22], where water molecules migrate from the second shell toward the first shell. If the value of $g(r)$ is close to one, we can write that $\ln[g(r)] \approx \ln[1 + g(r) - 1] \approx g(r) - 1$. Thus from Eq.(6.2),

$$
\begin{aligned}
S^{(2)} &\approx -2\pi\rho k_B \int \{g(r)[g(r) - 1] - [g(r) - 1]\}r^2 dr & (6.3)\\
&\approx -2\pi\rho k_B \int [g(r) - 1]^2 r^2 dr. & (6.4)
\end{aligned}
$$

Expression (6.4) is similar to the translational order parameter $t \equiv \int |g(r) - 1| dr$ [19, 29], which quantifies the degree to which a water molecule and its nearest neighbors adopt preferential separations. This similarity is the reason why $S^{(2)}$ and t show similar anomalies for water-like model liquids [19, 21, 28, 29, 87, 88].

We compute S_{ex} using Eq.(6.2). Figure 6.2(a) shows the temperature and density dependence of S_{ex} of TIP5P water, qualitatively reproducing the result for SPC/E water [103]. S_{ex} shows normal behavior for $T > 300$ K when it decreases with density. Below $T = 300$ K, S_{ex} develops anomalous behavior, increasing with density in an interval of density which widens upon cooling. This behavior is associated with the continuous change of structure upon compression and heating from the LDL-like local structure (open tetrahedral structure with low density, low entropy and low energy) to the HDL-like local structure (more closed structure with high density, high entropy and high energy) [22]. The anomalous change of S_{ex} is related to the density anomaly due to negative thermal expansion coefficient, arising from the relation $kTV\alpha_P = \langle \delta V \delta S \rangle$, which predicts the anti-correlation between the entropy and volume fluctuations. The S_{ex} anomaly is also related to the anomalous diffusivity increase with density due to Adam-Gibbs equation $D \propto \exp[-B/(TS_c)]$, where S_c is the configurational entropy [23].
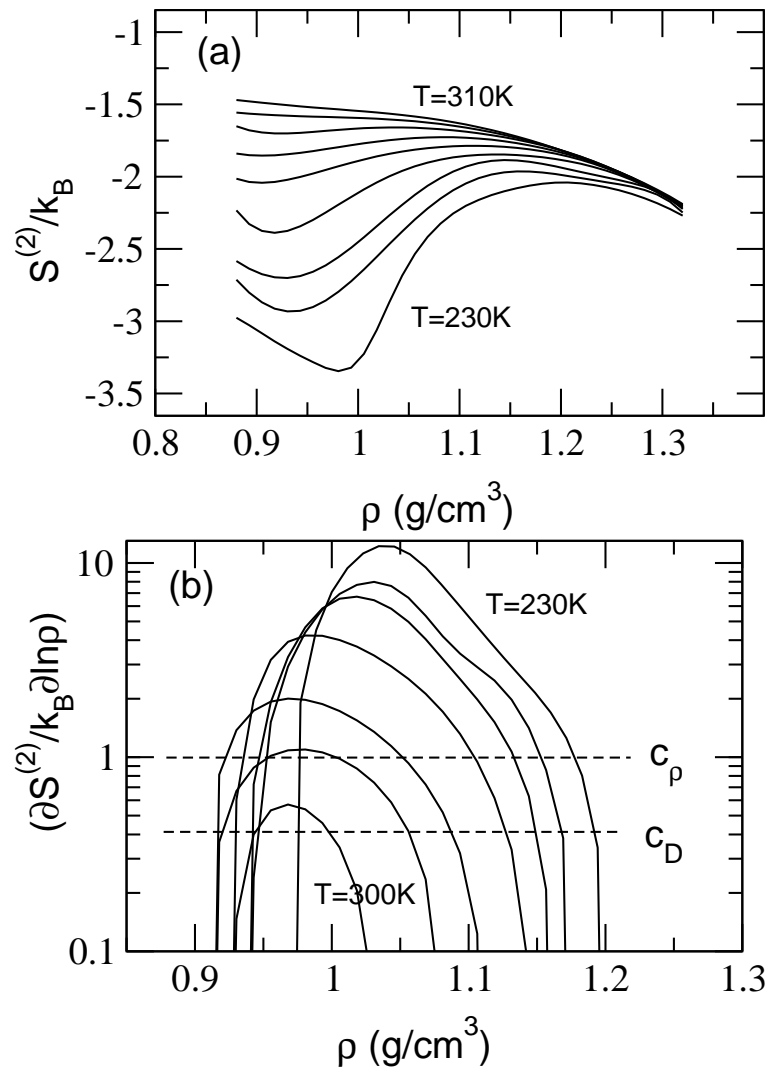
Figure 6.2: Excess entropy of the TIP5P model of water $S^{(2)}$. (a) Temperature and density dependence of $S^{(2)}$. From bottom to top, the isotherms correspond to $T = 230, 240, 259, 260, 270, 280, 290, 300, 310$ K. (b) Temperature and density dependence of $(\frac{\partial S^{(2)}}{\partial \ln \rho})_T$. From top to bottom, the isotherms correspond to $T = 230, 240, 259, 260, 270, 280, 290, 300$ K. The horizontal lines indicate the values of $(\frac{\partial S^{(2)}}{\partial \ln \rho})_T$ above which there is anomalous behavior of ρ and D respectively (see discussion below Eq.(6.5)). Note that $(\frac{\partial S^{(2)}}{\partial \ln \rho})_T$ is plotted in log scale, therefore only positive values can be seen, so the curve for $T = 310$ K is not shown.

6.3   Anomalies are Quantitatively Related to Excess Entropy

Ref. [88] has shown that in order to have waterlike density and diffusivity anomalies, $(\frac{\partial S_{ex}}{\partial \ln \rho})_T$ needs to be larger than some specific value. Due to the Maxwell relation, the density anomaly $(\frac{\partial \rho}{\partial T})_P > 0$ is equivalent to the entropy anomaly $(\frac{\partial S}{\partial \rho})_T > 0$. Thus from the definition of excess entropy in Eq. (6.1), it follows that $(\frac{\partial S_{ex}}{\partial \ln \rho})_T > c\ k_B$ with $c = 1$. From the empirical Rosenfied scaling relationship between diffusivity and excess entropy $D\frac{\rho^{1/3}}{T^{1/2}} = 0.6\ \exp(0.8 S_{ex}/k_B)$ established for various liquids [104], it follows that $(\frac{\partial S_{ex}}{\partial \ln \rho})_T > c\ k_B$ with $c = 0.42$ is a necessary condition for the diffusion anomaly.

Therefore the condition to have density and diffusivity anomalies can be written as

$$(\frac{\partial S_{ex}}{\partial \ln \rho})_T > c\ k_B, \tag{6.5}$$

where for the density anomaly $c = c_\rho = 1$, and for the diffusivity anomaly $c = c_D = 0.42$ [88]. To predict the regions of density and diffusivity anomalies, we show density and temperature dependence of $(\frac{\partial S^{(2)}}{k_B \partial \ln \rho})_T$ in Fig.6.2(b). The anomalous regions for density and diffusivity can be identified by finding the range of density between which the value of $(\frac{\partial S^{(2)}}{k_B \partial \ln \rho})_T$ for different T is greater than c_ρ or c_D, respectively.

Figure 6.3(a) and Figure 6.3(b) compare the regions of anomalies for density and diffusivity, respectively, in $T - \rho$ plane with the predictions of Eq. (6.5) (open symbols). Figure 6.3(c) compares the regions of structural anomaly quantified by the anomalous behavior of S_{ex} and the order parameters t and q obtained from MD simulations. These results indicate that Eq.(6.5), not only relates the behavior of the excess entropy to the anomalies in spherically symmetric ramp model [88], but also applies to water. It would be interesting to test the results of our simulation using experimental data on the O-O PCF for a wide range of temperatures and densities.
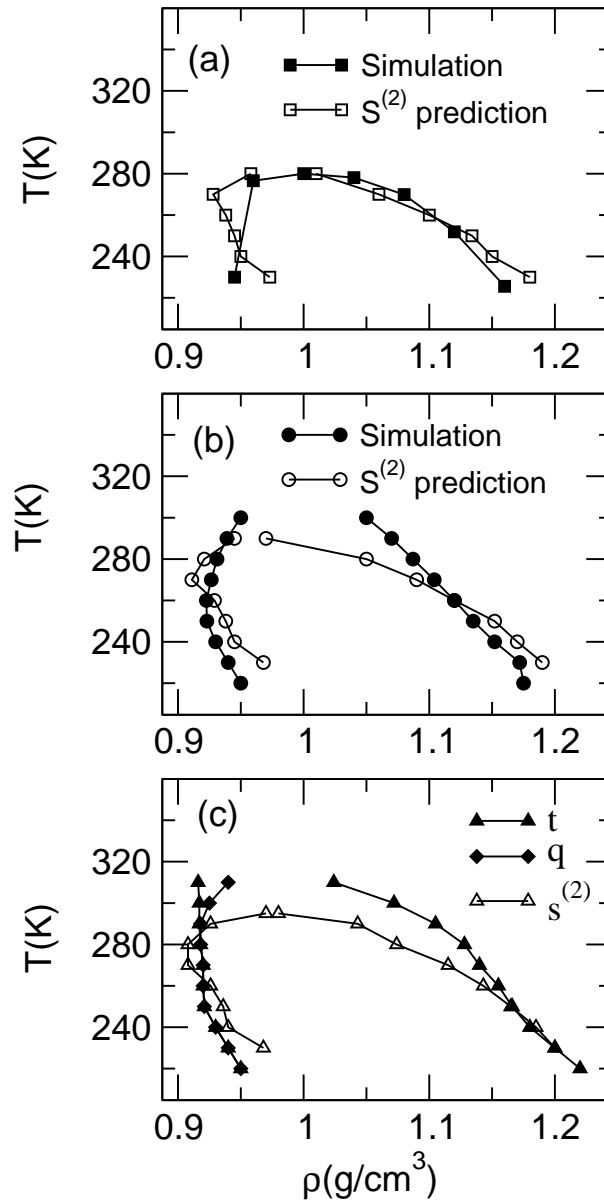
Figure 6.3: Comparison of the boundaries of anomalous regions with the prediction based on the excess entropy calculation within $T - \rho$ plane for TIP5P water. (a) Density anomaly region. (b) Diffusion anomaly region. Filled symbols are results based on MD simulations and open symbols are results based on the prediction of Eq.(6.5). (c) Comparison of the loci of excess entropy extrema from Fig. 6.2 with the structural anomaly regions found by MD simulations. The open triangles denote the loci of excess entropy $S^{(2)}$ extrema. The filled triangles denote the loci of extrema of translational order t. The filled diamonds denote loci of maxima of orientational order q.

6.4 Widom Line is Quantitatively Related to Excess Entropy

Near the critical point, the total correlation function $h(r) \equiv g(r) - 1$ has an asymptotic behavior for $r \to \infty$ [91]

$$h(r) \sim r^{-(d-2+\eta)} \exp(-r/\xi), \qquad (6.6)$$

where ξ is the correlation length, d is dimension (3 in our case) and $\eta \approx 0$ is correlation function decay exponent. So using Eq.(6.6), we can rewrite Eq.(6.4) as

$$\begin{aligned} S^{(2)} &\approx -2\pi\rho \int |h(r)|^2 r^2 dr \\ &\sim -2\pi\rho \int \exp(-2r/\xi) dr = -\pi\rho\xi. \end{aligned}$$

We find

$$(\frac{\partial S^{(2)}}{\partial \rho})_T \sim \xi + \rho(\frac{\partial \xi}{\partial \rho})_T = \xi + \rho(\frac{\partial \xi}{\partial P})_T(\frac{\partial P}{\partial \rho})_T. \qquad (6.7)$$

Near the critical point of fluids, the scaling law between P and ρ can be expressed as $|P - P_c| = A|\rho - \rho_c|^\delta$, where A is constant, P_c and ρ_c are critical pressure and density, and $\delta \approx 5$ is the critical exponent [91]. Therefore the term $(\frac{\partial P}{\partial \rho})_T \propto |\rho - \rho_c|^4 \to 0$ upon approaching ρ_c. Eq.(6.7) suggests that we can estimate the Widom line of water by finding the maximum of $(\frac{\partial S^{(2)}}{\partial \rho})$, since the Widom line corresponds to the locus of maxima of the correlation length.

Figure 6.4(a) shows that $(\frac{\partial S^{(2)}}{\partial \rho})_T$ as function of density and temperature reaches a maximum at a specific density $\rho_{max}(T)$ along fixed T path, or reach a maximum at a specific temperature $T_{max}(\rho)$ along fixed ρ path. The contour plot of $(\frac{\partial S^{(2)}}{\partial \rho})_T$ in Fig.6.4(b) predicts two lines corresponding to the loci of maxima in $(\frac{\partial S^{(2)}}{\partial \rho})_T$ along constant-T and constant-ρ paths. These two (bold) lines asymptotically approach each other as they come closer to the critical point. The common asymptote provides quantitative prediction of the Widom line based on the excess entropy. Therefore the excess entropy computed from O-O PCF can predict the location of the Widom line

and therefore the approximate location of other response functions maxima, such as C_P, K_T. The excess entropy can also predict the location of the dynamic transition from fragile to strong behavior in the supercooled water [11].

The relationship between configurational entropy S_c and diffusivity D of water is known to be well approximated by the Adam-Gibbs equation [23]. A different relation between S_{ex} and D was proposed for water-like core-softened repulsive simple potential liquid and binary Lennard-Jones alloy [109] and SPC/E water [103]: $D(T) \propto \exp[b(\rho)S_{ex}]$, where $b(\rho)$ is a T-independent parameter and ρ is constant. Our calculation (Fig. 6.5) confirms these results for the TIP5P water.

In summary using the TIP5P potential (five-site transferable intermolecular potential) we perform molecular dynamics simulations to investigate the relationship between the excess entropy and anomalies of water. We find that the two-body excess entropy is an ideal quantity to predict the regions of structural, dynamic and thermodynamic anomalies of water in its pressure-temperature and density-temperature phase diagrams. From the excess entropy we can also predict the location of the Widom line, associated with the hypothesized liquid-liquid critical point in supercooled water. Our results implies that it is possible to estimate the thermodynamic and dynamic anomalies of liquid from the structural change, and it is also possible to relate structural change to the correlation length maximum and therefore the hypothesized LDL/HDL critical point.
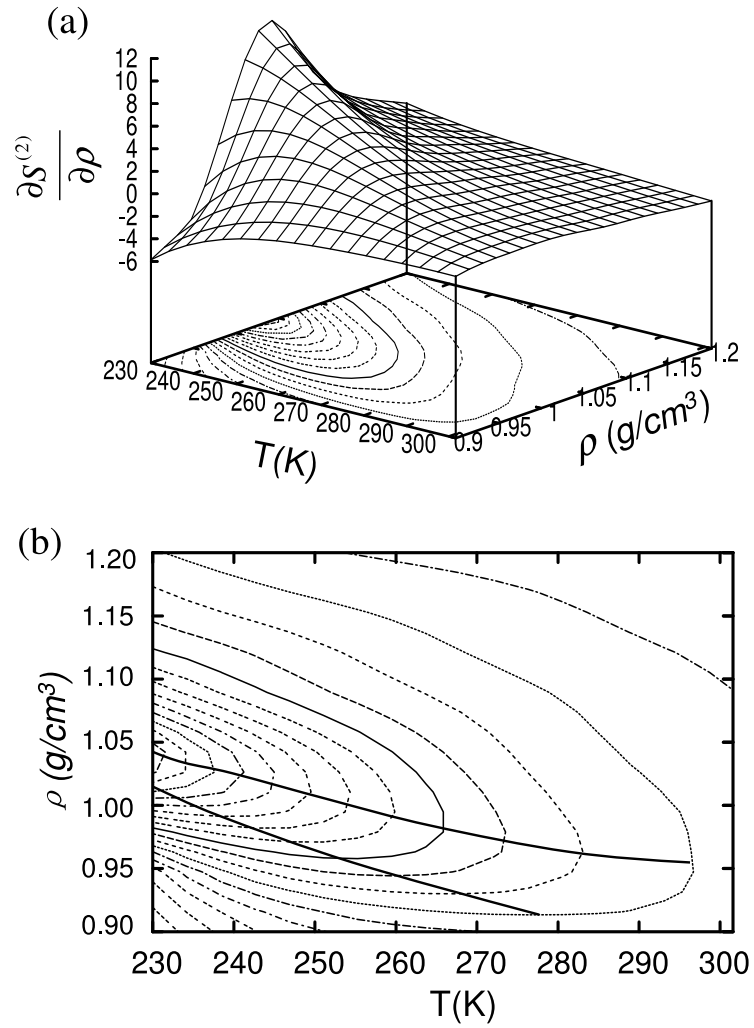
Figure 6.4: (a) The 3D plot shows the the temperature and density dependence of $(\frac{\partial S^{(2)}}{\partial \rho})_T$ with the contour plot projected on the $T - \rho$ plane. There is a locus of the maximum in $(\frac{\partial S^{(2)}}{\partial \rho})_T$ along the constant-T path and constant-ρ path. (b) The 2D contour plot of $(\frac{\partial S^{(2)}}{\partial \rho})_T$ shows that the locus of the maximum in $(\frac{\partial S^{(2)}}{\partial \rho})_T$ forms two lines (the bold lines) along constant-T path and constant-ρ path respectively.
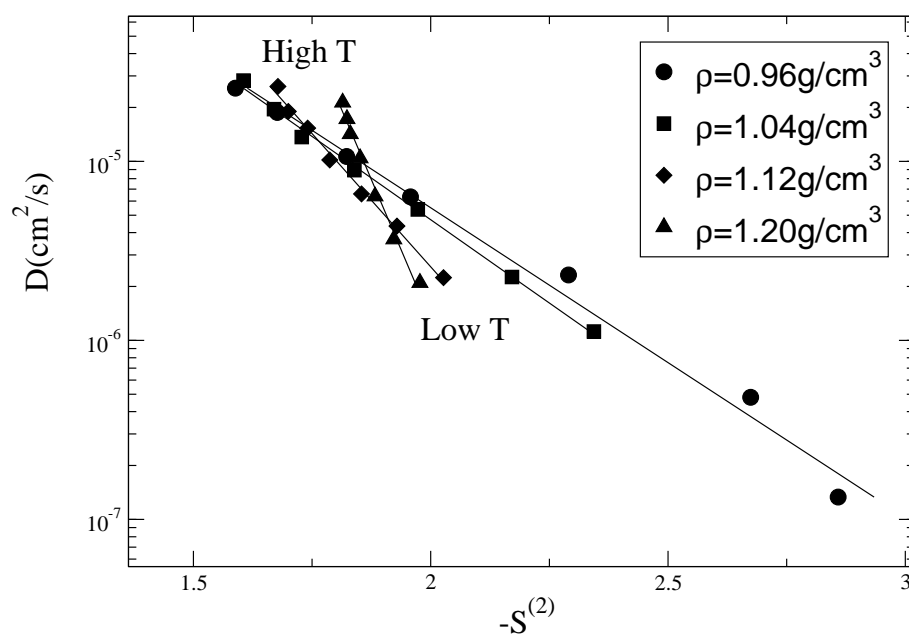
Figure 6.5: The relation between diffusivity and the negative of the excess entropy of water along isochores. The temperature range for each density is 240-300 K.

Appendix A

Molecular Dynamics Simulation

A.1 Temperature Computation in MD

The total energy of our system is defined as:

$$E_{tot} = \langle K \rangle + \langle U \rangle \ , \tag{A.1}$$

where K and U are the kinetic and potential energy, respectively. The kinetic energy is a sum of contributions from the individual particle $|p_i|^2/(2m_i)$, while the evaluation of the potential contribution involves summing over all pairs of interacting particles

$$\langle U \rangle = \sum U_{ij} \ . \tag{A.2}$$

For a three dimensional system of interacting hard-sphere particles, we have

$$\langle \sum_{i=1}^{N} |\vec{p_i}|^2/m_i \rangle = 2\langle K \rangle = 3Nk_BT \ , \tag{A.3}$$

where momentum of particle i is $\vec{p_i} = m_i\vec{v_i}$. The temperature in the system T is calculated according to Eq. (A.3) and the instantaneous temperature can be defined as

$$T = 2K/3Nk_B = \frac{1}{3Nk_B} \sum_{i=1}^{N} |\vec{p_i}|^2/m_i \ . \tag{A.4}$$

94

To maintain the temperature constant or to slowly cool the system down, we use the Berendson [110] method of velocity rescaling, multiplying all the velocities at each time step Δt by a factor $\sqrt{T'/T}$, which is determined by

$$\frac{T'}{T} = \left(1 + \frac{T_o}{T}(\kappa \Delta t) - \kappa \Delta t\right) . \tag{A.5}$$

Therefore, we use the relation

$$T' = T(1 - \kappa \Delta t) + \kappa \Delta t T_o , \tag{A.6}$$

where T_o is the temperature of the heat bath, T the instantaneous temperature before rescaling, T' the instantaneous temperature after rescaling, and κ the heat exchange coefficient. We choose $\kappa = 0.01$ to keep the temperature constant and $\kappa = 0.0001$ to slowly cool the system down. We calculate the time interval Δt as the time interval during which exactly N collisions occur. Average Δt is thus equal to two average collision intervals in a system.

A.2 Pressure Computation in MD

It is believed that the true thermodynamics average of a quantity f can be achieved in MD by averaging over sufficiently large time Δt,

$$\langle f \rangle_{\Delta t} \equiv \frac{\ell}{\Delta t} \int_t^{t+\Delta t} f(t) dt . \tag{A.7}$$

The calculation of pressure in MD has another difficulty, since in MD periodic boundaries are used and there are no container walls to create external pressure on the system. Nevertheless, pressure can be effectively computed using the virial theorem, which relates the time average of the total kinetic energy to the time average of the virial.

In classical mechanics, it can be proven that for any system kept for a sufficiently long period of time Δt in a finite region of the 6N dimensional phase space,

$$\left\langle \sum_{i=1}^{N} \frac{m_i v_i^2}{2} \right\rangle_{\Delta t} = -\left\langle \sum_{i=1}^{N} \frac{\vec{f_i} \cdot \vec{r_i}}{2} \right\rangle_{\Delta t} , \tag{A.8}$$

where $\vec{f}_i$ are the forces acting on the particles, $\vec{v}_i$ are the particle velocities, and $\vec{r}_i$ are the particle coordinates. The virial which is the right hand side of Eq. (A.8) can be presented as the contribution from external forces acting from the walls of the container and intermolecular forces

$$\vec{f}_i = \vec{f}_i^{\text{ext}} + \vec{f}_i^{\text{int}}; \tag{A.9}$$

$$\sum_{i=1}^{N} \vec{f}_i \cdot \vec{r}_i = \sum_{i=1}^{N} \vec{f}_i^{\text{int}} \cdot \vec{r}_i + \sum_{i=1}^{N} \vec{f}_i^{\text{ext}} \cdot \vec{r}_i . \tag{A.10}$$

For a liquid confined in a container with rigid walls in the absence of such external fields as gravity, the pressure acts perpendicular to the surface, pointing inside the container and is constant at any point of the surface. Thus

$$\left\langle \sum_{i=1}^{N} \vec{f}_i^{\text{ext}} \cdot \vec{r}_i \right\rangle = - \int_S dP \vec{r} \cdot \vec{n} dS = -PVd , \tag{A.11}$$

where n is normal to the surface, d is the dimensionality, and the integral is taken over the surface of the container S, where dS is the surface element. Combining Eqs. (A.8), (A.10), and (A.11) we have

$$P = \frac{2}{VD} \left\langle \sum_{i=1}^{N} \frac{m_i v_i^2}{2} \right\rangle_{\Delta t} - \frac{1}{VD} \left\langle \sum_{i=1}^{N} \vec{f}_i^{\text{int}} \cdot \vec{r}_i \right\rangle_{\Delta t} . \tag{A.12}$$

Note that $\sum_{i=1}^{N} m_i v_i^2 / 2$ is, by definition, equal to $(D/2)k_B NT$ and

$$P = \frac{NK_B}{V} \langle T \rangle_{\Delta t} - \frac{1}{VD} \left\langle \sum_{i=1}^{N} \vec{f}_i^{\text{int}} r_i \right\rangle_{\Delta t} . \tag{A.13}$$

When the system has walls, this equation gives the value of the pressure acting from the walls to the system. In the absence of walls, it gives the value of the internal pressure in the system. Thus this equation provides the basis for the computation of pressure in molecular dynamics simulations.

In discrete molecular dynamics, the force f_i^{int} is equal to zero except at the moments of collision with other particles, when it is equal to infinity. We count all the collisions of a given particle i with a given particle j that occur in the time interval

from t to $t + \Delta t$, using index $K_{ij} = 1, 2, 3, \ldots$ We denote the times of these collisions $t_{K_{ij}}$ and the change in momentum in particle i at the moment $t_{K_{ij}}$ as

$$\Delta \vec{P}_{K_{ij}} = m_i[\vec{v}_i(t_{K_{ij}} + \epsilon) - \vec{v}_i(t_{K_{ij}} - \epsilon)] \, , \tag{A.14}$$

where ϵ is an infinitesimally small value. Since the force acting on the particle i is the derivative of momentum with respect to time,

$$f_i^{\text{int}} = \sum_{j=1}^{N} \sum_{K_{ij}} \Delta P_{K_{ij}} \delta(t - t_{K_{ij}}) \, , \tag{A.15}$$

where $\delta(t - t_{K_{ij}})$ is a Dirac δ-function and the sum over K_{ij} is taken over all collisions between particle i and j during time interval $(t, t + \Delta t)$.

Integration involved in the averaging over time [see Eq. (A.7)] eliminates δ-functions and we obtain

$$P = \frac{NK_b}{V} \langle T \rangle_{\Delta t} - \frac{1}{\Delta t V D} \sum_{i=1}^{N} \sum_{K_{ij}} \sum_{j=1}^{N} (\Delta \vec{P}_{K_{ij}} \vec{r}_i) \, . \tag{A.16}$$

Finally, we can count all the collisions that occur in interval $(t, t + \Delta t)$ by index ℓ. Each collision is specified by the particles $i(\ell)$ and $j(\ell)$ involved in the collision $(i < j)$ and is counted twice in the sum of Eq. (A.16)—the first time when i is from the first sum and the second when i is from the second sum. According to momentum conservation, $\Delta P(\ell)i = -\Delta P(\ell)j$. Thus we rewrite (A.16) as

$$P = \frac{NK_b}{V} \langle T \rangle_{\Delta t} - \frac{1}{\Delta t V D} \sum_{\ell} \{\Delta \vec{P}_i(t_\ell)[\vec{r}_i(t_\ell) - \vec{r}_j(t_\ell)]\} \, , \tag{A.17}$$

where the sum is taken over all collisions ℓ that occur at moment t_ℓ during time interval Δt and

$$\Delta \vec{P}_i(\ell) = m_i[\vec{v}_i(t_\ell + \epsilon) - \vec{v}_i(t_\ell - \epsilon)] \, . \tag{A.18}$$

We use the Eq. (A.17) to compute the interval pressure in our system and record this value into a file at times which are multiples of Δt. We use $\Delta t = 100$, which corresponds to hundreds of collision intervals, so that the recorded pressure does not fluctuate much and it is also much smaller than the total simulation time, allowing us to perform the error analysis.

A.3   Discrete Molecular Dynamics

The molecular dynamics of molecules interacting via hard sphere discontinuous potentials, must be solved in a way which is qualitatively different form the molecular dynamics of soft bodies, such as Lennard-Jones type systems. Whenever the distance between two particles becomes equal to a point of discontinuity in the potential (i.e. at square-well distance or soft-core distance), then a collision occurs. Depending on the model, the particle velocities will suddenly change. The primary aim in the simulation is to locate the time, collision pairs, and all impact parameters for every collision occurring in the system, in chronological order.

Between collisions, particles move along straight lines with constant velocities. When the distance between the particles becomes equal to r, for which $U(r)$ has a discontinuity, the velocities of the interacting particles instantaneously change. The interaction time t_{ij} for two particles with coordinates $\vec{r}_i$, $\vec{r}_j$ and velocities $\vec{v}_i$, $\vec{v}_j$ satisfies the quadratic equation

$$(\vec{r}_{ij} + t_{ij}\vec{v}_{ij})^2 = R_{ij}^2,$$

where $R_{ij} = a, b, c$, depending on the initial distance between particles $\vec{r}_{ij} = \vec{r}_i - \vec{r}_j$ and their relative velocity $\vec{v}_{ij} = \vec{v}_i - \vec{v}_j$. This quadratic equation may have two positive roots, two negative roots, two roots of different signs, or no roots at all. The roots are determined by the formula

$$t_{ij} = \frac{-(\vec{v}_{ij}, \vec{r}_{ij}) \pm \sqrt{(\vec{v}_{ij}, \vec{r}_{ij})^2 + v_{ij}^2(R_{ij}^2 - r_{ij}^2)}}{v_{ij}^2},$$

where the sign is "plus" if roots have different signs or minus otherwise. The value of $R_{ij} = a, b, c$ is selected to minimize t_{ij}. If there are no positive roots, it means that the particles will not interact and $t_{ij} = \infty$.

We find the average particle collision interval

$$\delta t = \min_{i<j} t_{ij}$$

for all possible pairs of particles and propagate the system to time

$$t' = t + \delta t$$

so that

$$\vec{r'}_i = \vec{r}_i + \delta t \vec{v}_i.$$

At this moment, the distance between the centers of colliding particle-pairs becomes equal to a, b, or c.

Finally, we find the new velocities $\vec{v'}_i$ and $\vec{v'}_j$ after the interaction. These velocities must satisfy the momentum conservation law

$$m_i \vec{v}_i + m_j \vec{v}_j = m_i \vec{v'}_i + m_j \vec{v'}_j,$$

the angular momentum conservation law

$$m_i [\vec{r'}_i, \vec{v}_i] + m_j [\vec{r'}_j \vec{v}_j] = m_i [\vec{r'}_i, \vec{v'}_i] + m_j [\vec{r'}_j \vec{v'}_j],$$

and the energy conservation law

$$\frac{m_i v_i^2}{2} + \frac{m_j v_j^2}{2} + U_{ij} = \frac{m_i v_i'^2}{2} + \frac{m_j v_j'^2}{2} + U'_{ij},$$

where U_{ij} and U'_{ij}, are the values of the pair potential before and after interaction, equal to $U(R_{ij} \pm \epsilon)$, depending on the direction of the initial relative velocity $\vec{v}_{ij}$, initial distance $\vec{r}_{ij}$, and the value of R_{ij}. These equations are equivalent to six scalar equations, which are sufficient to determine the six unknown components of the velocities $\vec{v'}_i$ and $\vec{v'}_j$. Introducing a new coordinate system with the origin at the center of the particle j, and the x-axis collinear with the vector $\vec{r'}_{ij}$, we construct the expressions for the velocities that satisfy the momentum and the angular momentum conservation laws:

$$\vec{v'}_i = \vec{v}_i + A \vec{r'}_{ij} m_j,$$

$$\vec{v'}_j = \vec{v}_j - A \vec{r'}_{ij} m_i,$$

where constant A is determined from the energy conservation law:

$$A = a \frac{\pm \sqrt{1 + 2(U_{ij} - U'_{ij})(m_i + m_j)/(R_{ij}^2 a^2 m_i m_j)} - 1}{m_i + m_j},$$

where $a = (\vec{v}_{ij}, \vec{r}_{ij})/R_{ij}^2$. The sign "plus" in the expression for A corresponds to the motion after the collision in the same direction as before the collision, i.e., the particles penetrate into the attractive well or the soft core if they move toward each other before the collision, or leave them if they move away from each other. Note that this may happen only if the expression under the square root is positive, i.e, if there is enough kinetic energy to overcome the potential barrier

$$\frac{R_{ij}^2 a^2 m_i m_j}{2(m_i + m_j)} \geq U'_{ij} - U_{ij}.$$

Otherwise, the reflection happens, the particles do not change their state $U'_{ij} = U_{ij}$, and the sign in the expression for A must be "minus".

The minimization of the t_{ij} is optimized by dividing the system into small subsystems, so that collision times are computed only between particles in the neighboring subsystems. The final minimization is produced by a binary tree sorting among all the subsystems. In each collision, only the particles in the neighboring subsystems are updated. Each subsystem has its own collision table, in which the collision times and the indexes of colliding particles are recorded. After the collision, all the records involving colliding particles are removed from these tables and are replaced by the new records, corresponding to the new velocities. This optimization allows us to observe that the computational time grows as $N \ln N$.

A.4   Introduction to TIP5P Model

In this thesis, we present results obtained from molecular dynamics simulations using the TIP5P model for water. In the model, the molecules are rigid with two positive charges $q_1 = 0.241e$ located on each hydrogen atom and two negative charge $q_2 = -0.241e$ located on lone pair sites (see Fig. A.1).
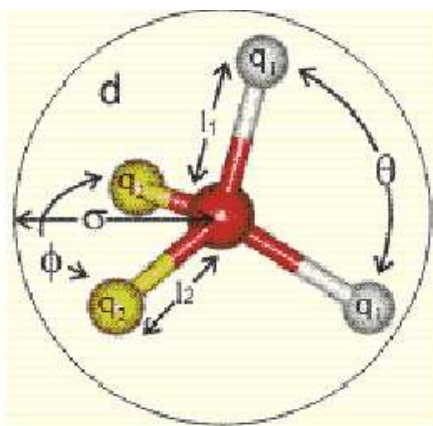
Figure A.1: TIP5P water model. In the TIP5P model water molecules are rigid with four point charges. Two positive charges $q_1 = 0.241e$ on each hydrogen atom and two negative charges with $q_2 = -q_1$ located on lone pairs. The OH distance is $l_1 = 0.09572$ nm and the O-lone pair distance is $l_2 = 0.070$ nm. The HOH angle is $\theta = 104.52^o$ and the lone pair-oxygen-lone pair angle is $\varphi = 109.47^o$. Oxygen atoms interact each other with a Lennard-Jones potential. (Figure from Prof. M. Chaplin http://www.lsbu.ac.uk/)

The distance between the oxygen and hydrogen atoms is $l_1 = 0.09572$ nm and the distance between the oxygen and the lone pair sites are $l_2 = 0.070$ nm. The hydrogen-oxygen-hydrogen angle is $\theta = 104.52^o$ and the lone pair-oxygen-lone pair angle is $\varphi = 109.47^o$. To avoid the overlapping the molecules, the model also use a Lennard-Jones potential between oxygen atoms,

$$V_{ij}(r) = 4\epsilon \left[\left(\frac{\sigma}{r_{ij}} \right)^{12} - \left(\frac{\sigma}{r_{ij}} \right)^{6} \right] \tag{A.19}$$

where rij is the distance between the $i-$th and $j-$th oxygen atoms. Here $\epsilon = 0.6694$ kJ/mol and $\sigma = 0.312$ nm.

The TIP5P water model is one the most used rigid-molecule pair-potential models for water, both for the study of the pure water simulations as well as for study of complex system such as solvation water of biomolecules (protein, DNA). It successfully reproduces experimental results, e.g., it shows a temperature of maximum density line in the phase diagram [79] and the temperature of maximum density at atmosphere pressure is $T = 277$ K, which is the best agreement with experiment among all water modles. It is also possibile to observe a liquid-crystal transition in water using MD simulation with TIP5P model [79], while it is very difficult to reproduce a crystalline phase with older model such as SPC/E model.

LIST OF JOURNAL ABBREVIATIONS

Phys. Rev. Lett.	Physical Review Letter
Phys. Rev. E	Physical Review E
Phys. Rev. B	Physical Review B
Phys. Rev. A	Physical Review A
J. Chem. Phys.	Journal of Chemical Physics
J. Phys. Chem.	Journal of Physical Chemistry
Phys. Chem. Chem. Phys.	Physical Chemistry Chemical Physics
Proc. Natl. Acad. Sci.	Proceedings of the National Academy of Sciences
Mol. Phys.	Molecular Physics
J. Stat. Phys.	Journal of Statistical Physics
J. Phys.: Condens. Matter	Journal of Physics: Condensed Matter
Faraday Disc.	Faraday Discussions

Bibliography

[1] P. V. Hobbs, *Ice Physics*, (Clarendon, Oxford, 1974).

[2] P. G. Debenedetti and H. E. Stanley, Supercooled and glassy water. Physics Today 56 (6), 40-46 (2003).

[3] O. Mishima and H. E. Stanley, Decompression-induced melting of ice IV and the liquid-liquid transition in water. Nature 392 (6672), 164-168 (1998).

[4] P. H. Poole, F. Sciortino, U. Essmann, and H. E. Stanley, Phase-Behavior of Metastable Water. Nature 360 (6402), 324-328 (1992).

[5] C. A. Angell, R. D. Bressel, M. Hemmati, E. J. Sare, and J. C. Tucker, Water and its anomalies in perspective: tetrahedral liquids with and without liquid-liquid phase transitions. Physical Chemistry Chemical Physics 2 (8), 1559-1566 (2000).

[6] Y. Katayama, T. Mizutani, W. Utsumi, O. Shimomura, M. Yamakata, and K. Funakoshi, A first-order liquid-liquid phase transition in phosphorus. Nature 403 (6766), 170-173 (2000).

[7] I. Saika-Voivod, F. Sciortino, and P. H. Poole, Computer simulations of liquid silica: Equation of state and liquid-liquid phase transition. Physical Review E 63 (1), 011202 (2001).

[8] S. Sastry and C. A. Angell, Liquid-liquid phase transition in supercooled silicon. Nature Materials 2 (11), 739-743 (2003).

[9] C. A. Angell, E. D. Finch, and P. Bach, Spin-echo diffusion coefficients of water to 2380 bar and -20 C. J. Chem. Phys. 65, 3063-3066 (1976).

[10] P. G. Debenedetti, *Metastable Liquids: Concepts and Principles* (Princeton University Press, Princeton, 1998).

[11] L. M. Xu, P. Kumar, S. V. Buldyrev, S. H. Chen, P. H. Poole, F. Sciortino, and H. E. Stanley, Relation between the Widom line and the dynamic crossover in systems with a liquid-liquid phase transition. Proceedings of the National Academy of Sciences of the United States of America 102 (46), 16558-16562 (2005); L. M. Xu, S. V. Buldyrev, C. A. Angell, and H. E. Stanley, Thermodynamics and dynamics of the two-scale spherically symmetric Jagla ramp model of anomalous liquids. Physical Review E 74 (3), 031108 (2006).

[12] A. B. de Oliveira, G. Franzese, P. A. Netz, and M. C. Barbosa, Waterlike hierarchy of anomalies in a continuous spherical shouldered potential. Journal of Chemical Physics 128 (6), 064901 (2008).

[13] H. E. Stanley, J. Teixeira, A. Geiger, and R. L. Blumberg, Interpretation of the Unusual Behavior of H2O and D2O at Low Temperature: Are Concepts of Percolation Relevant to the Puzzle of Liquid Water? Physica A 106, 260-277 (1981).

[14] P. A. Netz, F. W. Starr, H. E. Stanley, and M. C. Barbosa, Static and dynamic properties of stretched water. Journal of Chemical Physics 115 (1), 344-348 (2001).

[15] F. N. Keutsch and R. J. Saykally, Water clusters: Untangling the mysteries of the liquid, one molecule at a time. Proceedings of the National Academy of Sciences of the United States of America 98 (19), 10533-10540 (2001).

[16] J. D. Eaves, J. J. Loparo, C. J. Fecko, S. T. Roberts, A. Tokmakoff, and P. L. Geissler, Hydrogen bonds in liquid water are broken only fleetingly. Proceedings of the National Academy of Sciences of the United States of America 102 (37), 13019-13022 (2005).

[17] J. J. Loparo, S. T. Roberts, and A. Tokmakoff, Multidimensional infrared spectroscopy of water. I. Vibrational dynamics in two-dimensional IR line shapes. Journal of Chemical Physics 125 (19), 194521 (2006).

[18] J. J. Loparo, S. T. Roberts, and A. Tokmakoff, Multidimensional infrared spectroscopy of water. II. Hydrogen bond switching dynamics. Journal of Chemical Physics 125 (19), 194522 (2006).

[19] J. R. Errington and P. G. Debenedetti, Relationship between structural order and the anomalies of liquid water. Nature 409 (6818), 318-321 (2001).

[20] J. R. Errington, P. G. Debenedetti, and S. Torquato, Quantification of order in the Lennard-Jones system. Journal of Chemical Physics 118 (5), 2256-2263 (2003).

[21] Z. Y. Yan, S. V. Buldyrev, N. Giovambattista, and H. E. Stanley, Structural order for one-scale and two-scale potentials. Physical Review Letters 95 (13), 130604 (2005).

[22] A. K. Soper and M. A. Ricci, Structures of high-density and low-density water. Physical Review Letters 84 (13), 2881-2884 (2000); S. Klotz, G. Hamel, J. S. Loveday, R. J. Nelmes, M. Guthrie, and A. K. Soper, Structure of high-density amorphous ice under pressure. Physical Review Letters 89 (28), 285502 (2002).

[23] A. Scala, F. W. Starr, E. La Nave, F. Sciortino, and H. E. Stanley, Configurational entropy and diffusivity of supercooled water. Nature 406 (6792), 166-169 (2000).

[24] P. L. Chau and A. J. Hardwick, A new order parameter for tetrahedral configurations. Molecular Physics 93 (3), 511-518 (1998).

[25] S. Sastry, Water structure - Order and oddities. Nature 409 (6818), 300-301 (2001).

[26] S. Torquato, T. M. Truskett, and P. G. Debenedetti, Is random close packing of spheres well defined? Physical Review Letters 84 (10), 2064-2067 (2000).

[27] H. J. C. Berendsen, J. R. Grigera, and T. P. Straatsma, The Missing Term in Effective Pair Potentials. Journal of Physical Chemistry 91 (24), 6269-6271 (1987).

[28] M. S. Shell, P. G. Debenedetti, and A. Z. Panagiotopoulos, Molecular structural order and anomalies in liquid silica. Physical Review E 66 (1), 011202 (2002).

[29] T. M. Truskett, S. Torquato, and P. G. Debenedetti, Towards a quantification of disorder in materials: Distinguishing equilibrium and glassy sphere packings. Physical Review E 62 (1), 993-1001 (2000).

[30] P. J. Steinhardt, D. R. Nelson, and M. Ronchetti, Bond-Orientational Order in Liquids and Glasses. Physical Review B 28 (2), 784-805 (1983).

[31] Z. Y. Yan, S. V. Buldyrev, P. Kumar, N. Giovambattista, and H. E. Stanley, Correspondence between phase diagrams of the TIP5P water model and a spherically symmetric repulsive ramp potential with two characteristic length scales. Physical Review E 77 (4), 042201 (2008).

[32] P. C. Hemmer and G. Stell, Fluids with Several Phase Transitions, Phys. Rev. Lett. 24 (23), 1284 - 1287 (1970).

[33] F. H. Stillinger and D. K. Stillinger, Negative thermal expansion in the Gaussian core model. Physica A 244 (1-4), 358-369 (1997).

[34] E. A. Jagla, Core-softened potentials and the anomalous properties of water. Journal of Chemical Physics 111 (19), 8980-8986 (1999).

[35] E. A. Jagla, Low-temperature behavior of core-softened models: Water and silica behavior. Physical Review E 63 (6), 061509 (2001).

[36] M. R. Sadr-Lahijany, A. Scala, S. V. Buldyrev, and H. E. Stanley, Liquid-state anomalies and the Stell-Hemmer core-softened potential. Physical Review Letters 81 (22), 4895-4898 (1998); M. R. Sadr-Lahijany, A. Scala, S. V. Buldyrev, and H. E. Stanley, Waterlike anomalies for core-softened models of fluids: One dimension. Physical Review E 60 (6), 6714-6721 (1999).

[37] A. Scala, M. R. Sadr-Lahijany, N. Giovambattista, S. V. Buldyrev, and H. E. Stanley, Applications of the Stell-Hemmer potential to understanding second critical points in real systems. Journal of Statistical Physics 100 (1-2), 97-106 (2000); A. Scala, M. R. Sadr-Lahijany, N. Giovambattista, S. V. Buldyrev, and H. E. Stanley, Waterlike anomalies for core-softened models of fluids: Two-dimensional systems. Physical Review E 63 (4), 041202 (2001).

[38] G. Franzese, G. Franzese, G. Malescio, A. Skibinsky, S. V. Buldyrev, and H. E. Stanley, Generic mechanism for generating a liquid-liquid phase transition. Nature 409 (6821), 692-695 (2001); G. Franzese, G. Malescio, A. Skibinsky, S. V. Buldyrev, and H. E. Stanley, Metastable liquid-liquid phase transition in a single-component system with only one crystal phase and no density anomaly. Physical Review E 66 (5), 051206 (2002).

[39] P. Kumar, S. V. Buldyrev, F. W. Starr, N. Giovambattista, and H. E. Stanley, Thermodynamics, structure, and dynamics of water confined between hydrophobic plates. Physical Review E 72 (5), 021501 (2005).

[40] P. G. Debenedetti, V. S. Raghavan, and S. S. Borick, Spinodal Curve of Some Supercooled Liquids. Journal of Physical Chemistry 95 (11), 4540-4551 (1991).

[41] G. Stell and P. C. Hemmer, Phase Transitions Due to Softness of the Potential Core. J. Chem. Phys. 56 (9), 4274-4286 (1972).

[42] A. B. de Oliveira, P. A. Netz, T. Colla, and M. C. Barbosa, Structural anomalies for a three dimensional isotropic core-softened potential. Journal of Chemical Physics 125 (12), 124503 (2006).

[43] S. V. Buldyrev et al., G. Franzese, N. Giovambattista, G. Malescio, M. R. Sadr-Lahijany, A. Scala, A. Skibinsky, and H. E. Stanley, in *New Kinds of Phase Transitions: Transformations in Disordered Substances*, NATO Advanced Research Workshop, Volga River, edited by V. Brazhkin et al., S. V. Buldyrev, V. Ryzhov, and H. E. Stanley (Kluwer, Dordrecht, 2002), pp. 97–120.

[44] A. Huerta, G. G. Naumis, D. T. Wasan, D. Henderson, and A. Trokhymchuk, Attraction-driven disorder in a hard-core colloidal monolayer. Journal of Chemical Physics 120 (3), 1506-1510 (2004).

[45] In Refs. [20, 26, 29], $\overline{Y}_{\ell m}(\theta, \varphi)$ denotes the average over *all* the bonds in the *system*, and the orientational order is defined for the whole system, and not just for single molecules. However, for water and silica [19, 28] the orientational order is defined for each molecule and its average is used.

[46] J. M. Kincaid, G. Stell and C. K. Hall, Isostructural phase transitions due to core collapse. I. A one-dimensional model. J. Chem. Phys. 65 (6), 2161-2171 (1976).

[47] J. M. Kincaid, G. Stell and E. Goldmark, Isostructural phase transitions due to core collapse. II. A three-dimensional model with a solidCsolid critical poin. J. Chem. Phys. 65 () 2172-2179 (1976).

[48] J. M. Kincaid and G. Stell, Isostructural phase transitions due to core collapse. III. A model for solid mixtures. J. Chem. Phys. 67 (2), 420-429 (1977).

[49] M. P. Allen and D. J. Tildesley, *Computer Simulation of Liquids* (Clarendon Press, Oxford, 1990).

[50] C. N. Likos, A. Lang, M. Watzlawek, and H. Lowen, Criterion for determining clustering versus reentrant melting behavior for bounded interaction potentials. Physical Review E 63 (3), 031206 (2001).

[51] F. Sciortino, A. Geiger, and H. E. Stanley, Network Defects and Molecular Mobility in Liquid Water. Journal of Chemical Physics 96 (5), 3857-3865 (1992).

[52] F. F. Stillinger, Phase transitions in the Gaussian core system. J. Chem. Phys. 65 (10), 3968-3974 (1976).

[53] S. Sastry, P. G. Debenedetti, F. Sciortino, and H. E. Stanley, Singularity-free interpretation of the thermodynamics of supercooled water. Physical Review E 53 (6), 6144-6154 (1996).

[54] Y. Katayama, Y. Inamura, T. Mizutani, M. Yamakata, W. Utsumi, and O. Shimomura, Macroscopic separation of dense fluid phase and liquid phase of phosphorus. Science 306 (5697), 848-851 (2004).

[55] R. Kurita and H. Tanaka, On the abundance and general nature of the liquid-liquid phase transition in molecular systems. Journal of Physics-Condensed Matter 17 (27), L293-L302 (2005).

[56] R. Kurita and H. Tanaka, Critical-like phenomena associated with liquid-liquid transition in a molecular liquid. Science 306 (5697), 845-848 (2004).

[57] O. Mishima, Liquid-liquid critical point in heavy water. Physical Review Letters 85 (2), 334-336 (2000).

[58] O. Mishima and Y. Suzuki, Propagation of the polyamorphic transition of ice and the liquid-liquid critical point. Nature 419 (6907), 599-603 (2002).

[59] D. J. Lacks, First-order amorphous-amorphous transformation in silica. Physical Review Letters 84 (20), 4629-4632 (2000).

[60] J. N. Glosli and F. H. Ree, Liquid-liquid phase transformation in carbon. Physical Review Letters 82 (23), 4659-4662 (1999).

[61] S. Harrington, R. Zhang, P. H. Poole, F. Sciortino, and H. E. Stanley, Liquid-liquid phase transition: Evidence from simulations. Physical Review Letters 78 (12), 2409-2412 (1997).

[62] M. Yamada, H. E. Stanley, and F. Sciortino, Equation of state of supercooled water from the sedimentation profile. Physical Review E 67 (1), 010202(R) (2003).

[63] P. H. Poole, I. Saika-Voivod, and F. Sciortino, Density minimum and liquid-liquid phase transition. Journal of Physics-Condensed Matter 17 (43), L431-L437 (2005).

[64] M. Yamada, S. Mossa, H. E. Stanley, and F. Sciortino, Interplay between time-temperature transformation and the liquid-liquid phase transition in water. Physical Review Letters 88 (19), 195701 (2002).

[65] I. Brovchenko, A. Geiger, and A. Oleinikova, Multiple liquid-liquid transitions in supercooled water. Journal of Chemical Physics 118 (21), 9473-9476 (2003).

[66] I. Brovchenko, A. Geiger, and A. Oleinikova, Liquid-liquid phase transitions in supercooled water studied by computer simulations of various water models. Journal of Chemical Physics 123 (4), 044515 (2005).

[67] P. H. Poole, T. Grande, C. A. Angell, and P. F. McMillan, Polymorphic phase transitions in liquids and glasses. Science 275 (5298), 322-323 (1997).

[68] J. L. Yarger and G. H. Wolf, Chemistry - Polymorphism in liquids. Science 306 (5697), 820-821 (2004).

[69] L. Bosio, S. H. Chen, and J. Teixeira, Isochoric Temperature Differential of the X-Ray Structure Factor and Structural Rearrangements in Low-Temperature Heavy-Water. Physical Review A 27 (3), 1468-1475 (1983).

[70] S. Klotz, G. Hamel, J. S. Loveday, R. J. Nelmes, M. Guthrie, and A. K. Soper, Structure of high-density amorphous ice under pressure. Physical Review Letters 89 (28), 285502 (2002).

[71] A. Botti, F. Bruni, A. Isopo, M. A. Ricci, and A. K. Soper, Experimental determination of the site-site radial distribution functions of supercooled ultrapure bulk water. Journal of Chemical Physics 117 (13), 6196-6199 (2002).

[72] T. Strassle, A. M. Saitta, Y. Le Godec, G. Hamel, S. Klotz, J. S. Loveday, and R. J. Nelmes, Structure of dense liquid water by neutron scattering to 6.5 GPa and 670 K. Physical Review Letters 96 (6), 067801 (2006).

[73] M. Canpolat, F. W. Starr, A. Scala, M. R. Sadr-Lahijany, O. Mishima, S. Havlin, and H. E. Stanley, Local structural heterogeneities in liquid water under pressure. Chemical Physics Letters 294 (1-3), 9-12 (1998).

[74] E. Schwegler, G. Galli, and F. Gygi, Water under pressure. Physical Review Letters 84 (11), 2429-2432 (2000).

[75] E. Schwegler, G. Galli, F. Gygi, and R. Q. Hood, Dissociation of water under pressure. Physical Review Letters 87 (26), 265501 (2001).

[76] A. M. Saitta and F. Datchi, Structure and phase diagram of high-density water: The role of interstitial molecules. Physical Review E 67 (2), 020201(R) (2003).

[77] F. Sciortino, A. Geiger, and H. E. Stanley, Isochoric Differential Scattering Functions in Liquid Water - the 5th Neighbor as a Network Defect. Physical Review Letters 65 (27), 3452-3455 (1990).

[78] C. H. Cho, S. Singh, and G. W. Robinson, An explanation of the density maximum in water. Physical Review Letters 76 (10), 1651-1654 (1996); C. H. Cho, S. Singh, and G. W. Robinson, Liquid water and biological systems: The most important problem in science that hardly anyone wants to see solved. Faraday Discussions (103), 19-27 (1996).

[79] M. W. Mahoney and W. L. Jorgensen, A five-site model for liquid water and the reproduction of the density anomaly by rigid, nonpolarizable potential functions. Journal of Chemical Physics 112 (20), 8910-8922 (2000).

[80] C. Vega, E. Sanz, and J. L. F. Abascal, The melting temperature of the most common models of water. Journal of Chemical Physics 122 (11), 114507 (2005).

[81] F. Sciortino, A. Geiger, and H. E. Stanley, Effect of Defects on Molecular Mobility in Liquid Water. Nature 354 (6350), 218-221 (1991).

[82] V. Molinero, S. Sastry, and C. A. Angell, Tuning of tetrahedrality in a silicon potential yields a series of monatomic (metal-like) glass formers of very high fragility. Physical Review Letters 97 (7), 075701 (2006).

[83] M. Esposito and S. Mukamel, Fluctuation theorems for quantum master equations. Physical Review E 73 (4), 040502 (2006).

[84] M. R. Sadr-Lahijany, A. Scala, S. V. Buldyrev, and H. E. Stanley, Liquid-state anomalies and the stell-hemmer core-softened potential. Physical Review Letters 81 (22), 4895-4898 (1998).

[85] N. B. Wilding and J. E. Magee, Phase behavior and thermodynamic anomalies of core-softened fluids. Physical Review E 66 (3), 031509 (2002).

[86] Z. Y. Yan, S. V. Buldyrev, N. Giovambattista, P. G. Debenedetti, and H. E. Stanley, Family of tunable spherically symmetric potentials that span the range

from hard spheres to waterlike behavior. Physical Review E 73 (5), 051204 (2006).

[87] R. Sharma, S. N. Chakraborty, and C. Chakravarty, Entropy, diffusivity, and structural order in liquids with waterlike anomalies. Journal of Chemical Physics 125 (20), 204501 (2006).

[88] R. Sharma, S. N. Chakraborty, and C. Chakravarty, Entropy, diffusivity, and structural order in liquids with waterlike anomalies. Journal of Chemical Physics 125 (20), 244502 (2006).

[89] Z. Y. Yan, S. V. Buldyrev, P. Kumar, N. Giovambattista, P. G. Debenedetti, and H. E. Stanley, Structure of the first- and second-neighbor shells of simulated water: Quantitative relation to translational and orientational order. Physical Review E 76 (5), 051201 (2007).

[90] T. Headgordon and F. H. Stillinger, An Orientational Perturbation-Theory for Pure Liquid Water. Journal of Chemical Physics 98 (4), 3313-3327 (1993).

[91] J.P Hansen and I. R. McDonald, *Theory of Simple Liquids* (Academic, London, 1986).

[92] M. E. Johnson, T. Head-Gordon, and A. A. Louis, Representability problems for coarse-grained water potentials. Journal of Chemical Physics 126 (14), 144509 (2007).

[93] G. E. Walrafen, Raman spectral studies of water structure. J. Chem. Phys. 40 (11), 3249-3256 (1964).

[94] The pressure is defined as $P = nkT+ < W(N)/3V >$, where $W(N)$ is the virial expression and n is the number density [see, e.g., M. P. Allen and D. J. Tildesley, *Computer simulations of liquids*, Oxford University Press., New

York, 2004]. Therefore in the present case the ramp potential number density doubles, the values of pressure also doubles.

[95] See data from IAPWS (http://www.iapws.org/relguide/fundam.pdf).

[96] H. E. Stanley, M. C. Barbosa, S. Mossa, P. A. Netz, F. Sciortino, F. W. Starr, and M. Yamada, Statistical Physics and Liquid Water at Negative Pressures, Physica A 315 (1), 281-290 (2002).

[97] S. B. Kiselev and J. F. Ely, Parametric crossover model and physical limit of stability in supercooled water. Journal of Chemical Physics 116 (13), 5657-5665 (2002).

[98] D. Paschek, How the liquid-liquid transition affects hydrophobic hydration in deeply supercooled water. Physical Review Letters 94 (21), 217802 (2005).

[99] S. Harrington, P. H. Poole, F. Sciortino, and H. E. Stanley, Equation of state of supercooled water simulated using the extended simple point charge intermolecular potential. Journal of Chemical Physics 107 (18), 7443-7450 (1997).

[100] P. Kumar, S. V. Buldyrev, S. R. Becker, P. H. Poole, F. W. Starr, and H. E. Stanley, Relation between the Widom line and the breakdown of the Stokes-Einstein relation in supercooled water. Proceedings of the National Academy of Sciences of the United States of America 104 (23), 9575-9579 (2007).

[101] A. B. Oliveira, G. Franzese, P. A. Netz, and M. C. Barbosa, J. Chem. Phys. **128**, 064901 (2008).

[102] W. P. Krekelberg, J. Mittal, V. Ganesan, and T. M. Truskett, Structural anomalies of fluids: Origins in second and higher coordination shells. Physical Review E 77 (4), 041201 (2008).

[103] J. Mittal, J. R. Errington, and T. M. Truskett, Quantitative link between single-particle dynamics and static structure of supercooled liquids. Journal of Physical Chemistry B 110 (37), 18147-18150 (2006).

[104] Y. Rosenfeld, Relation between the transport coefficients and the internal entropy of simple systems. Phys. Rev. A 15 (6), 2545-2549 (1977).

[105] R. E. Nettleton and M. S. Green, Expression in Terms of Molecular Distribution Functions for the Entropy Density in an Infinite System. J. Chem. Phys. 29 (6), 1365-1370 (1958).

[106] A. Baranyai and D. J. Evans, Direct Entropy Calculation from Computer-Simulation of Liquids. Physical Review A 40 (7), 3817-3822 (1989).

[107] J. L. Bretonnet, Self-diffusion coefficient of dense fluids from the pair correlation function. Journal of Chemical Physics 117 (20), 9370-9373 (2002).

[108] I. Yokoyama, On Dzugutov's scaling law for atomic diffusion in condensed matter. Physica B 269 (3-4), 244-248 (1999).

[109] J. Mittal, J. R. Errington, and T. M. Truskett, Relationship between thermo-dynamics and dynamics of supercooled liquids. Journal of Chemical Physics 125 (7), 076102 (2006).

[110] H. J. C. Berendsen, J. P. M. Postma, W. F. Vangunsteren, A. Dinola, and J. R. Haak, Molecular-Dynamics with Coupling to an External Bath. Journal of Chemical Physics 81 (8), 3684-3690 (1984).

CURRICULUM VITAE

Zhenyu Yan

Boston University, Physics Department

Center For Polymer Studies

590 Commonwealth Avenue

Boston, Massachusetts 02215 USA

Telephone: 617/353-4836

Facsimile: 617/353-9393 or 617/353-3783

E-mail: zyan@buphy.bu.edu

http://buphy.bu.edu/~zyan/home

EDUCATION

- Ph.D., 2009 Physics; Boston University, Boston, MA.

  Academic advisor: Professor H. Eugene Stanley.

- M.S., 2002 - Physics; Clark Atlanta University, Atlanta, GA.

- B.S., 2000 - Applied Physics; Tongji University, Shanghai, P.R. China.

ACADEMIC APPOINTMENTS

- *Research Assistant* [2004.9 - present] Center for Polymer Studies and Physics Department, Boston University.

- *Teaching Assistant* [2002.9 - 2004.9] Physics Department, Boston University.

PROGRAMMING EXPERIENCE

- **OS** - LINUX & Windows.

- **Languages** - C/C++, Fortran 77/90, shell script, Perl, Matlab, HTML.

SELECTED PUBLICATIONS

- **Z. Yan**, S. V. Buldyrev, P. Kumar, N. Giovambattista, , H. E. Stanley, "Correspondence Between the Phase Diagrams of TIP5P Water and a Spherically Symmetric Repulsive Ramp Potential", Phys. Rev. E 77, 042201 (2008).

- **Z. Yan**, S. V. Buldyrev, P. Kumar, N. Giovambattista, P. G. Debenedetti, H. E. Stanley, Structure of the First and Second Neighbor Shells of Water: Quantitative Relation with Translational and Orientational Order, Phys Rev E, **76**, 051201 (2007).

- P. Kumar, **Z. Yan**, L. Xu, M. G. Mazza, S. V. Buldyrev, S.-H. Chen, S. Sastry, and H. E. Stanley, Glass Transition in Biomolecules and the Liquid-Liquid Critical Point of Water", Phys. Rev. Lett. **97**, 177802 (2006).

- **Z. Yan**, S. V. Buldyrev, N. Giovambattista, P. G. Debenedetti, and H. E. Stanley, Family of tunable spherically symmetric potentials that span the range from hard spheres to waterlike behavior, Phys. Rev. E **73**, 051204 (2006).

- **Z. Yan**, S. V. Buldyrev, N. Giovambattista, and H. E. Stanley, Structure Order of one-scale and two-scale potentials, Phys. Rev. Lett. **95**, 130604 (2005).

- C R Handy, A Z Msezane and **Z. Yan**, Generation of converging Regge-pole bounds for arbitrary rational fraction scattering potentials J. Phys. A: Math. Gen. **35**, 6359-6382 (2002).

- **Z. Yan** and C R Handy, Extension of a spectral bounding method to the PT-invariant states of the -(iX)N non-Hermitian potential, J. Phys. A: Math. Gen. **34**, 9907-9922 (2001).